Zeitschrift für angewandte Mathematik und Physik

ZAMP

Journal of Applied Mathematics and Physics
Journal de Mathématiques et de Physique appliquées

INHALT – CONTENTS – SOMMAIRE

ZAMP	Vol. XII	Fasc. 2	Pag. 89—184	25. 3. 61

Birkhäuser Verlag · Basel und Stuttgart

Zeitschrift für angewandte Mathematik und Physik
Journal of Applied Mathematics and Physics
Journal de Mathématiques et de Physique appliquées
ZAMP

Redaktor/Editor/rédacteur: Prof. Dr. R. Sänger, Postfach Zürich 23 (Schweiz)

ZAMP erscheint regelmässig alle zwei Monate. *Redaktionsschluss:* spätestens 12 Wochen vor Erscheinungstermin. Manuskripte und alle die Redaktion betreffenden Zuschriften sind an den Redaktor zu richten. Manuskripte für *Kurze Mitteilungen* können, falls die Autoren auf Zustellung eines Korrekturabzuges verzichten, 8 Wochen vor Erscheinungstermin eingereicht werden. Die Beiträge werden in deutscher, englischer, französischer oder italienischer Sprache publiziert, doch soll jeder *Originalarbeit* und *Kurzen Mitteilung* eine kurze Zusammenfassung in einer andern als der Originalsprache beigegeben werden. *Abbildungsvorlagen* sollen reproduktionsfertig mit Reduktionsmaßstab versehen eingeliefert werden, hingegen soll die Beschriftung nur mit Bleistift, am besten auf einem lose vorgeklebten, durchsichtigen Papier, ausgeführt werden. Autoren von Originalarbeiten, welche einen Umfang von mehr als 16 Druckseiten aufweisen, haben einen *Satzbeitrag* zu entrichten. Dieser beträgt sFr. 30.– pro Seite von der 17. bis 24. Seite, sFr. 46.– pro Seite von der 25. bis 32. Seite und sFr. 57.– pro Seite von der 33. Seite an. Die Verfasser von *Zusammenfassenden Berichten, Originalarbeiten* und *Kurzen Mitteilungen* erhalten 50 Gratisseparata ohne Umschlag.

ZAMP is published regularly every two months. All papers must be in the hand of the editor at least 12 weeks before publication of the issue. Manuscripts and all other correspondence concerning contributions to the periodical should be addressed *to the Editor*. Manuscripts of *Brief Reports* can be submitted 8 weeks before publication of the issue, if the authors dispense with proof-reading. The contributions will be published in English, German, French, or Italian; to each *Original Paper* and *Brief Report* should be added a brief summary in a language other than the original one. Drawings and photographs for *illustrations* should be sent ready for reproduction with indication of the proposed reduction; lettering on the illustrations should be entered in pencil, preferably on a loosely attached transparent sheet. Authors of Original Papers exceeding 16 printed pages are requested to pay a *contribution* of Sw.Frs. 30.– per page for pages 17–24, Sw. Frs. 46.– per page for pages 25–32, and Sw. Frs. 57.– per page for pages 33 and over. The authors of *Survey Articles, Original Papers*, and *Brief Reports* receive 50 free separata prints without cover.

ZAMP paraît régulièrement tous les deux mois. Derniers délais pour présenter les manuscrits: trois mois avant la parution de chaque numéro. Tous les manuscrits et toute correspondance relatifs à la rédaction sont à adresser au rédacteur. Les manuscrits pour des *communications brèves* peuvent être présentés huit semaines avant la parution, si les auteurs renoncent à contrôler les épreuves. Les articles seront publiés en langues française, anglaise, allemande ou italienne; cependant, chaque *article original* et toute *communication brève* devront être accompagnés d'un résumé en une autre langue. Les *illustrations* doivent être prêtes à la reproduction et il faudra y indiquer l'échelle de réduction. Le légende devra être inscrite au crayon, de préférence sur papier transparent, légèrement collé à l'illustration. Pour articles originaux qui dépassent 16 pages imprimées, une *contribution* de frs.s. 30.– par page doit être payée pour les pages 17–24 et de frs.s. 46.– par page pour les pages 25–32; à partir de page 33 la contribution est de frs.s. 57.– par page. Les auteurs de *comptes rendus*, ainsi que ceux d'*articles originaux* et de *communications brèves* recevront 50 tirés à part sans couverture de leur article.

Jahresabonnement, Annual subscription, Abonnement annuel:
(6 Nummern, 6 issues, 6 numéros) sFr. 78.– (DM 78.–)
Einzelnummer, single copy, le numéro, sFr. 16.–

Electromagnetic Field Theory Solution of the Infinite Tapered-Plane Transmission Line

By Noach Amitay, Abrahim Lavi, and Frederick Young, Pittsburgh, Pennsylvania, U.S.A.[1])

Introduction

Aside from a few isolated cases an exact solution to the nonuniform tapered transmission line problem is very difficult and consequently certain simplifying approximations become mandatory in arriving at a reasonable accurate solution. The methods employed in the literature are based mainly upon the telegraphy equations. The series and shunt impedances are obtained either from the step-line approximation where the line is broken into segments of parallel planes, or are assumed to vary according to an arbitrary function. The correlation between the mathematical solution and the actual physical structure is lacking in many cases. In this work a new approach is presented which bridges the missing link between the circuit theory analysis and the line geometry. The mathematical technique used is based upon the exact electromagnetic field theory solution of the oblique-planes line in conjunction with Lagrange's method of variation of parameters.

Wave Propagation between Two Infinite Oblique Conducting Planes

Prior to the analysis of an arbitrary tapered-plane transmission line, the solution of the two infinite oblique-planes line of figure 1 is briefly stated. Assuming an isotropic and nondissipative medium, ε and μ are both constant scalars, and assuming the planes to have a very high conductivity, the solution of the TM modes of propagation is given by

$$H_z = [C_{1m} H_m^{(1)}(k r) + C_{2m} H_m^{(2)}(k r)] (A_m \cos m\theta + B_m \sin m\theta) , \qquad (1)$$

$$E_r = \frac{m}{i \omega \varepsilon r} [C_{1m} H_m^{(1)}(k r) + C_{2m} H_m^{(2)}(k r)] (B_m \cos m\theta - A_m \sin m\theta) , \qquad (2)$$

$$E_\theta = \frac{1}{i \omega \varepsilon} \frac{d}{dr} [C_{1m} H_m^{(1)}(k r) + C_{2m} H_m^{(2)}(k r)] (A_m \cos m\theta + B_m \sin m\theta) , \qquad (3)$$

where $H_m^{(1)}(k r)$ and $H_m^{(2)}(k r)$ are Hankel functions of the first and second kind

[1]) Carnegie Institute of Technology, Department of Electrical Engineering. This work was submitted by Noach Amitay in partial fulfillment of the Degree Doctor of Philosophy.

of m^{th} order and C_{1m}; C_{2m}; A_m; B_m and m are constants of integration and separation. $k^2 = \omega^2 \mu \varepsilon = (2\pi/\lambda)^2$, λ being the free space wave length.

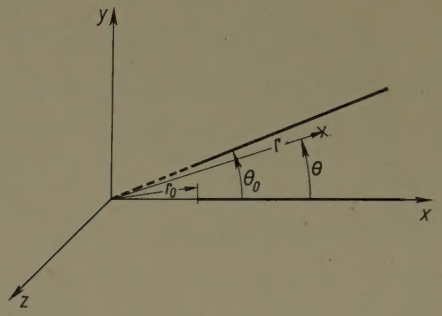

Figure 1
Two infinite oblique planes.

For a TEM mode $m = 0$ and hence

$$H_z = C_1 H_0^{(1)}(k r) + C_2 H_0^{(2)}(k r) , \tag{4}$$

$$E_\theta = -i \sqrt{\frac{\mu}{\varepsilon}} \left[C_1 H_1^{(1)}(k r) + C_2 H_1^{(2)}(k r)\right] . \tag{5}$$

It can easily be shown that higher order modes will be eliminated if $r\,\theta_0 < \lambda/2$.

Wave Propagation in an Infinite Tapered-plane Transmission Line

Consider the case of two conducting sheets extending from $z = -\infty$ to $z = +\infty$ as shown in figure 2. One plane lies along the x-axis ($y = 0$) while

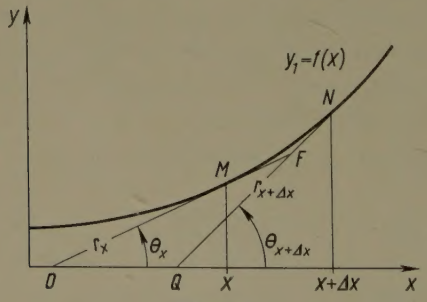

Figure 2
Infinite tapered plane transmission line.

the other is given by $y_1 = f(x)$ where $f(x)$ is an arbitrary function of x. Draw tangents to the tapered plane y_1 at the points M and N of figure 2. These

tangents intersect the x-axis at O and Q, while intersecting one another at the point F. Designate the length $\overline{OM}$ as r_x, the length $\overline{QN}$ as $r_{x+\Delta x}$, the angle between $\overline{OM}$ and the x-axis as θ_x and the angle between $\overline{QN}$ and the x-axis as $\theta_{x+\Delta x}$. Then

$$\tan\theta_x = \left.\frac{dy_1}{dx}\right|_x \quad \text{and} \quad \tan\theta_{x+\Delta x} = \left.\frac{dy_1}{dx}\right|_{x+\Delta x}. \tag{6}$$

Divide the tapered line into small sections VF, FG and so on, as shown in figure 3. Each section is a portion of an oblique plane making an angle of θ_x with the x-axis. The electromagnetic field quantities in each section are given by (4) and (5).

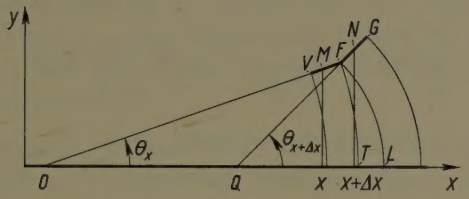

Figure 3

Two small sections of an infinite tapered-plane transmission line.

It should be emphasized here that r_x and θ_x are functions of x for a certain $y_1 = f(x)$ and thus the coefficients C_1 and C_2 of (4) and (5) vary from one section to another depending on x while being constants over each section. The field quantities everywhere between the planes are determined by requiring the magnitudes of the corresponding electromagnetic field components at the end of a section to equal those at the beginning of the following section, while taking the limit as $\Delta x \to 0$.

Consider the section $\overline{VF}$ of figure 3. With center O and radius $\overline{OF}$ draw the arc $\widehat{FT}$, where T is its point of intersection with the x-axis; with center Q and radius $\overline{QF}$ draw the arc $\widehat{QL}$, where L is its point of intersection with the x-axis. Since the mode of propagation considered is the TEM, the arcs $\widehat{FT}$ and $\widehat{FL}$ represent the wave fronts for the sections bounded by $\overline{VF}$ and $\overline{FG}$ respectively. The corresponding electromagnetic field quantities are matched along these arcs as stated above.

In a typical section $\overline{VF}$,

$$H_{z1} = C_1(x)\, H_0^{(1)}(k\,r) + C_2(x)\, H_0^{(2)}(k\,r)\,, \tag{7}$$

$$E_{\theta 1} = -i\,Z\,[C_1(x)\, H_1^{(1)}(k\,r) + C_2(x)\, H_1^{(2)}(k\,r)]\,, \tag{8}$$

where $\overline{OV} \leqq r \leqq \overline{OF}$ and $Z = \sqrt{\mu/\varepsilon}$.

In the adjacent section $\overline{FG}$,

$$H_{z2} = C_1(x + \Delta x)\, H_0^{(1)}(k\, r) + C_2(x + \Delta x)\, H_0^{(2)}(k\, r)\,, \tag{9}$$

$$E_{\theta 2} = -i\, Z\, [C_1(x + \Delta x)\, H_1^{(1)}(k\, r) + C_2(x + \Delta x)\, H_1^{(2)}(k\, r)]\,, \tag{10}$$

where $\overline{QF} \leqq r \leqq \overline{QG}$.

For values of $kr \gg 1$ or q, the Hankel functions can be replaced by their asymptotic form

$$H_q^{(1)}(k\, r) = \left(\frac{2}{\pi\, k\, r}\right)^{1/2} e^{i\,[k\, r - (2\,q+1)\,\pi/4]}\,, \tag{11}$$

$$H_q^{(2)}(k\, r) = \left(\frac{2}{\pi\, k\, r}\right)^{1/2} e^{-i\,[k\, r - (2\,q+1)\,\pi/4]}\,. \tag{12}$$

For $q = 1$ and $k\, r = \pi$ the error introduced is about 3%.

Matching the corresponding field quantities along the arcs $\widehat{FT}$ and $\widehat{FL}$ while $\Delta x \to 0$ implies

$$\lim_{\Delta x \to 0} H_{z1}|_{r=\overline{OF}} = \lim_{\Delta x \to 0} H_{z2}|_{r=\overline{QF}}\,, \tag{13}$$

$$\lim_{\Delta x \to 0} E_{\theta 1}|_{r=\overline{OF}} = \lim_{\Delta x \to 0} E_{\theta 2}|_{r=\overline{QF}}\,. \tag{14}$$

From figures 2 and 3

$$\overline{OF} = r_x + \frac{a\, \Delta x}{\cos\theta_x}\,, \tag{15}$$

$$\overline{QF} = r_{x+\Delta x} - \frac{(1-a)\, \Delta x}{\cos\theta_{x+\Delta x}}\,, \tag{16}$$

where $0 \leqq a \leqq 1$.

Upon the substitution of the asymptotic form of the Hankel functions (13) and (14) become

$$\lim_{\Delta x \to 0}\left[\frac{2}{\pi\, k\left(r_x + \dfrac{a\, \Delta x}{\cos\theta_x}\right)}\right]^{1/2}\left[C_1(x)\, e^{i\left[k\left(r_x + \frac{a\,\Delta x}{\cos\theta_x}\right) - \frac{\pi}{4}\right]} + C_2(x)\, e^{-i\left[k\left(r_x + \frac{a\,\Delta x}{\cos\theta_x}\right) - \frac{\pi}{4}\right]}\right]$$

$$= \lim_{\Delta x \to 0}\left[\frac{2}{\pi\, k\left(r_{x+\Delta x} - \dfrac{(1-a)\, \Delta x}{\cos\theta_{x+\Delta x}}\right)}\right]^{1/2}\left[C_1(x + \Delta x)\, e^{i\left[k\left(r_{x+\Delta x} - \frac{(1-a)\,\Delta x}{\cos\theta_{x+\Delta x}}\right) - \frac{\pi}{4}\right]}\right.$$

$$\left. + C_2(x + \Delta x)\, e^{-i\left[k\left(r_{x+\Delta x} - \frac{(1-a)\,\Delta x}{\cos\theta_{x+\Delta x}}\right) - \frac{\pi}{4}\right]}\right].$$

$$\left.\begin{aligned}\lim_{\Delta x\to 0}\left[\frac{2}{\pi k\left(r_x+\frac{a\,\Delta x}{\cos\theta_x}\right)}\right]^{1/2}&\left[C_1(x)\,e^{i\left[k\left(r_x+\frac{a\,\Delta x}{\cos\theta_x}\right)-\frac{3\pi}{4}\right]}\right.\\&\left.+\,C_2(x)\,e^{-i\left[k\left(r_x+\frac{a\,\Delta x}{\cos\theta_x}\right)-\frac{3\pi}{4}\right]}\right]\\=\lim_{\Delta x\to 0}\left[\frac{2}{\pi k\left(r_{x+\Delta x}-\frac{(1-a)\,\Delta x}{\cos\theta_{x+\Delta x}}\right)}\right]^{1/2}&\left[C_1(x+\Delta x)\,e^{i\left[k\left(r_{x+\Delta x}-\frac{(1-a)\,\Delta x}{\cos\theta_{x+\Delta x}}\right)-\frac{3\pi}{4}\right]}\right.\\&\left.+\,C_2(x+\Delta x)\,e^{-i\left[k\left(r_{x+\Delta x}-\frac{(1-a)\,\Delta x}{\cos\theta_{x+\Delta x}}\right)-\frac{3\pi}{4}\right]}\right].\end{aligned}\right\}\tag{18}$$

The mathematical solution is carried out by expanding $C_1(x+\Delta x)$; $C_2(x+\Delta x)$; $r_{x+\Delta x}$ and $\theta_{x+\Delta x}$ into Taylor series around the point x. Taking the limit as $\Delta x \to 0$, (17) and (18) produce two differential equations for the coefficients $C_1(x)$ and $C_2(x)$ given by

$$\frac{dC_1(x)}{dx} = C_1(x)\left(\frac{dr_x}{dx}-\frac{1}{\cos\theta_x}\right)\left(\frac{1}{2\,r_x}-i\,k\right),\tag{19}$$

$$\frac{dC_2(x)}{dx} = C_2(x)\left(\frac{dr_x}{dx}-\frac{1}{\cos\theta_x}\right)\left(\frac{1}{2\,r_x}+i\,k\right).\tag{20}$$

Integration of (19) and (20) yields

$$\log C_1(x) = \log A + \frac{1}{2}\log r_x - i\,k\,r_x - \frac{1}{2}\int\frac{dx}{r_x\cos\theta_x} + i\,k\int\frac{dx}{\cos\theta_x},\tag{21}$$

$$\log C_2(x) = \log B + \frac{1}{2}\log r_x + i\,k\,r_x - \frac{1}{2}\int\frac{dx}{r_x\cos\theta_x} - i\,k\int\frac{dx}{\cos\theta_x},\tag{22}$$

where $\log A$ and $\log B$ are constants of integration.

Referring to figures 2 and 3, the following relations can be derived.

$$r_x^2 = y_1^2 + \left(\frac{y_1}{\frac{dy_1}{dx}}\right)^2 = \left(\frac{y_1}{\frac{dy_1}{dx}}\right)^2\left[1+\left(\frac{dy_1}{dx}\right)^2\right],\tag{23}$$

$$\frac{1}{\cos^2\theta_x} = 1+\tan^2\theta_x = 1+\left(\frac{dy_1}{dx}\right)^2.\tag{24}$$

The use of (23) and (24) in the evaluation of the last two integrals in (21) and (22) gives

$$\int\frac{dx}{r_x\cos\theta_x} = \int\left[1+\left(\frac{dy_1}{dx}\right)^2\right]^{1/2}dx\Bigg/\left(\frac{y_1}{\frac{dy_1}{dx}}\right)\left[1+\left(\frac{dy_1}{dx}\right)^2\right]^{1/2} = \int\frac{dy_1}{y_1} = \log y_1,\tag{25}$$

$$\int \frac{dx}{\cos\theta_x} = \int_{x_0}^{x} \left[1 + \left(\frac{dy_1}{dx}\right)^2\right]^{1/2} dx = s_{x_0 x}\,, \tag{26}$$

where $s_{x_0 x}$ is the length of the tapered line arc between an arbitrary fixed point $[x_0; y_1(x_0)]$ and the point $[x; y_1(x)]$.

In this case, the choice is $x_0 = 0$. Thus, (21) and (22) assume the form which is given by

$$C_1(x) = A\left(\frac{r_x}{y_1}\right)^{1/2} e^{ik(s_x - r_x)}\,, \tag{27}$$

$$C_2(x) = B\left(\frac{r_x}{y_1}\right)^{1/2} e^{-ik(s_x - r_x)}\,. \tag{28}$$

The final equations of the electromagnetic field quantities are

$$\left.\begin{aligned} H_z = \left(\frac{2}{\pi k r_x}\right)^{1/2} &\left[A\left(\frac{r_x}{y_1}\right)^{1/2} e^{ik\left[r_x - \frac{\pi}{4} + (s_x - r_x)\right]} + B\left(\frac{r_x}{y_1}\right)^{1/2} e^{-ik\left[r_x - \frac{\pi}{4} + (s_x - r_x)\right]}\right] \\ &= y_1^{-1/2}\left[A_1 e^{iks_x} + A_2 e^{-iks_x}\right], \end{aligned}\right\}$$

$$\left.\begin{aligned} E_\theta = -iZ\left(\frac{2}{\pi k r_x}\right)^{1/2} &\left(\frac{r_x}{y_1}\right)^{1/2}\left[A e^{i\left[ks_x - \frac{3\pi}{4}\right]} + B e^{-i\left[ks_x - \frac{3\pi}{4}\right]}\right] \\ &= Z y_1^{-1/2}\left(-A_1 e^{iks_x} + A_2 e^{-iks_x}\right), \end{aligned}\right\} \tag{30}$$

where $A_1 = A\,(2/\pi k)^{1/2}\, e^{-i\pi/4}$ and $A_2 = B\,(2/\pi k)^{1/2}\, e^{i\pi/4}$.

To distinguish this solution from the exact field solution derived directly from MAXWELL'S equations, and from the solution obtained from the telegraphy equations, this solution will be henceforth designated as the 'Approximate field solution' of the tapered line.

Since energy is conserved and the transmission line is assumed to be lossless, the instantaneous power flow per unit of z width through any transverse cross-section extending between the two planes should be constant. The RMS power flow is

$$P = \frac{1}{2}\int_0^{\theta_x} \mathrm{Re}[E_\theta H_z^*]\, r_x\, d\theta = \text{const.} \tag{31}$$

Upon the substitution of (29) and (30) into (31)

$$\left.\begin{aligned} P &= \frac{Z r_x}{2 y_1}\int_0^{\theta_x} \mathrm{Re}\left[(A_2 e^{-iks_x} - A_1 e^{iks_x})\,(A_2^* e^{iks_x} + A_1^* e^{-iks_x})\right] d\theta \\ &= \frac{Z}{2}\left(|A_2|^2 - |A_1|^2\right)\frac{r_x \theta_x}{y_1} = \frac{Z}{2}\left(|A_2|^2 - |A_1|^2\right)\frac{\theta_x}{\sin\theta_x}. \end{aligned}\right\} \tag{32}$$

It appears that the power P flowing through any transverse cross-sectional surface is a function of x. The dependence of P on x expressed by $\gamma_x = \theta_x/\sin\theta_x$ violates the law of conservation of energy.

However, γ_x is very close to unity for $0 \leqq \theta_x \leqq \pi/6$ (at $\theta_x = \pi/6$; $\gamma_x = 1{\cdot}04$). Therefore, if θ_x is kept below $\pi/6$ for any point along the line, no serious error is introduced.

This limitation on the tapering angle is not surprising if it is realized that in the procedure of matching the corresponding field quantities between two adjacent segments (see (17) and (18), the wave fronts were assumed to be cylindrical surfaces. Obviously this assumption breaks down at large angles which are not common in the art. Hence, for all practical purposes the law of conservation of energy is not violated.

Transformations by the Nonuniform Line

Any transmission line that may be considered as a four terminal network has the property of impedance transformation. Thus, designating the ratio of input voltage to input current as the input impedance, Z_i, and the ratio of output voltage to output current as the output impedance (terminating impedance), Z_s, the impedance transformation ratio is given by Z_s/Z_i.

In the general transmission line of figure 4, the voltage between points P_1 and P_2 is

$$V_x = \int_0^{\theta_x} E_\theta r_x \, d\theta = Z\,(A_2 e^{-iks_x} - A_1 e^{iks_x}) \frac{r_x \theta_x}{\sqrt{y_1}}. \tag{33}$$

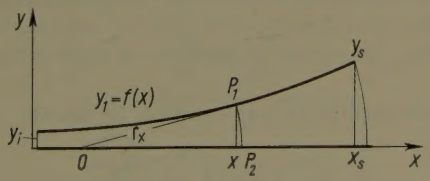

Figure 4
General transmission line.

The current flowing in a strip of width d is

$$I_x = H_z d = \frac{d}{\sqrt{y_1}} (A_2 e^{-iks_x} + A_1 e^{iks_x}). \tag{34}$$

For a finite length line having the total arc length

$$S = \int_0^{x_S} \left[1 + \left(\frac{dy_1}{dx}\right)^2\right]^{1/2} dx$$

as in figure 4, A_1 and A_2 are expressed in terms of the voltage and the current at the end of the line (V_S and I_S respectively).

Thus, the voltage and current at any point x along the line are

$$V_x = \frac{Z}{2}\left(\frac{y_S}{y_1}\right)^{1/2}\left\{\left(\frac{I_S}{d}+\frac{V_S}{Z\,r_S\,\theta_S}\right)e^{ik(S-s_x)}-\left(\frac{I_S}{d}-\frac{V_S}{Z\,r_S\,\theta_S}\right)e^{-ik(S-s_x)}\right\}r_x\,\theta_x\,, \tag{35}$$

$$I_x = \frac{d}{2}\left(\frac{y_S}{y_1}\right)^{1/2}\left\{\left(\frac{I_S}{d}+\frac{V_S}{Z\,r_S\,\theta_S}\right)e^{ik(S-s_x)}+\left(\frac{I_S}{d}-\frac{V_S}{Z\,r_S\,\theta_S}\right)e^{-ik(S-s_x)}\right\}. \tag{36}$$

In order to suppress reflection in the line, the following relation must hold

$$Z_S = \frac{V_S}{I_S} = Z\,\frac{r_S\,\theta_S}{d}\,. \tag{37}$$

In other words, if the line is terminated with a load impedance Z_S, no reflections occur. In this case the input voltage and current ($x = 0$) are

$$V_i = V_S\left(\frac{y_S}{y_i}\right)^{1/2}e^{ikS}\,\frac{r_i\,\theta_i}{r_S\,\theta_S} \approx V_S\left(\frac{y_i}{y_S}\right)^{1/2}e^{ikS}\,, \tag{38}$$

$$I_i = \left(\frac{y_S}{y_i}\right)^{1/2}\frac{dV_S}{Z\,r_S\,\theta_S}\,e^{ikS} = \left(\frac{y_S}{y_i}\right)^{1/2}I_S\,e^{ikS}\,, \tag{39}$$

and the input impedance is

$$Z_i = \frac{V_i}{I_i} = \frac{V_S}{I_S}\,\frac{y_i}{y_S} = Z_S\,\frac{y_i}{y_S}\,. \tag{40}$$

The impedance transformation ratio for this case becomes

$$\frac{Z_S}{Z_i} = \frac{y_S}{y_i}\,. \tag{41}$$

While the voltage and current transformation ratios are

$$\frac{V_S}{V_i} = \left(\frac{y_S}{y_i}\right)^{1/2}e^{-ikS}\,, \tag{42}$$

$$\frac{I_S}{I_i} = \left(\frac{y_S}{y_i}\right)^{-1/2}e^{-ikS}\,. \tag{43}$$

It is interesting to note that the transformation ratios are explicitly expressed in terms of the function y_1, and the impedance transformation ratio depends solely on the ratio of the output to input vertical separation between the lines. The actual shape of the line has no bearing whatsoever on the impedance transformation ratio; that is, given two lines described by $y_1 = f_1(x)$ and $y_1 = f_2(x)$ such that $f_1(0) = f_2(0)$ and $f_1(L) = f_2(L)$ as in figure 5, the impedance transformation ratio for both lines is identical as long as both lines satisfy the conditions imposed previously.

The previous conclusion has to be modified, however, when the voltage (or current) transformation ratio is evaluated. The absolute value of the ratio is again independent of the function, y_1, but there is definitely a phase dependence upon the length of the arc S. Therefore, for the two lines $f_1(x)$ and $f_2(x)$ of figure 5, if

$$\int_0^L \left[1 + \left(\frac{df_1(x)}{dx}\right)^2\right]^{1/2} dx \neq \int_0^L \left[1 + \left(\frac{df_2(x)}{dx}\right)^2\right]^{1/2} dx \tag{44}$$

then the two lines do not behave identically phase-wise although $f_1(L) = f_2(L)$.

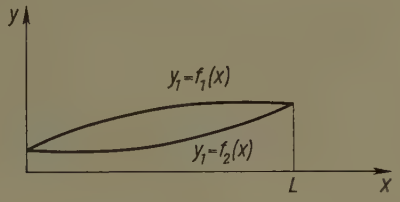

Figure 5
Two transmission lines having the same impedance transformation ratio.

Design Considerations

The limitation $\theta_{max} \leqq \pi/6$ in conjunction with $r/\lambda > 1/2$ and $\theta_{max}\, r/\lambda < 1/2$ define the region within which the solution is valid. These three conditions are represented in figure 6. The shaded area gives the permissible combinations for r/λ and θ_{max}. It is interesting to note that in order to increase the bandwidth while retaining the same impedance transformation θ_{max} must be decreased.

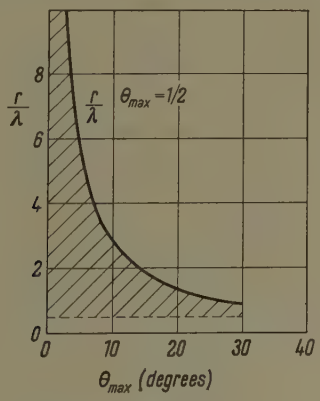

Figure 6
Impedance transformation region.

Comparison with other Existing Solutions

The solutions of other tapered lines obtained from the telegraphy equations check in certain respects with those obtained from the approximate field solution. It has been found that the impedance transformation in Bessel and exponential lines depends upon the ratio of the vertical separations between the electrodes at the two ends of the line. However, a discrepancy in phase is observed. The phase variation in the approximate field solution depends upon the length of the arc while in the telegraphy equations solution the phase variation depends upon the linear distance x. This error in phase is not surprising in view of the fact that for the simple case of the two oblique-planes line the phase variation obtained from the telegraphy equations solution is in disagreement with the solution obtained directly from MAXWELL's equations. On the other hand in the approximate field solution, the phase variation is expected to be more accurate because the shape of the wave fronts is accounted for. Moreover, the boundary conditions (i. e. the electric field is perpendicular to the conducting surfaces) are satisfied in contrast with the situation in the step-line approximation.

The agreements between the telegraphy equations solution and the approximate field solution are encouraging but certainly not profound. While the approximate field solution yields quick and accurate results for any arbitrary tapering function y_1, the telegraphy equations in conjunction with the step line approximation lack this generality.

Conclusion

A new method for the study of the steady state performance of infinite tapered-plane transmission lines has been presented. This method is advantageous because it offers a quick and accurate evaluation of the transformation properties of the line. The impedance transformation ratio as well as the absolute values of the voltage and current transformation ratios of a matched line depends upon the ratio of the initial and final separations regardless of the tapering function of the line. In contrast to previous works, this paper accounts for the phase variation which is proportional to the tapered-line arc.

In addition, design criteria are presented, which limit the tapering of the line and determine the bandwidth.

The results derived in this work hold true for tapered strip lines as well as coaxial cables where the radial separation between the electrodes is small compared to the radius of the electrodes.

REFERENCES

[1] C. RAVUT, *Propagation des courants sinusoïdaux sur des lignes quelconques*, Rev. gén. Elect., 7 (1920).

[2] S. Ballantine, *Nonuniform Lumped Electric Lines*, J. Franklin Inst., *203*, 561–582; (1927).
[3] J. W. Arnold and P. F. Bechberger, *Sinusoidal Currents in Linearly Tapered Loaded Transmission Lines*, Proc. IRE, 19, 304–310 (1931).
[4] A. T. Starr, *The Nonuniform Transmission Line*, Proc. IRE, *20*, 1052–1063, (1932).
[5] S. A. Schelkunoff, *Transmission Theory of Plane Electromagnetic Waves*, Proc. IRE, *25*, 1457–1492 (1937).
[6] C. R. Burrows, *The Exponential Transmission Line*, BSTJ, *17*, 555–573 (1938).
[7] H. A. Wheeler, *Transmission Lines with Exponential Taper*, Proc. IRE, *27*, 65–71 (1939).
[8] J. R. Pierce, *Note on the Transmission Line Equations in Terms of Impedance*, BSTJ, *22*, 263–265 (1943).
[9] R. L. Walker and N. Wax, *Nonuniform Transmission Lines and Reflection Coefficients*, J. Appl. Phys. *17*, 1043–1045 (1946).
[10] E. R. Schatz and E. M. Williams, *Pulse Transients in Exponential Transmission Lines*, Proc. IRE, *38*, 1208–1212 (1950).
[11] M. E. Zhabotinski, W. L. Levin, and S. M. Rytov, *The Telegraphy Equations for Generalized Transmission Lines with Small Losses*, J. Tech. Phys., Moscow, *20*, 257–281 (1950).
[12] F. Bolinder, *Fourier Transforms in the Theory of Inhomogeneous Transmission Lines*, Proc. IRE, *38*, 1354 (1950).
[13] H. Kaufman, *Bibliography of Nonuniform Transmission Lines*, Trans. IRE, AP–*3*, 218–220 (1955).
[14] S. A. Schelkunoff, *Conversion of Maxwell's Equations into Generalized Telegraphist's Equations*, BSTJ, *34*, 995–1044 (1955).
[15] R. W. Klopfenstein, *A Transmission Line Taper of Improved Design*, Proc. IRE, *44*, 31–35 (1956).
[16] J. Willis and N. K. Sinha, *Nonuniform Transmission Line as Impedance Transformer*, Proc. IEE, *103* [B], 166–172 (1956).
[17] R. E. Collin, *The Optimum Tapered Transmission Line Matching Section*, Proc. IRE, *44*, 539–547 (1956).
[18] R. N. Ghose, *Exponential Transmission Lines as Resonators and Transformers*, Trans. IRE, MTT-*5*, 213–227 (1957).
[19] R. Codelupi, *Teoria delle linee non-uniformi*, Alta Frequenza, *26*, 226–282 (1957).
[20] B. G. Kazanski, *Outline of a Theory of Nonuniform Transmission Lines*, Proc. IEE, *105* [C], 126–138 (1958).
[21] L. Solymar, *Some Notes on Optimum Design of Stepped Transmission Line Transformer*, Trans. IRE, MTT-*6*, 374–378 (1958).
[22] F. J. Young, E. R. Schatz, and J. B. Woodford, *The Transient Response of Tapered Transmission Lines*, Communication and Electronics, *43*, 223–228 (1959).

Zusammenfassung

Für den eingeschwungenen Zustand der *tapered-plane transmission line* wird eine neue Lösungsmethode beschrieben und gezeigt, dass die Impedanztransformation direkt vom Verhältnis der Abstände zwischen Anfang und Ende der leitenden Ebenen bestimmt wird. Die Phasendifferenz der Spannungen zwischen den Leitungsenden ist dem Öffnungswinkel der beiden Ebenen proportional. Kriterien für den Entwurf solcher Leitungen lassen sich angeben.

(Received: August 30, 1960.)

Duct Flow in Magnetohydrodynamics

By Chieh C. Chang and Thomas S. Lundgren, Minneapolis, Minnesota, USA[1])

Introduction

This paper is an extension of the work of Hartmann [2][2]) and Shercliff [3, 4] on the steady flow of conducting fluids through ducts under transverse magnetic fields – the simplest class of magnetohydrodynamic problems. We are concerned here mainly with the boundary value problems associated with flow in ducts with conducting walls.

Equations and Boundary Conditions

The following set of vector equations appears to give an adequate description of the steady state interaction between electromagnetic and hydrodynamic forces:

$$\text{curl } \boldsymbol{B} = \mu_0 \boldsymbol{j} , \tag{1}$$

$$\text{div } \boldsymbol{B} = 0 , \tag{2}$$

$$\text{curl } \boldsymbol{E} = 0 , \tag{3}$$

$$\text{div } \boldsymbol{E} = \varrho_e/\varepsilon_0 , \tag{4}$$

$$\boldsymbol{j} = \sigma (\boldsymbol{B} + \boldsymbol{V} \times \boldsymbol{B}) + \varrho_e \boldsymbol{V} , \tag{5}$$

$$\varrho \boldsymbol{V} \cdot \nabla \boldsymbol{V} = -\nabla p + \varrho \nu \nabla^2 \boldsymbol{V} + \boldsymbol{j} \times \boldsymbol{B} + \varrho_e E \tag{6}$$

$$\text{div } \boldsymbol{V} = 0 . \tag{7}$$

It is assumed that the magnetic and dielectric properties of the medium are the same as in a vacuum; μ_0 and ε_0 are the magnetic permeability and dielectric constant in vacuum. In (5), Ohm's law, the electrical conductivity σ is assumed constant for a homogeneous medium. Equations (6) and (7) are the momentum and continuity equations which describe the steady motion of an incompressible fluid. If the system to be analyzed is composed partly of fluid and partly of solid or vacuum, the last two equations, (6) and (7), only have to be satisfied in the fluid, while the first five equations must be satisfied throughout all space. The description of the system is completed by specifying zero velocity at rigid boundaries and imposing continuity of tangential components of $\boldsymbol{E}$ and of

[1]) Department of Aeronautical Engineering, University of Minnesota.

[2]) Numbers in brackets refer to References, page 114.

normal and tangential components of $\boldsymbol{B}$ at interfaces, plus boundary conditions on $\boldsymbol{B}$ and $\boldsymbol{E}$ at infinity. It should be mentioned that continuity of tangential components of $\boldsymbol{B}$ implies no surface currents. This is the case, since in non-magnetic materials surface currents occur only in the presence of *unsteady* magnetic fields.

In equations (5) and (6) the free charge ϱ_e will be neglected. It will be retained in (4), which serves only to determine the free charge once $\boldsymbol{E}$ is known. This can be considered as the first step in an iterative process, the second step being to substitute the value of ϱ_e calculated in the first step into (5) and (6).

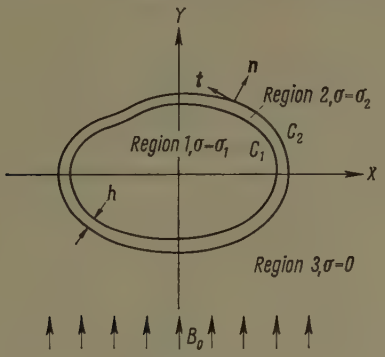

Figure 1
Cross-section of duct.

Figure 1 is a sketch of the system under study. An electrically conducting incompressible fluid (region 1) flows in the z-direction through a straight duct whose walls are of constant thickness (region 2). The electrical conductivity of the wall is σ_2. Outside of the duct (region 3) the conductivity is zero, and at infinity a uniform magnetic field B_0 acts in the y-direction.

If it is assumed that the velocity has only a z-component, that all physical quantities (except pressure) are independent of z, and that there is no net flow of current in the z-direction, then it can be shown that $B_x = 0$, $B_y = B_0$, and $j_z = E_z = 0$.

Using the results of the previous paragraph, the vector equations from (1) to (7) can be reduced to two second order linear partial differential equations, namely, the z-component of the momentum equation

$$\frac{\partial p}{\partial z} = \varrho \nu \nabla^2 V_z + \frac{B_0}{\mu_0} \frac{\partial B_z}{dy} \tag{8}$$

and the z-component of the curl of OHM's law,

$$\nabla^2 B_z + \sigma \mu_0 B_0 \frac{\partial V_z}{\partial y} = 0 . \tag{9}$$

In the first of these $\partial p/\partial z$ is a constant, since from (6) ∇p is independent of z. In the fluid, region 1, both (8) and (9) are valid, while outside of the fluid, regions 2 and 3, only (9) is true with $V_z = 0$. In addition, since region 3 is non-conducting, the current must be zero there. This fact and (1) imply that B_z is constant. Therefore, since B_z goes to zero at infinity, B_z must be identically zero in region 3.

Across the boundaries of the several regions, B_z and the tangential component of electric field must be continuous. Using OHM's law, the condition on the electric field can be written

$$\left[\frac{j_t}{\sigma}\right] = 0$$

where j_t is the current in the direction of the tangent to the interface. (A square bracket around a quantity means the discontinuity in this quantity.) This is true since the velocity vanishes at the boundary, causing the $\boldsymbol{V} \times \boldsymbol{B}$ term in OHM's law to vanish. Observe now that the x- and y-components of (1) are

$$\mu_0 \, j_x = \frac{\partial B_z}{\partial y}, \qquad \mu_0 \, j_y = -\frac{\partial B_z}{\partial x}$$

so B_z can be considered as a 'stream function' for $\mu_0 \boldsymbol{j}$ — the current flows along the lines $B_z =$ constant. This shows that

$$\mu_0 \, j_t = -\frac{\partial B_z}{\partial n},$$

where $\boldsymbol{n}$ is the outward normal. Using this result, continuity of E_t becomes

$$\left[\sigma^{-1} \frac{\partial B_z}{\partial n}\right] = 0.$$

Before summing up the results of the last few paragraphs, let new dimensionless variables be introduced by

$$\left.\begin{aligned} \xi &= \frac{x}{a}, \\ \eta &= \frac{y}{a}, \\ V &= -\frac{V_z}{(a^2/\nu\,\varrho)\,(\partial p/\partial z)}, \\ B &= -\frac{B_z}{(a^2/\nu\,\varrho)\,(\partial p/\partial z)\,\mu_0\,(\nu\,\varrho\,\sigma)^{1/2}}, \\ M &= B_0\, a \left(\frac{\sigma}{\nu\,\varrho}\right)^{1/2}, \end{aligned}\right\} \tag{10}$$

where a is a characteristic dimension of the duct and M is the Hartmann number. With this new notation and using subscripts 1 and 2 to denote the region, the problem is to solve

$$\nabla^2 V_1 + M \frac{\partial B_1}{\partial \eta} = -1, \tag{11}$$

$$\nabla^2 B_1 + M \frac{\partial V_1}{\partial \eta} = 0, \tag{12}$$

in region 1, and

$$\nabla^2 B_2 = 0 \tag{13}$$

in region 2. The boundary conditions are: $B_2 = 0$ on C_2, the boundary between 2 and 3; and $V_1 = 0$, $B_1 = B_2$, $\sigma_2 \, \partial B_1/\partial n = \sigma_1 \, \partial B_2/\partial n$ on C_1, the boundary between 1 and 2.

This problem is difficult since it involves two domains and two sets of boundary conditions. In special cases it can be simplified. If the duct wall is a perfect insulator ($\sigma_2 = 0$), then $B_2 = 0$ so that it is only necessary to solve (11) and (12) with $V_1 = 0$ and $B_1 = 0$ on C_1. If the duct wall is a perfect conductor ($\sigma_2 = \infty$) the boundary conditions become: $V_1 = 0$ and $\partial B_1/\partial n = 0$ on C_1. There is another limiting case discovered by SHERCLIFF [4], for which the problem reduces to solving (11) and (12) in region 1 with boundary conditions given on C_1. Suppose the thickness of the duct wall (h/a in the new notation) is much smaller than unity. To a good approximation the harmonic function B_2 is locally linear, that is, it varies linearly across the duct wall.This can be seen clearly by considering the membrane analogy for solutions of LAPLACE'S equation. Then $\partial B_2/\partial n = -\, a\, B_1/h$ on C_1. The boundary conditions become $V_1 = 0$, $\partial B_1/\partial n + B_1/\varphi = 0$, where $\varphi = \sigma_2 \, h/\sigma_1 \, a$. It should be noted that the cases $\sigma_2 = 0$ and $\sigma_2 = \infty$ are included in the last boundary condition with $\varphi = 0$ and $\varphi = \infty$ respectively.

Parallel Sided Duct

There is one situation in which the approximate boundary condition becomes exact. This is the case of flow in a rectangular duct when the walls parallel to the applied magnetic field are at infinity. In this problem the harmonic function B_2 is independent of ξ, and hence must be a linear function of η.

With the dimensionless variables defined in the previous section, the problem is to solve

$$\frac{d^2V}{d\eta^2} + M \frac{dB}{d\eta} = -1, \qquad \frac{d^2B}{d\eta^2} + M \frac{dV}{d\eta} = 0,$$

with boundary conditions $V = 0$, $dB/d\eta \pm B/\varphi = 0$ when $\eta = \pm 1$ respectively. Here, half the duct height has been taken as the characteristic length, a. The

solution of the above equations is easily found to be

$$V = \frac{1}{M} \frac{\varphi + 1}{M\varphi + \tanh M} \left(1 - \frac{\cosh M\eta}{\cosh M}\right), \tag{14}$$

$$B = -\frac{\eta}{M} + \frac{1}{M} \frac{\varphi + 1}{M\varphi + \tanh M} \frac{\sinh M\eta}{\cosh M}. \tag{15}$$

HARTMANN [2] gave this solution for the case $\varphi = 0$. For given φ, the velocity, which is parabolic for $M = 0$, becomes flatter in the center as M increases. When M is very large it tends to be uniform except in a boundary layer of thickness the order of $1/M$. Asymptotically,

$$V \sim \frac{1}{M} \frac{\varphi + 1}{M\varphi + 1}. \tag{16}$$

This shows that $V \sim 1/M$ for non-conducting walls while $V \sim 1/M^2$ for perfectly conducting walls: increasing the wall conductivity decreases the velocity.

Another quantity of interest is $M\, dB/d\eta$, the ratio of Lorentz force to the magnitude of the pressure gradient. This is also proportional to the current density. By an easy calculation,

$$M \frac{dB}{d\eta} = -1 + M \frac{\varphi + 1}{M\varphi + \tanh M} \frac{\cosh M\eta}{\cosh M}.$$

This is plotted in Figure 2 for $M = 3$, $\varphi = 1$, $h = 0{\cdot}5\, a$, to give a typical example. The value of this quantity in the wall,

$$\frac{a}{h} \varphi \left(\frac{M - \tanh M}{M\varphi + \tanh M}\right),$$

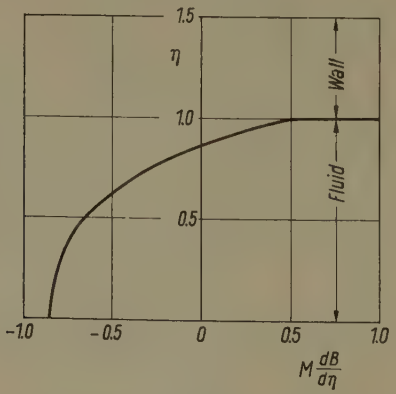

Figure 2

The current distribution across half of a parallel sided duct for $M = 3$, $\varphi = 1$, $h = 0{\cdot}5\, a$.

is also plotted. From this figure it is seen that near the center of the duct the current flows to the left. This gives a Lorentz force which tends to help the viscous forces balance the pressure gradient. Near the wall the current flows to the right giving a Lorentz force which opposes the viscous forces, so that the viscous forces have to be larger in order that the pressure gradient be balanced. For large M

$$M \frac{dB}{d\eta} \sim 1$$

except in a boundary layer of thickness the order of $1/M$, and in the wall. This shows that for large M, the Lorentz force completely balances the pressure gradient except in a thin boundary layer along the wall.

Stated differently, the current distribution tends to be uniform to the left and of a magnitude such as to make the Lorentz force balance the pressure gradient. Since the total current flow must be zero, part of the return current flows in the boundary layer and part in the wall. When the wall conductivity is larger a greater proportion of the return current flows in the wall, taking the path of least resistance. This shows that for fixed M (large), less current flows in the boundary layer when the wall conductivity is high, indicating that the Lorentz force opposing the viscous forces is less. Therefore the viscous forces must be smaller in order that the pressure gradient be balanced. Now if the viscous forces near the wall are smaller, the second derivatives of the velocity will be smaller; hence the velocity of the core will be smaller. This shows why the velocity becomes smaller when the wall conductivity increases.

Consider the dimensionless mass flow

$$Q = \int_{-1}^{1} V \, d\eta = \frac{\text{Mass flow per unit width}}{(a^3/\nu)\,(-\partial p/\partial z)}$$

$$= \frac{\varphi + 1}{M^2} \frac{M - \tanh M}{M\varphi + \tanh M}.$$

The reciprocal of Q is essentially the pressure gradient required to maintain a given mass flow. In Figure 3

$$\frac{Q(M=0)}{Q} = \frac{1}{3} \frac{M^2}{\varphi + 1} \frac{M\varphi + \tanh M}{M - \tanh M} \tag{17}$$

is plotted versus M for various values of φ. This can be interpreted as the ratio of the pressure gradient to the pressure gradient required to maintain a non-magnetic flow with the same mass flow. Notice that for a given mass flow a much larger pressure gradient is required to maintain flow through a perfectly conducting duct than through a non-conducting duct.

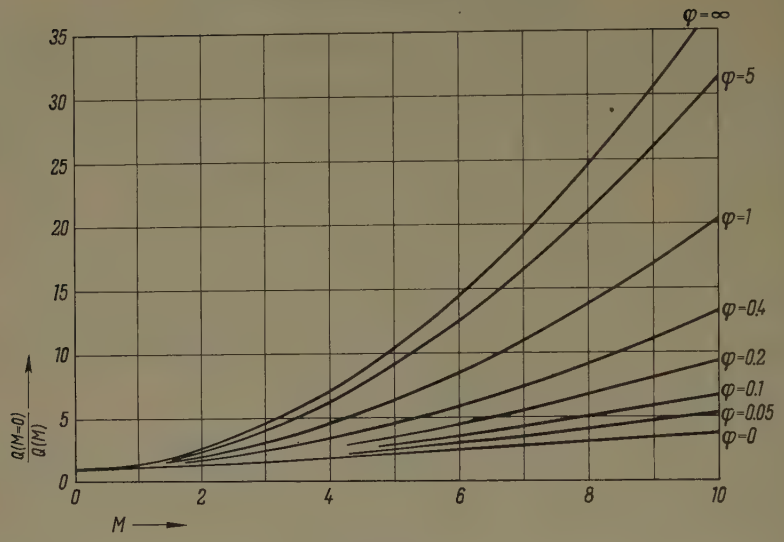

Figure 3

The pressure gradient versus M for various values of φ in a parallel sided duct.

Perfectly Conducting Rectangular Duct

In this section, the flow through a finite rectangular duct with perfectly conducting walls is considered. Regrettably, we have been unable to solve the problem for arbitrary wall conductivity.

The problem to be solved is

$$\nabla^2 V + M \frac{\partial B}{\partial \eta} = -1, \qquad \nabla^2 B + M \frac{\partial V}{\partial \eta} = 0$$

in a rectangle of width $2l$ and height 2, with $V = 0$ on all the walls, $\partial B/\partial \xi = 0$ on the vertical walls, and $\partial B/\partial \eta = 0$ on the horizontal walls. The expansions

$$V = \sum_{j=0}^{\infty} v_j \cos \beta_j \eta, \qquad B = \sum_{j=0}^{\infty} b_j \sin \beta_j \eta, \qquad 1 = \sum_{j=1}^{\infty} a_j \cos \beta_j \eta,$$

where $\beta_j = (j + 1/2)\pi$, satisfies the boundary conditions on the horizontal walls and allows the differential equations to be written as ordinary differential equations for v_j and b_j —

$$\frac{d^2 v_j}{d\xi^2} - \beta_j^2 v_j + M \beta_j b_j = -a_j, \qquad \frac{d^2 b_j}{d\xi^2} - \beta_j^2 b_j - M \beta_j v_j = 0.$$

Solutions of these which satisfy the boundary conditions on the vertical walls are

$$v_j = \frac{a_j}{\beta_j^2 + M^2} \left(1 - \frac{r_{2j} \sinh r_{2j} l \cosh r_{1j} \sinh \xi + r_{1j} \sinh r_{1j} l \cosh r_{2j} \xi}{r_{2j} \cosh r_{1j} l \sinh r_{2j} l + r_{1j} \cosh r_{2j} l \sinh r_{1j} l}\right) \tag{18}$$

and

$$b_j = \frac{a_j}{\beta_j^2 + M^2}\left(\frac{M}{\beta_j} + i\,\frac{r_{2j}\sinh r_{2j}\,l\cosh r_{1j}\,\xi - r_{1j}\sinh r_{1j}\,l\cosh r_{2j}\,\xi}{r_{2j}\cosh r_{1j}\,l\sinh r_{2j}\,l + r_{1j}\cosh r_{2j}\,l\sinh r_{1j}\,l}\right) \tag{19}$$

where

$$r_{1j} = (\beta_j^2 + i\,M\,\beta_j)^{1/2}, \quad r_{2j} = (\beta_j^2 - i\,M\,\beta_j)^{1/2}$$

are complex. r_{1j} and r_{2j} may be separated into their real and imaginary parts, namely,

$$r_{1j} = \alpha_j + i\,\gamma_j$$

and

$$r_{2j} = \alpha_j - i\,\gamma_j\,,$$

where

$$\alpha_j = \left(\frac{\beta_j}{2}\right)^{1/2}[\beta_j + (\beta_j^2 + M^2)^{1/2}]^{1/2}, \quad \gamma_j = \left(\frac{\beta_j}{2}\right)^{1/2}[-\beta_j + (\beta_j + M^2)^{1/2}]^{1/2}.$$

After some algebra to express v_j and b_j in terms of the real quantities α_j and γ_j the final result becomes

$$V = \sum_{j=0}^{\infty} \frac{2\,(-1)^j}{\beta_j}\,\frac{\cos\beta_j\,\eta}{\beta_j^2 + M^2}\left\{1 - \frac{\alpha_j\,E_j(\xi) - \gamma_j\,F_j(\xi)}{\alpha_j\sinh 2\,\alpha_j\,l - \gamma_j\sin 2\,\gamma_j\,l}\right\}, \tag{20}$$

$$B = \sum_{j=0}^{\infty} \frac{2\,(-1)^j}{\beta_j}\,\frac{\sin\beta_j\,\eta}{\beta_j^2 + M^2}\left\{\frac{M}{\beta_j} + \frac{\alpha_j\,F_j(\xi) + \gamma_j\,E_j(\xi)}{\alpha_j\sinh 2\,\alpha_j\,l - \gamma_j\sin 2\,\gamma_j\,l}\right\}, \tag{21}$$

where

$$E_j(\xi) = \frac{1}{4}\,[\cos\gamma_j\,(l-\xi)\sinh\alpha_j\,(l+\xi) + \cos\gamma_j\,(l+\xi)\sinh\alpha_j\,(l-\xi)]\,,$$

$$F_j(\xi) = \frac{1}{4}\,[\sin\gamma_j\,(l-\xi)\cosh\alpha_j\,(l+\xi) + \sin\gamma_j\,(l+\xi)\cosh\alpha_j\,(l-\xi)]\,.$$

The calculation of mass flow per unit pressure gradient is more easily accomplished by integrating the complex form of the velocity. The result is

$$Q = 8\,l\sum_{j=0}^{\infty}\frac{1}{\beta_j^2\,(\beta_j^2 + M^2)}\left\{1 - \frac{\beta_j}{l\,(\beta_j^2 + M^2)^{1/2}}\,\frac{\cosh 2\,\alpha_j\,l - \cos 2\,\alpha_j\,l}{\alpha_j\sinh 2\,\alpha_j\,l - \gamma_j\sin 2\,\gamma_j\,l}\right\}. \tag{22}$$

$Q(M=0)/Q(M)$ is plotted versus M in Figure 4 for a square duct. The corresponding result for non-conducting walls, SHERCLIFF [3], is included for comparison.

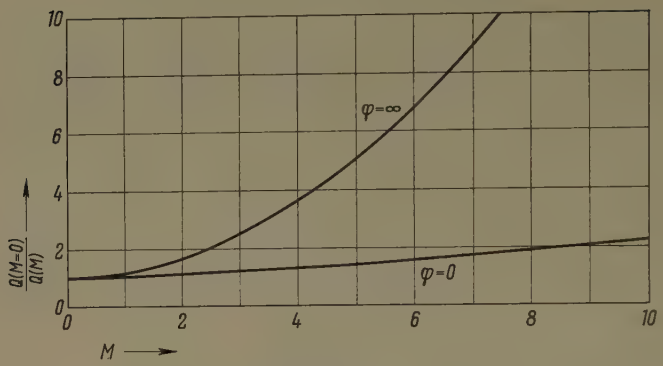

Figure 4
Pressure gradient versus M for $\varphi = 0$ and $\varphi = \infty$, square duct.

Flow in Arbitrary Symmetrical Duct for Large M

It has been seen for rectangular ducts that the velocity distribution for large M consists of a uniform core with a boundary layer near the walls in which the velocity changes rapidly. The purpose of the present section is to investigate how the cross-section form and wall conductivity affect the velocity distribution in the core. This question has been answered for non-conducting walls by SHERCLIFF [3] and for circular ducts with walls of small conductivity by SHERCLIFF [4].

Let the duct be as indicated in Figure 1, except symmetrical about the x-axis. Let the upper surface be described by $\eta = Y(\xi)$ the lower surface by $\eta = -Y(\xi)$. The problem is to solve

$$\nabla^2 V + M \frac{\partial B}{\partial \eta} = -1, \tag{23}$$

$$\nabla^2 B + M \frac{\partial V}{\partial \eta} = 0 \tag{24}$$

with $V = 0$ and $\partial B/\partial n + B/\varphi = 0$ at the wall. Let $Z_1 = M(V + B), Z_2 = M(V - B)$. Adding and subtracting (23) and (24) gives

$$\nabla^2 Z_1 + M \frac{\partial Z_1}{\partial \eta} = -M, \tag{25}$$

$$\nabla^2 Z_2 - M \frac{\partial Z_2}{\partial \eta} = -M. \tag{26}$$

Singular perturbation theory, LEVINSON [1], says that at interior points and at points on the upper surface

$$Z_1 = Z_{1i} + O\left(\frac{1}{M^{1/2}}\right),$$

where Z_{1i} is the solution of

$$\frac{\partial Z_{1i}}{\partial \eta} = -1$$

which takes the given boundary values on the upper surface. There is a boundary layer near the lower surface and ends. Specifically, this is true when Z_1 is given on the boundary. In the present problem the value of Z_1 on the boundary is unknown but the above result should still be true, since if the exact solution of (23) and (24) were known the values which Z_1 takes on the boundary could be calculated and the problem formulated as a first boundary value problem. The analysis of Z_2 is similar, with Z_2 tending to the solution $\partial Z_{2i}/\partial \eta = 1$ which assumes the boundary values on the *lower* surface. This reasoning gives asymptotic solutions

$$Z_{1i} = Y(\xi) - \eta + Z_1(\xi, Y(\xi)), \tag{27}$$

$$Z_{2i} = \eta + Y(\xi) + Z_2(\xi_1, -Y(\xi)), \tag{28}$$

where $Z_1(\xi, Y(\xi))$ and $Z_2(\xi, -Y(\xi))$ are the values which the exact solutions of (25) and (26) assume on the boundaries. Since $Z_1 = M(V + B)$, $Z_2 = M(V - B)$ and V is zero on the boundaries, it must be the case that

$$Z_1(\xi, Y(\xi)) = M B(\xi, Y(\xi)), \tag{29}$$

$$Z_2(\xi, -Y(\xi)) = -M B(\xi, -Y(\xi)).$$

But by the symmetry of the boundaries, B is an odd function of η, therefore

$$Z_2(\xi, -Y(\xi)) = M B(\xi, Y(\xi)). \tag{30}$$

Also, the velocity and induced field in the interior tend to

$$V_i = \frac{Z_{1i} + Z_{2i}}{2M} = B(\xi, Y(\xi)) + \frac{Y(\xi)}{M}, \tag{31}$$

$$B_i = \frac{Z_{1i} - Z_{2i}}{2M} = -\frac{\eta}{M}. \tag{32}$$

In order to find $B(\xi, Y(\xi))$ it is necessary to have a relation between quantities across the boundary layer. By integrating $\nabla^2 B + M\,\partial V/\partial \eta = 0$ over a small cylinder which extends through the boundary layer, and using GREEN's third identity, one finds

$$\frac{\partial B}{\partial n} - \frac{\partial B_i}{\partial n} + M(V - V_i)\cos(n, \eta) = 0, \tag{33}$$

where n is the outward normal. This result is equivalent to imposing continuity of tangential components of the electric field across the boundary layer. Now using $V = 0$ and $\partial B/\partial n + B/\varphi = 0$ on the boundaries, it is found that

$$\frac{B}{\varphi} = -\frac{\partial B_i}{\partial n} - M_i \cos(n, \eta) \tag{34}$$

on the boundary. Observe that

$$\frac{\partial B_i}{\partial n} = \frac{\partial B_i}{\partial \xi}\cos(n, \xi) + \frac{\partial B_i}{\partial \eta}\cos(n, \eta) = -M^{-1}\cos(n, \eta) \tag{35}$$

whence

$$\frac{B}{\varphi} = [M^{-1} - (M\, B(\xi, Y(\xi)) + Y(\xi))]\cos(n, \eta) \tag{36}$$

on the boundary.

In particular this is true on the upper surface where $B = B(\xi, Y(\xi))$ and $\cos(n, \eta) = (1 + Y'^2)^{-1/2}$. Substituting these into (36) and solving for $B(\xi, Y(\xi))$ gives

$$B(\xi, Y(\xi)) = \frac{M^{-1} - Y}{M + \varphi^{-1}(1 + Y'^2)^{1/2}}. \tag{37}$$

With (37) and (31), V_i is solved —

$$V_i = \frac{1}{M}\left\{\frac{Y + \varphi(1 + Y'^2)^{-1/2}}{1 + M\varphi(1 + Y'^2)^{-1/2}}\right\}. \tag{38}$$

This checks with (16) for the case $Y = 1$. Note, when the walls are non-conducting ($\varphi = 0$) that $V_i = Y(\xi)/M$ as shown by SHERCLIFF [3]. In this case the velocity distribution has the same shape as the cross-section of the duct. In fact this result is also true for non-symmetrical ducts with non-conducting walls, that is, if the upper surface is $\eta = Y_1(\xi)$ and the lower surface is $\eta = -Y_2(\xi)$ then $V_i = (Y_1(\xi) + Y_2(\xi))/2M$. On the other hand for perfectly conducting walls ($\varphi = \infty$), $V_i = 1/M^2$ which shows the velocity to be uniform in the core. Also, in this case, the dimensional velocity V_z is independent of viscosity – $V_z = -(\partial p/\partial z)/(\sigma B_0^2)$.

For a circular cross-section, $Y = (1 - \xi^2)^{1/2}$, a small calculation shows

$$V_i = \frac{1 + \varphi}{M}\,\frac{(1 - \xi^2)^{1/2}}{1 + M\varphi(1 - \xi^2)^{1/2}}.$$

This differs from SHERCLIFF [4] in the occurence of the factor $1 + \varphi$; SHERCLIFF restricted φ to be small. The volume flow through the circular duct is given by

$$
\begin{aligned}
Q &= \int_{-1}^{1} 2\, Y(\xi)\, V_i(\xi)\, d\xi \\
&= 4 \int_{0}^{1} \frac{1+\varphi}{M} \frac{1-\xi^2}{1+M\varphi\,(1-\xi^2)^{1/2}}\, d\xi \\
&= 4\,\frac{1+\varphi}{M} \int_{0}^{\pi/2} \frac{\cos^3\theta}{1+M\varphi\cos\theta}\, d\theta \\
&= 4\,\frac{1+\varphi}{M}\left[\frac{\pi/4}{M\varphi} - \frac{1}{(M\varphi)^2} + \frac{\pi/2}{(M\varphi)^3} - \frac{1}{(M\varphi)^3}\,\frac{2}{1+M\varphi}\right. \\
&\qquad \left. \times \tan^{-1}\left(\frac{1-M\varphi}{1+M\varphi}\right)^{1/2} \Big/ \left(\frac{1-M\varphi}{1+M\varphi}\right)\right]^{1/2}.
\end{aligned}
\tag{39}
$$

Note that the expression for Q, (39), does *not* have a singularity at $M\varphi = 0$, the inverse powers are absorbed by the last term on the right. In fact when $M\varphi$ is small

$$
Q = 4\,\frac{1+\varphi}{M}\left(\frac{2}{3} - \frac{3\pi}{16}\,M\varphi + \frac{8}{15}\,(M\varphi)^2 + \cdots\right).
$$

In Figure 5 $(Q/\pi)\,[4\,M/(1+\varphi)]$ is plotted versus $M\varphi$. Q/π is the average (dimensionless) velocity. In Figure 6 V_i/V_{av} is plotted versus ξ with $M\varphi$ as parameter. The latter figure shows the effect of wall conductivity on the shape of the

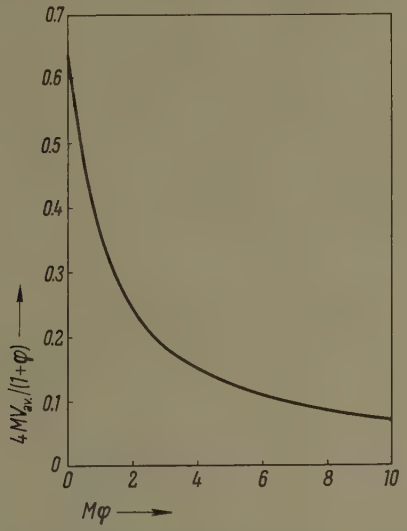

Figure 5

$4\,M\,V_{av}/(1+\varphi)$ versus M for circular duct, large M.

velocity profile for the case of a circular duct. It should be noted in this case that the *shape* depends only on the product $M\varphi$.

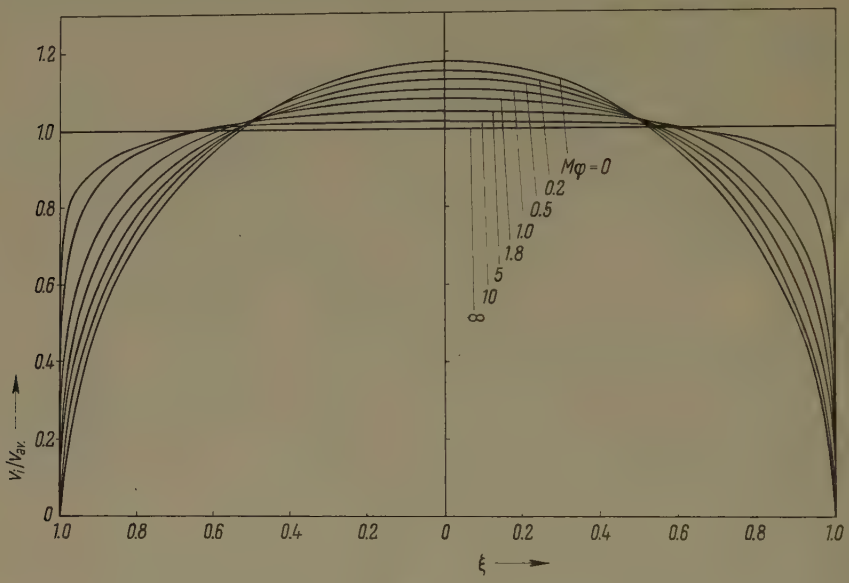

Figure 6
Velocity distribution in a circular duct with $M\varphi$ as parameter.

The Effect of the Free Charge on the Electric Field

In the introduction we stated that the free charge would be neglected in OHM's law and in the momentum equation, but would be retained in (4). We have seen that B_z and V_z can be determined without using (4), therefore $\boldsymbol{E}$ can be determined from OHM's law leaving (4) for the determination of ϱ_e. This is done simply by taking the divergence of (5), with the result

$$\varrho_e = -\varepsilon_0 \operatorname{div} (\boldsymbol{V} \times \boldsymbol{B}) . \tag{40}$$

We shall now check to see that ϱ_e was negligible in (5) and (6) for the class of problems which we have considered. We note that in this case (40) becomes

$$\varrho_e = \varepsilon_0 B_0 \frac{\partial V_z}{\partial x} . \tag{41}$$

For large M it is apparent that ϱ_e will be largest in the boundary layer. To be more specific it will be largest near that part of the boundary which is parallel to the applied magnetic field. SHERCLIFF [3] has shown that the boundary layer has thickness of the order of $a/\sqrt{M}$ on walls parallel to the applied magnetic

field. This allows us to estimate $\partial V_z/\partial x$ by $V_{z\,av}\sqrt{M}/a$ at this point ($V_{z\,av}$ is the average or core velocity) which makes

$$\varrho_e = O\left(\varepsilon_0 B_0 V_{z\,av} \frac{\sqrt{M}}{a}\right). \tag{42}$$

We note that in equations (5) and (6) the terms with ϱ_e will be small compared to $\sigma V \times B$ and $j \times B$ respectively provided the inequality $\varrho_e/\sigma B_0 \ll 1$ is satisfied. With (42) this inequality can be put in the form

$$\frac{V_{z\,av}}{c} \ll \frac{\lambda R_c}{\sqrt{M}}, \tag{43}$$

where c is the speed of light, $\lambda = \mu_0 \sigma \nu$ and $R_c = a c/\nu$ is a 'Reynolds' number based on the speed of light. As an example consider the case of mercury where $\lambda \cong 10^{-7}$, $M = 100$ (the experimental upper limit) and $R_c = O(10^{15})$ (with $a = 1$ cm). In this case (43) becomes $V_{z\,av}/c \ll 10^7$ which is obviously always satisfied.

It should not be concluded from the previous paragraph that the effect of ϱ_e is completely negligible, for it has a dominant effect on the electric field. The free charge in the boundary causes the electric field to make a large increase on passing through this layer. This is best illustrated by a concrete example. Consider a long rectangular duct with non-conducting walls. Except in the boundary layer near the ends the solution is essentially that given by equations (14) and (15), with $\varphi = 0$. Using this solution we can calculate $\boldsymbol{E}$ from equation (5), that is

$$E_x = \frac{1}{\sigma \mu_0} \frac{\partial B_z}{\partial y} + V_z B_0, \tag{44}$$

$$E_y = -\frac{1}{\sigma \mu_0} \frac{\partial B_z}{\partial x}.$$

From (14) and (15) we get

$$E_x = \frac{a}{\sqrt{\nu \varrho \sigma}} \frac{\partial p}{\partial z} \left\{\frac{1}{M} - \frac{1}{\tanh M}\right\}, \tag{45}$$

$$E_y = 0.$$

It is seen that E_x is constant. One might suppose that E_x is constant all the way to the end of the duct, taking a jump through the surface of the wall. This is *not* the case, since for nonconducting walls B_z is zero at the wall, therefore $\partial B_z/\partial y$ is zero on the vertical wall, and equation (44) then shows that $E_x = 0$ on the vertical wall. We conclude that E_x varies from zero at the wall to the value given by (45) as we go through a boundary layer of thickness $a/\sqrt{M}$. This is due to the free charge in this boundary layer. (There is some question as to whether the free charge causes the variation in electric field or whether the variation in electric field causes the free charge.)

Conclusion

In the flow of conducting fluids through ducts, in general, the domain of the equations describing the flow is not the same as the domain of the fluid. It was found that the problem reduced to two sets of equations, one set, (11) and (12), in the fluid, and one set, (13), in the wall, with boundary conditions specified on the outer boundary of the wall and across the inner boundary of the wall. The known special cases (SHERCLIFF [3, 4]) where this problem reduces to an ordinary boundary value problem with boundary conditions given at the boundary of the fluid, follow as limiting cases of the above formulations. These are $\varphi \to 0$, $\varphi \to \infty$ and $h \to 0$.

In the bulk of the paper the flow through rectangular ducts was considered. The essential conclusion is that increasing the wall conductivity tends to decrease the average velocity if the pressure gradient is the same in the two cases. Stated differently, when the wall conductivity is increased, the pressure gradient must be increased in order to maintain the same mass flow.

The flow through arbitrarily shaped symmetrical ducts was considered for large M and arbitrary wall conductivity. It was found that when $\varphi \to \infty$ the velocity tends to be uniform except in a thin boundary layer along the wall.

In the final section the effect of the neglected free charge was considered. We found that free charge tends to accumulate near walls which are parallel to the applied field, but not enough to effect the velocity distribution.

REFERENCES

[1] N. LEVINSON, Ann. Math. *51*, 428 (1950).
[2] J. HARTMANN, 1937, Math.-fys. Medd. *15*, 6 (1937).
[3] J. A. SHERCLIFF, Proc. Camb. phil. Soc. *49*, 136 (1953).
[4] J. A. SHERCLIFF, J. Fluid Mech. *1*, 644 (1956).

Zusammenfassung

In dieser Arbeit wird die Strömung einer elektrisch-leitenden Flüssigkeit durch ein gerades Rohr mit einem gleichförmigen, querlaufenden magnetischen Feld betrachtet. Das Problem wird unter Berücksichtigung des elektromagnetischen Feldes sowohl innerhalb als ausserhalb der Flüssigkeit formuliert. Besondere Aufmerksamkeit wird auf die Ableitung der Randbedingungen gerichtet. Es wird klargemacht, dass, wenn die Wände des Rohres endliche Leitfähigkeit haben, das Problem, abgesehen von Einzelfällen, kein gewöhnliches Randwertproblem darstellt. Eine Lösung wird für die Strömung durch ein rechteckiges Rohr mit unendlich fernen, dem äusseren Feld parallelen Wänden bei beliebiger Wandleitfähigkeit gefunden, ebenso für die Strömung durch ein endliches rechteckiges Rohr mit idealleitenden Wänden. Es gelingt, die asymptotische Geschwindigkeitsverteilung bei grosser Hartmannscher Zahl für ein dünnwandiges symmetrisches Rohr bei beliebiger Wandleitfähigkeit anzugeben.

(Received: June 14, 1960.)

The Influence of Turbulence on the Transfer of Heat to Cylinders near the Stagnation Point

By J. Kestin[1]), P. F. Maeder[1]), and H. H. Sogin[2]), Providence, R. I., USA

1. Introduction

In a previous paper [1][3]) two of the authors have shown that the intensity of turbulence of a free stream exerts an important influence on the rate of heat transfer from a cylinder in cross-flow. The most noteworthy conclusion from that investigation was the realization that the effect was a local one and additional to the expected influence from the effect of free-stream turbulence on transition and separation. In another paper [2] it was shown that this local effect was absent in the case of a flat plate at zero incidence, but that it re-appeared when a favorable pressure gradient was imposed on it. In both cases, the local Nusselt number increased by amounts of the order of 25–50% when the turbulence intensity increased relatively little, say from 0·5 to 2%. A plausible explanation for these effects was given elsewhere [3], it being conjectured that the local Nusselt number increased as a result of the oscillations carried by the free stream; it was, namely, shown that any oscillations accompanied by a pressure gradient must be expected to modify the mean velocity profile of an associated boundary layer. Changes in the velocity profile will, in turn, modify the temperature profile and hence the local Nusselt number.

Although the preceding explanation appears plausible, the details of the mechanism operating under such conditions are far from being clarified and understood. Nevertheless, if the explanation is plausible, one must expect large local increases in the rate of heat transfer in the neighborhood of the forward stagnation point of a cylinder (or any bluff body) in cross-flow when the boundary layer is laminar and where the free-stream velocity gradient is large, and where, therefore, there exists a large downstream gradient in the amplitude of oscillation, as required by the theory advanced in reference [3]. The present paper addresses itself to the experimental verification of this point.

The increase in the local rate of heat transfer from a bluff body which is produced by an increase in the free-stream turbulence intensity has been observed before. Even more, it appears that evidence of this effect can be

[1]) Department of Engineering, Brown University.
[2]) Department of Mechanical Engineering, Tulane University, formerly with Brown University.
[3]) Numbers in brackets denote the References, page 131.

discerned in experimental investigations which were carried out at a time when the importance of the turbulence in the free stream in general had not yet been discovered.

Figure 1 shows a comparison between the classical experiments performed by SCHMIDT and WENNER [4] and the theoretical calculations due to FRÖSSLING [5]. Since the resulting variation of the Nusselt number with the angular co-ordinate φ is fairly sensitive to the assumed variation of free-stream velocity U with the co-ordinate $x = R\varphi$ (φ = radians), the equation given by FRÖSSLING was re-evaluated with the aid of the following series expansion for U, where U_∞ is the velocity of approach, D being the diameter of the cylinder:

$$U = U_\infty \left\{3{\cdot}631 \left(\frac{x}{D}\right) - 3{\cdot}275 \left(\frac{x}{D}\right)^3 - 0{\cdot}168 \left(\frac{x}{D}\right)^5\right\}. \tag{1}$$

The coefficients in equation (1) were given by ECKERT [6] who deduced them from SCHMIDT and WENNER's measurements at a Reynolds number $Re = 170000$. Thus we were led to the expression

$$\frac{Nu}{(Re)^{1/2}} = 0{\cdot}9449 - 0{\cdot}7693 \left(\frac{x}{D}\right)^2 - 0{\cdot}3009 \left(\frac{x}{D}\right)^4, \quad (Pr = 0{\cdot}7) \tag{2}$$

in which the Reynolds and Nusselt numbers are referred to the diameter D. The group $Nu/Re^{1/2}$ is very convenient for presenting experimental results, because it is independent of Reynolds number and is a unique function of the angular coordinate φ for a given Prandtl number, Pr, as long as the coefficients in the expansion in equation (1) have been chosen properly.

The diagram presents three series of results, each for a different diameter D but for similar ranges of velocities U_∞. Hence the ranges of Reynolds numbers are also different. For the sake of simplicity, the same theoretical curve, equation (2) is shown in all three graphs, but strictly speaking, the power-expansion in equation (1) most closely corresponds to the diagram in Figure 1c. In any case its accuracy becomes questionable at $\varphi = 60°$.

From the nature of the theoretical calculation which neglects free-stream oscillations, it is clear that it refers to a stream with zero intensity of turbulence, i. e. to a laminar stream. The diagrams show that all measured points indicate a higher rate of heat transfer for the range of the angular coordinate ($0 < \varphi < 60°$) where the boundary layer is expected to be laminar, as compared with the theoretical curve. The fact that all points lie above the theoretical curve suggests that the deviations are not due to random experimental errors. Furthermore, at the highest Reynolds numbers (Re = 52800, 170000, 426000 respectively) the Nusselt numbers at the stagnation point exceed the calculated value by 7%, 13% and 16% approximately which is considerably larger than the 5% margin of error of the determination. This suggests that the deviations are systematic and increase as the Reynolds number is increased. In actual

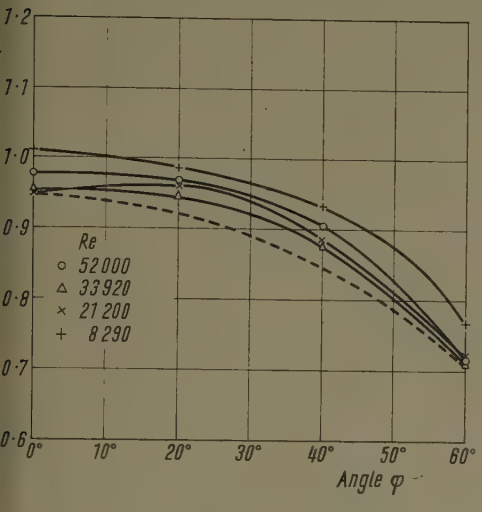

a

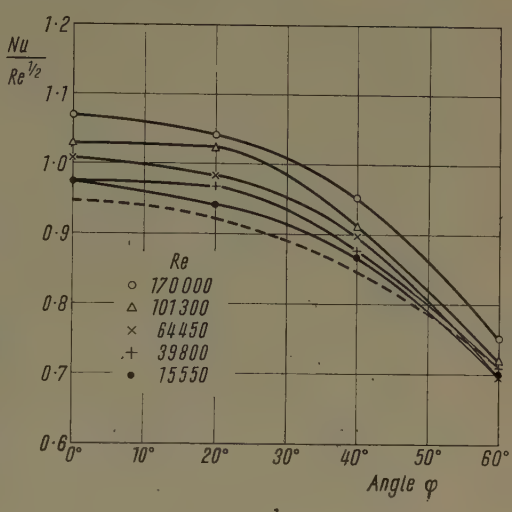

b

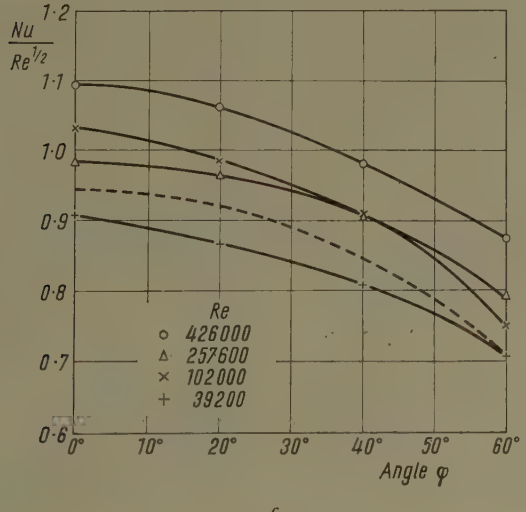

c

Figure 1

Local rate of heat transfer from forward portion of a cylinder. Comparison between experiments due to Schmidt and Wenner [4] and calculations due to Froessling [5], $Pr = 0{\cdot}7$, free-stream velocity from equation (1).

a $8290 < Re < 52800$, $D = 5$ cm.
b $15550 < Re < 170000$, $D = 10$ cm.
c $39200 < Re < 426000$, $D = 25$ cm.

fact, as was shown in reference [1], it is highly probable that the free stream available to SCHMIDT and WENNER was one of relatively low turbulence intensity (of order 0·9%), but also one in which the intensity of turbulence increased with the velocity, and hence with the Reynolds number. Thus the apparent increase in Nusselt number with the Reynolds number can possibly by interpreted as an increase with increasing intensity of turbulence.

If this hypothesis is correct, then the curves for a given velocity, and hence for a given intensity of turbulence, should most nearly coincide, the only difference being now due to the different pressure distributions, as expressed by $U(x)$ and associated with different cylinder diameters.

The results for the two groups of Reynolds numbers, 52800 in Figure 1*a*, 101300 in Figure 1*b*, and 257600 in Figure 1*c* satisfy this condition reasonably closely. The two sets of results have been replotted in Figure 2 whose appearance confirms our guess, in so far as the general spread in the values has now decreased.

Figure 3 shows a comparison between the measurements performed by five groups of investigators [4] and [7–10] all at about the same Reynolds number of $Re = 39600$. For illustrative purposes, FRÖSSLING's curve from equation (2) has also been drawn. Once again all measured values exceed the calculated ones and the excess at the stagnation point reaches an order of magnitude of 60–70%. It is unlikely that so many experimental investigations

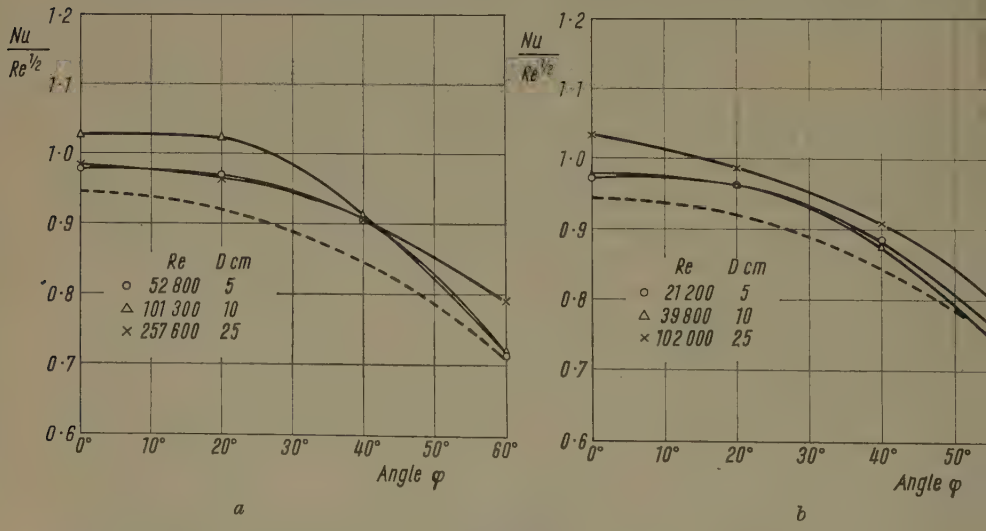

Figure 2

Verification for two sets of three Reynolds numbers which correspond to approximately equal velocities (and turbulence intensities). Replot from Figure 1.

a $Re = 52800$, $D = 5$ cm; $Re = 101300$, $D = 10$ cm; $Re = 257600$, $D = 25$ cm;
b $Re = 21200$, $D = 5$ cm; $Re = 39800$, $D = 10$ cm; $Re = 102000$, $D = 25$ cm.

could show such large errors, all of them positive, and it is probable that they are due to systematic differences in the recorded intensities of turbulence in the various streams.

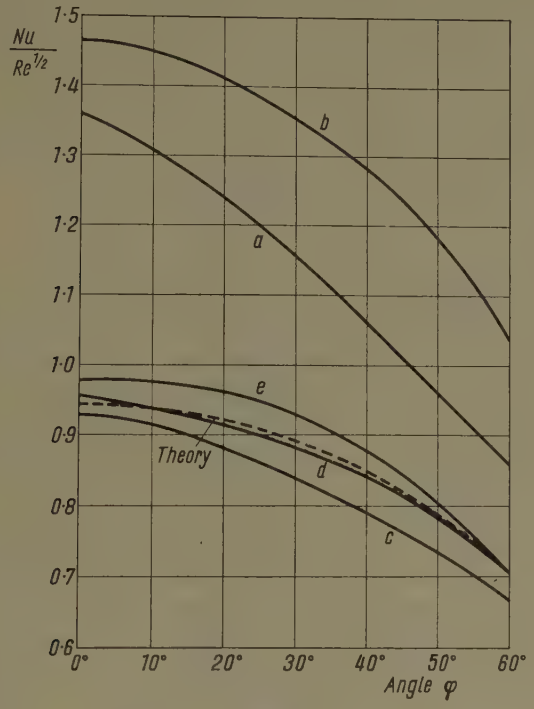

Figure 3

Variation of local Nusselt number with angular co-ordinate for cylinder in cross-flow at $Re = 39\,600$ (or a value close to it). Measurements by five groups of investigators, theory by Frössling [5].
a Krujilin [7], $Re = 39\,500$, *d* Klein [10], $Re = 39\,600$,
b Small [8], $Re = 39\,600$, *e* Schmidt and Wenner [4], $Re = 39\,800$.
c Drew and Ryan [9], $Re = 39\,600$,

2. Scope of the Investigation

During the present experimental investigation, measurements were made of the local coefficient of heat transfer from a vertical cylinder placed in a wind tunnel. The measurements were made at varying velocities and with intensities of turbulence which were increased by placing suitable screens upstream of the model. Hence the two parameters, the Reynolds number Re, and the intensity of turbulence, Tu, were varied nearly independently. A completely independent adjustment proved to be impossible because the intensity of turbulence produced by a given screen turned out to be a function of air speed [1]. Finally, measurements were made over the full range of angular positions φ, from 0°

to 180°, but owing to the complexity of the results, and the difficulties in their interpretation, the present paper will discuss exclusively the case of the laminar boundary layer, say up to $\varphi = 60°$.

The measurements covered a range of Reynolds numbers

$$120 \times 10^3 < Re = \frac{U_\infty D}{\nu} < 290 \times 10^3$$

and a range of turbulence intensities (based on the longitudinal fluctuation u')

$$0{\cdot}5\% < Tu = \frac{(\overline{u'^2})^{1/2}}{U_\infty} < 2{\cdot}7\% .$$

3. Description of Experimental Arrangement

The model used in the present investigation consisted of a 4·21″ *OD* brass tube provided with a 1/2″ × 10″ strip heater, similar to that used by SCHMIDT and WENNER [4]. The tube was placed vertically in the 20″ × 32″ Brown University low-speed tunnel, [1], and could be rotated about its vertical axis. The angle of turn was set with the aid of two indexing plates accommodated outside the tunnel test-section.

The design of the tube is depicted in Figure 4 which contains two cross-sections and a view of the model. The heat transfer tube B was placed in a slot in the brass tube A, and consisted of a specially wound, sheathed nichrome spiral C cast into a copper slab. The copper slab was enclosed in a housing D milled out of a solid brass bar. The housing insulated the element from the interior of tube A, and a brass pipe E provided an outlet for the heater leads, as well as for several thermocouples. A micarta slab F connected the heat transfer element to the housing, insulating it thermally. The thin gap C between the tube wall and heater slab was filled with a plastic, heat resistant paint. The housing D together with the element B were joined to tube A with screws, and the whole assembly was turned to size and polished in a lathe. Upon heating, the heater element had a tendency to protrude somewhat, but the resulting unevenness was less than 0·001″.

The interior of tube A was supplied with saturated steam from a small electrical boiler, and the heater C was supplied with DC current of a highly stabilized voltage. During an experiment, the current supplied to the heat transfer element was so adjusted as to keep its surface temperature substantially equal to the surface temperature of the tube. At low speeds the maximum difference in temperature did not exceed 0·5°C rising to 2°C at the highest wind speeds. In this manner, nearly all the Joule heat evolved in the electric heater was forced to leave through the exposed surface of the heat transfer element, and was inhibited from leaking out sideways by the small temperature difference coupled to a high thermal resistance. Sample calculations showed

that possible leaks did not exceed 5% of the quantity measured. Since no greater accuracy was intended, no correction for heat leaks was applied to the final result. Thus, in contrast with most other investigations [7, 11, 12, 13], the measurement of the rate of heat transfer was direct. Strictly speaking, the measurement extended over a width of 1/2″ (14·5° of angle), and thus contri-

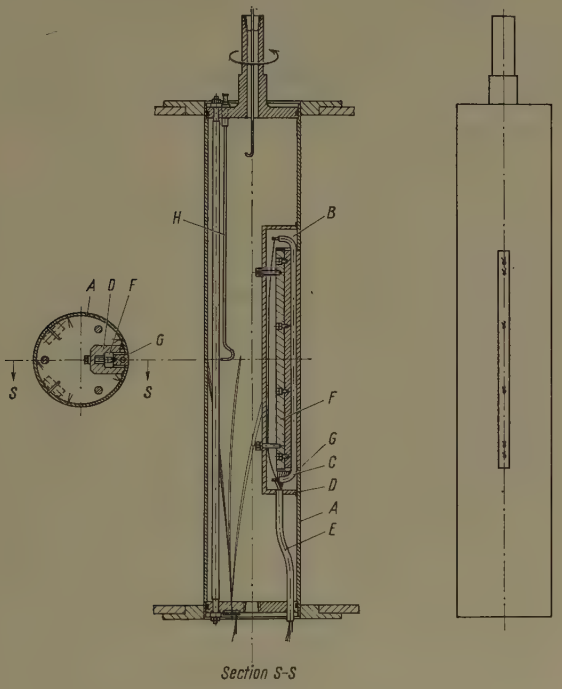

Figure 4
The experimental tube.

buted a mean measurement over a fraction of the circumference. It can be easily shown that for the measured variation of Nusselt number with angular coordinate (convex upwards), this averaging tended to underestimate the rate of heat transfer.

The electrical input was measured with the aid of a sensitive potentiometer, as described in reference [1]. The temperatures were measured with the aid of copper-constantan surface thermocouples whose location is shown in Figure 4. The wires were led out of the assembly through a tube shown in the drawing. In addition, provision was made by two radiation-shielded thermocouples, one inside cylinder A to measure the steam temperature, and one in the settling chamber of the wind tunnel to measure the air temperature. All temperatures were measured differentially with respect to the steam junction, and the EMF's

were recorded on a Brown potentiometer-recorder using a scale of 1 mV to 25 cm. In all, temperatures were measured with an accuracy of 0·15°C.

The tube was provided with two static-pressure probes H, Figure 4, placed symmetrically with respect to the center plane of the heater; they were used to position the tube with respect to the wind.

All remaining details and procedures, including those for the evaluation of the results were identical with the ones described in reference [1] and need not be repeated here, except for re-stating that the Nusselt and Reynolds numbers were evaluated with thermal properties averaged integrally over the boundary layer thickness, as in reference [4].

4. Experimental Results

The experimental results cover measurements in three distinct, non-overlapping ranges of turbulence intensity. The ranges were obtained in the free tunnel and by putting two, different, turbulence-producing screens, 12 inches upstream of the model. As already mentioned, neither in the free tunnel, nor in the presence of the screens, did the turbulence intensity remain constant over the range of wind velocities available in the tunnel and it was necessary to calibrate the turbulence intensity in terms of air velocity. The calibration curves, reproduced from reference [1], are shown in Figure 5 for easy access. The resulting ranges of parameters covered in the three runs are shown summarized in Table 1. It will be noticed that the runs were arranged to avoid overlapping in turbulence intensity so that at any Reynolds number a point in run 1 had the lowest, a point in run 2 had an intermediate, and a point in run 3 had the highest intensity of turbulence.

Table 1
Ranges of parameters covered

Series	Screen			Range of turbulence intensity, Tu	Range of Reynolds numbers, Re
	Designation	Mesh	Wire diameter		
Run 1 Low Intensity	None	None	None	1·0 to 0·5	132×10^3 to 290×10^3
Run 2 Intermediate Intensity	No. 2	$1/2''$	0·062″	1·9 to 1·5	130×10^3 to 260×10^3
Run 3 High Intensity. . . .	No. 1	$3/4''$	0·148″	2·1 to 2·7	120×10^3 to 220×10^3

In carrying out the experimental program, it was found impracticable to adjust the tunnel to a given speed and to make measurements over the whole

range of angular positions. Instead, the heater was turned to a given position, and measurements were performed over a range of Reynolds numbers. In all cases, measurements were made at two symmetrical positions, denoted by $+\varphi$ and $-\varphi$ respectively, and averaged graphically. Owing to the tunnel characteristic, a certain lack of symmetry was unavoidable.

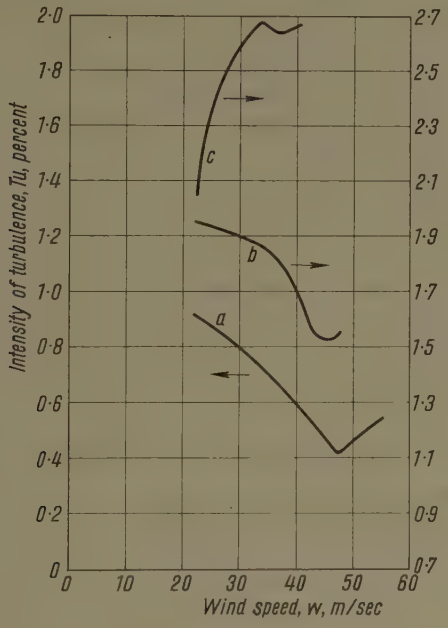

Figure 5

Turbulence intensity in terms of air velocity from reference [1].
a) Low intensity, no screen.
b) Intermediate intensity, screen No. 2 at 12″.
c) High intensity, screen No. 1 at 12″.

The direct experimental results are seen plotted in Figure 6. They are plotted in the form of a diagram of the group $Nu/Re^{1/2}$ because for a given Prandtl number, this ratio is a unique function of the angular coordinate φ at $Tu = 0$, as already stated earlier. It is, however, necessary to remember that equation (2) remains valid only for a given pressure distribution near the stagnation line. Hence the variation of $Nu/Re^{1/2}$ with Reynolds number may be due to two causes. First, as the Reynolds number varies, the pressure distribution may vary somewhat, causing a variation in $Nu/Re^{1/2}$; it is supposed that this is a small variation. Secondly, as the Reynolds number varies, the turbulence intensity varies, and affects the value of $Nu/Re^{1/2}$; it is supposed that this constitutes the major effect.

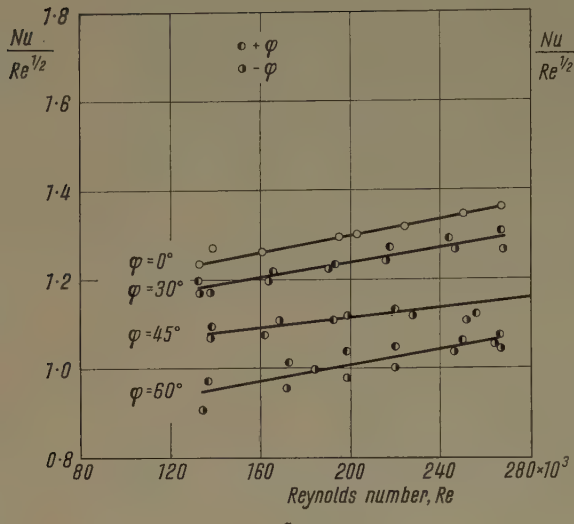

a

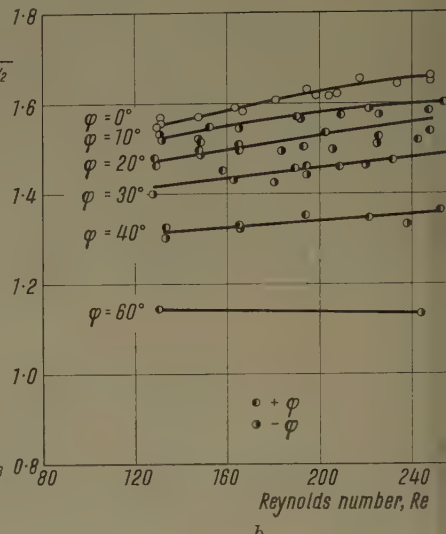

b

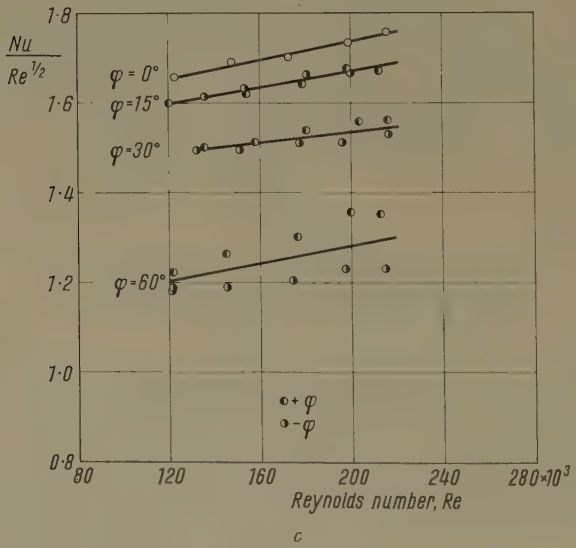

c

Figure 6

Experimental results plotted as the ratio $Nu/Re^{1/2}$ *versus* the Reynolds number Re, at different angular positions $\pm\varphi$.

a Run 1, lowest turbulence intensity,

b Run 2, intermediate turbulence intensity,

c Run 3, highest turbulence intensity.

An idea about the effect of different pressure distributions can be formed with reference to Figure 7 which contains plots of the variation of the heat transfer parameter $Nu/Re^{1/2}$ with the angular coordinate φ for two pressure

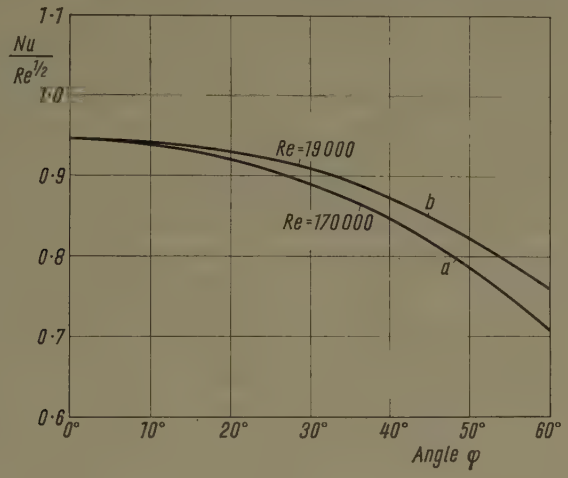

Figure 7

Effect of pressure distribution on heat transfer parameter $Nu/Re^{1/2}$
a $Re = 170000$, equation (2), *b* $Re = 19000$, equation (3).

distributions. The lower curve is a plot of equation (2) which corresponds to the pressure distribution implied in equation (1) and obtained experimentally at a Reynolds number of $Re = 170000$. The upper curve corresponds to FRÖSSLING's [5] explicit equation

$$\frac{Nu}{Re^{1/2}} = \left\{0{\cdot}9449 - 0{\cdot}5100\left(\frac{x}{D}\right)^2 - 0{\cdot}5956\left(\frac{x}{D}\right)^4\right\}, \quad (Pr = 0{\cdot}7) \qquad (3)$$

obtained from the pressure distribution measured by HIEMENZ [4] at a Reynolds number $Re = 19000$ and corresponding to the velocity distribution

$$U = U_\infty\left\{3{\cdot}6314\left(\frac{x}{D}\right) - 2{\cdot}1709\left(\frac{x}{D}\right)^3 - 1{\cdot}5144\left(\frac{x}{D}\right)^5\right\}. \qquad (4)$$

It is seen that the two results agree very closely near the stagnation point, diverging as the angular coordinate φ increases. The discrepancy reaches a value of 6·5% at $\varphi = 60°$ which means that the preceding argument ceases to be valid there.

The two Reynolds numbers of 19000 and 170000 extend over a sufficiently large range to make it certain that in the range of Reynolds numbers covered in the present investigation, the possible discrepancies from this source would be smaller than those suggested by the diagram in Figure 7.

In order to exhibit the local effect of turbulence intensity, it is best to proceed by cross-plotting the results from Figure 6 for several Reynolds numbers. At a constant Reynolds number, and for a given screen configuration, the intensity of turbulence is constant. Since the difference between the three runs consists only in the insertion of a screen ahead of the model for runs 2 and 3, the pressure distribution will remain virtually unaffected near the stagnation region, as confirmed by a subsequent investigation [14]. If there were no local influence from turbulence intensity, all such cross-plots should arrange themselves around the theoretical curve, equation (2), in a band corresponding to the accuracy of the measurement. In the contrary case, they should form a distinct family of curves, with the intensity of turbulence as a parameter. Three such crossplots are shown in Figure 8. The intensity of turbulence corresponding to each point plotted was obtained with reference to the calibration curves given in Figure 5. The theoretical curve from equation (2) has been drawn in for comparison; it corresponds to $Tu = 0$.

The diagrams unmistakably demonstrate the local effect of turbulence intensity on the rate of heat transfer and hence on the characteristics of the associated laminar boundary layer. The effect is unexpectedly large, reaching a value of 80% at the stagnation point for a change of turbulence intensity from 0% (calculated) to less than 3% (measured).

The same results are seen plotted in an alternative way in Figure 9 in which the group $Nu/Re^{1/2}$ has been plotted against Reynolds number for different values of the angular co-ordinate φ. The important feature to be noticed in this diagram is the fact that, once more, the experimental points do not group themselves around the theoretical constant values shown in broken lines. It will be remembered that along each curve the turbulence intensity, and possibly the pressure distribution, vary somewhat with Reynolds number. However, owing to the fact that the three ranges of turbulence intensity do not overlap, the local effect on the rate of heat transfer exerted by turbulence intensity all along the laminar boundary layer is apparent. At one given Reynolds number, particularly near the stagnation point, the pressure distribution is insensitive to turbulence intensity, and the diagram clearly demonstrates that the heat transfer parameter $Nu/Re^{1/2}$ increases from run to run, as the turbulence intensity is increased.

In order to gain an insight into the effect of turbulence intensity, it is convenient to cross-plot the experimental results from Figure 6 in yet another form. The diagram in Figure 10 shows the variation of the ratio $Nu/Re^{1/2}$ at a given intensity of turbulence to that at zero intensity, denoted $(Nu/Re^{1/2})_0$, at different angular co-ordinates φ and for different Reynolds numbers. It is seen that the effect is larger at lower intensities of turbulence and nearer the stagnation point and that it depends to some extent on the Reynolds number. Hence it may be concluded that a given increase in the turbulence intensity

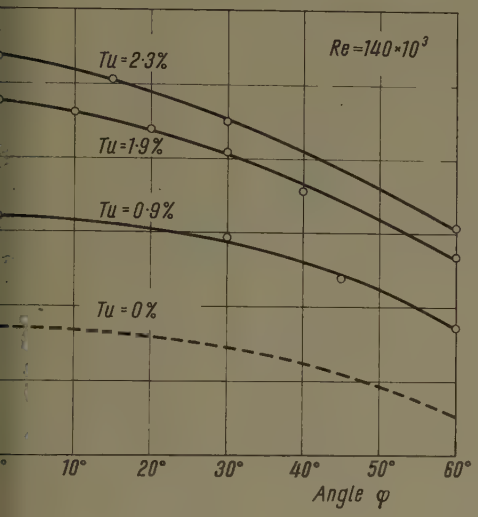

a

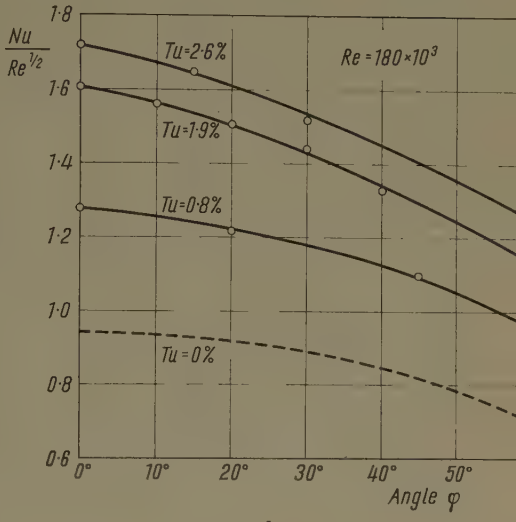

b

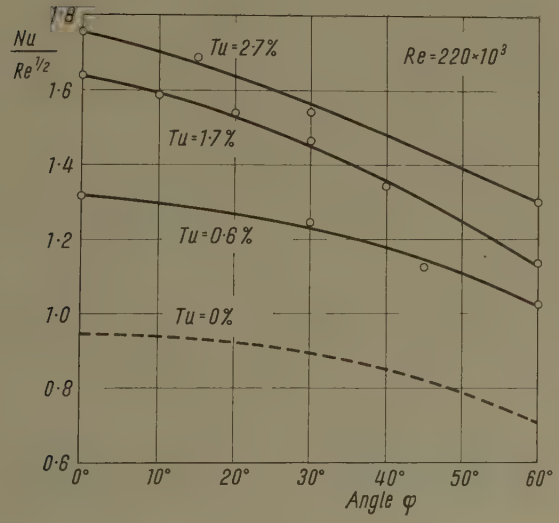

c

Figure 8

Variation of local Nusselt number on a circular cylinder with turbulence intensity Tu and angular co-ordinate φ. Crossplot from Figure 6.

a $Re = 140 \times 10^3$, *b* $Re = 180 \times 10^3$, *c* $Re = 220 \times 10^3$;
– – – – – theory after FROESSLING [5], equation (2).

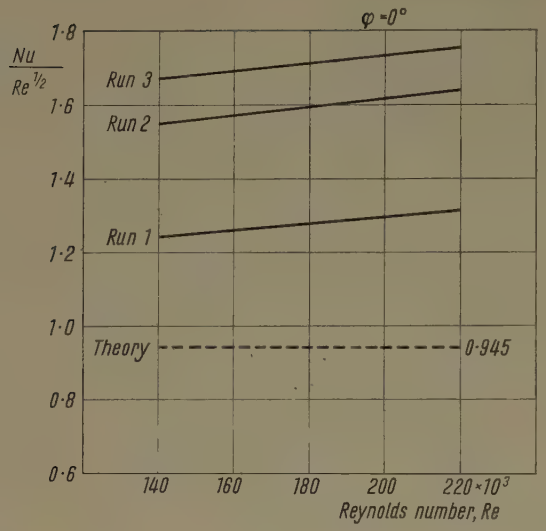

a

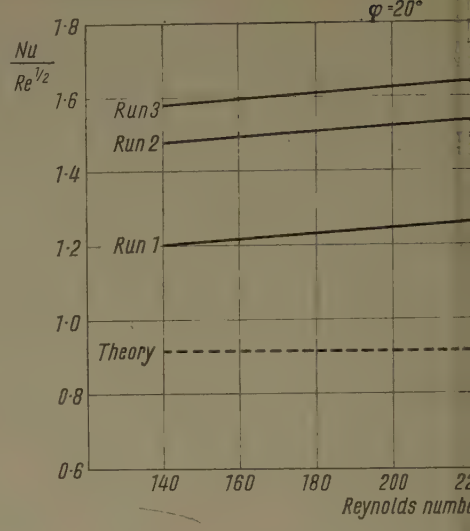

b

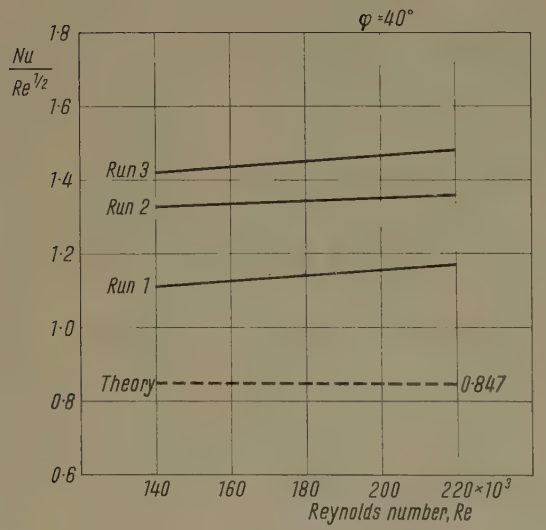

c

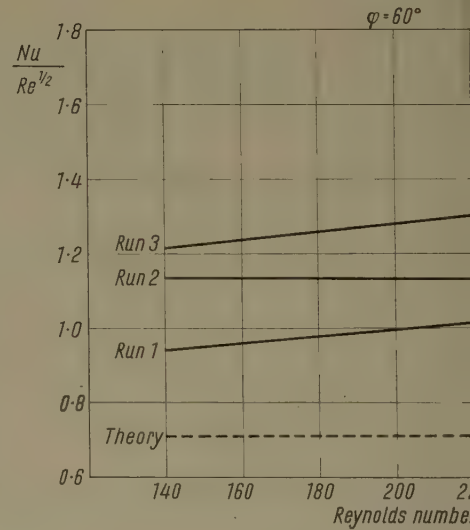

d

Figure 9

Variation of local Nusselt number on a circular cylinder with turbulence intensity Tu and angular co-ordinate φ. Crossplot from Figure 8. Runs 1, 2, 3 correspond to non-overlapping bands of increasing turbulence intensity.

a $\varphi = 0°$, *b* $\varphi = 20°$, *c* $\varphi = 40°$, *d* $\varphi = 60°$,
– – – – – theoretical value after FROESSLING [5], equation (2).

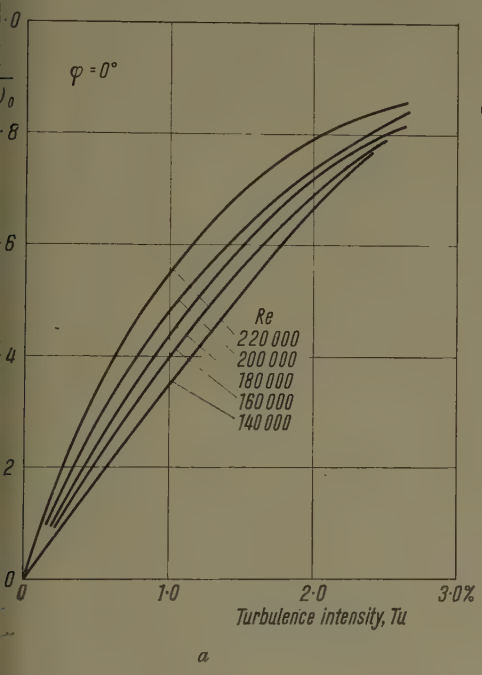

a

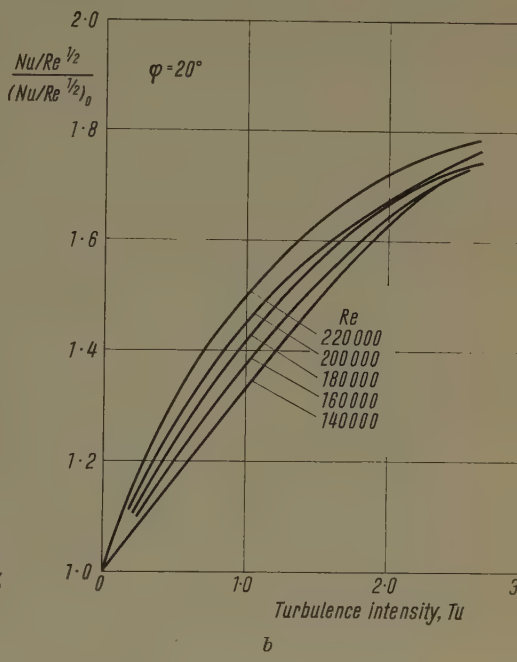

b

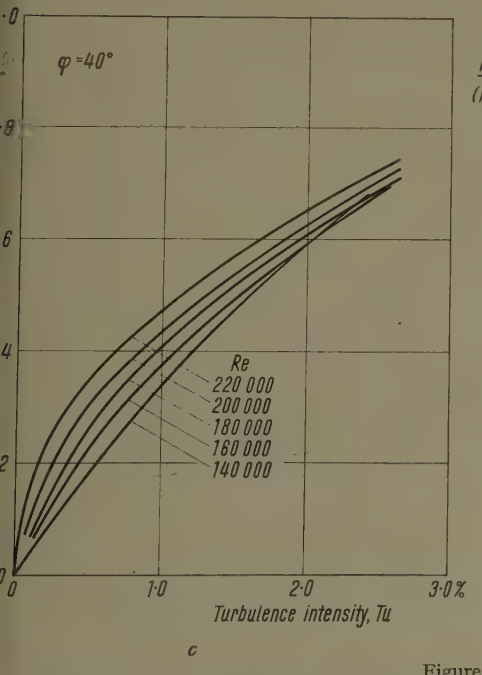

c

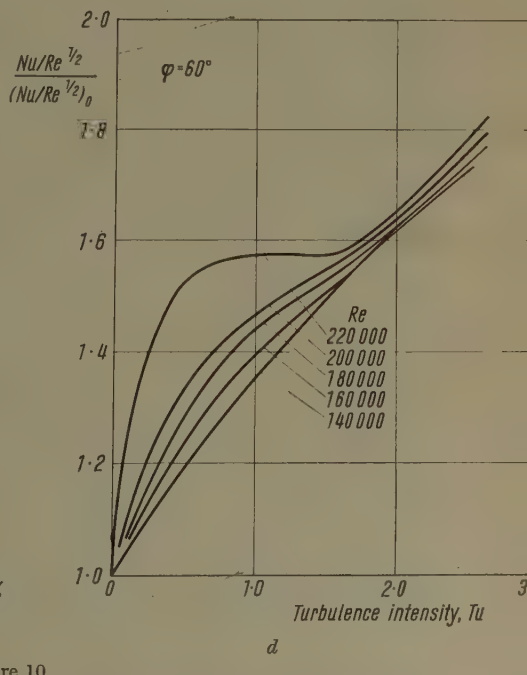

d

Figure 10

Variation of the ratio $(Nu/Re^{1/2})/(Nu/Re^{1/2})_0$ of the heat transfer parameter at given intensity of turbulence to that at zero intensity of turbulence with turbulence intensity Tu at different angular coordinates φ and different Reynolds numbers Re. $(Nu/Re^{1/2})_0$ denotes the theoretical value of the ratio at given angular coordinate φ from equation (2) i. e. for $Tu = 0$.

a $\varphi = 0°$, *b* $\varphi = 20°$, *c* $\varphi = 40°$, *d* $\varphi = 60°$.

produces a larger increase in the Nusselt number in regions where the gradient of free-stream velocity is larger.

5. Concluding Remarks

The preceding, preliminary investigation demonstrates clearly the existence of a local effect from turbulence intensity on the Nusselt number across a laminar boundary layer with a favorable pressure gradient imposed on it. The effect appears to be largest at low intensity of turbulence and at points associated with the largest gradients of free-stream velocity.

The present measurements are not considered to have been of a sufficiently high precision in order to permit us to supply definite, quantitative measures for this effect, but the magnitude of the effect was sufficiently large to justify the preceding qualitative conclusions.

The preceding discussion, admittedly, constitutes a somewhat simplified interpretation of the experimental results. This is due to the fact that the changes in the structure of the free stream were not investigated in detail in the distance between the entrance section and the model. It is well-known that the oscillations carried by a free stream are amplified along streamlines, the largest amplification occurring along the stagnation streamline. It is, therefore, clear that the modification in the velocity profiles in the laminar boundary layer caused by oscillations will be governed by their amplitude outside the boundary layer, and not by those in the free tunnel. However, the detailed mechanism of amplification is not known, and one can only surmise that the increase in the heat transfer parameter $Nu/Re^{1/2}$ with Reynolds number evident in Figures 6 and 8, even for the clear tunnel and for screen No. 2 for which the intensity of turbulence decreases with Reynolds number, is a consequence of this phenomenon. It is clear that a complete explanation cannot be obtained other than by further detailed measurements.

It is pertinent to remark here that in a subsequent investigation on the effect of turbulence intensity on mass transfer from a cylinder in cross-flow, by H. H. SOGIN, V. SUBRAMANIAN and R. J. SOGIN [14] confirmed the preceding qualitative results. Quantitatively they found that the rate of mass transfer at a turbulence intensity of the order of $Tu = 1{\cdot}0\%$ agreed quite well with the theoretical values showing a much smaller effect in the range 0–1%. By a suitable choice of average values of the transport properties, namely by forming the Reynolds and Nusselt numbers with values of viscosity and conductivity corrrsponding to the mean boundary layer temperature, and by inserting the free-stream density into the Reynolds number, it is possible to bring the values of the heat transfer parameter $Nu/Re^{1/2}$ for the clear tunnel to good agreement with equation (2). The essential point, however, is that a further increase in turbulence intensity causes large further increases in the Nusselt

number. Hence it may be concluded that the particular manner in which the properties μ, k and ϱ are averaged, has no bearing on the qualitative conclusions advanced in this paper.

6. Acknowledgements

The authors wish to acknowledge the financial support received from the then National Advisory Committee for Aeronautict (now the National Space and Aeronautics Administration) which made the present investigation possible. The authors were aided in their work by Mr. E. SCHAFRANIK, Research Associate at Brown University who designed the model, and by Dr. H. E. WANG, then Research Assistant at Brown University, who helped to perform the experiments and the calculations.

REFERENCES

[1] J. KESTIN and P. F. MAEDER, *Influence of Turbulence on the Transfer of Heat from Cylinders*, NACA TN 4018 (1957).

[2] J. KESTIN, P. F. MAEDER, and H. E. WANG, *Influence of Turbulence on the Transfer of Heat from Plates with and without a Pressure Gradient*, to be presented at 2nd. Intern. Heat Transfer Conference.

[3] J. KESTIN, P. F. MAEDER, and H. E. WANG, *On Boundary Layers Associated with Oscillating Streams*, Appl. Sci. Res. A *10*, 1 (1961).

[4] E. SCHMIDT and K. WENNER, *Wärmeabgabe über Umfang eines angeblasenen geheizten Zylinders*, Forschung *12*, 65 (1941).

[5] N. FROESSLING, *Verdunstung, Wärmeübertragung und Geschwindigkeitsverteilung bei zweidimensionaler und rotationssymmetrischer Grenzschichtströmung*, Lunds Univ. Årsskrift. N. F. 2, *36*, Nr. 4 (1940).

[6] E. R. G. ECKERT, *Die Berechnung des Wärmeüberganges in der laminaren Grenzschicht umströmter Körper*, Forschungsh. 416B (1942).

[7] G. KROUJILIN, *The Heat Transfer of a Circular Cylinder in a Transverse Airflow in the Range of Re = 6000–425,000*, Techn. Phys. USSR *5*, 289 (1938).

[8] J. SMALL, *The Temperature Field in an Air Current Flowing across a Hot Cylinder*, Phil. Mag. 7, *19*, 21 (1935); *The Average and Local Rates of Heat Transfer from the Surface of a Hot Cylinder in a Transverse Stream of Fluid*, Phil. Mag. 7, *19*, 251 (1935).

[9] T. B. DREW and W. P. RYAN, *The Mechanism of Heat Transmission: Distribution of Heat Flow about the Circumference of a Pipe in a Stream of Fluid – I.* Trans. Am. Inst. Chem. Eng. *26*, 118 (1931).

[10] V. KLEIN, *Bestimmung der örtlichen Wärmeübergangszahl an Rohren im Kreuzstrom durch Abschmelzversuche*, Arch. Wärmewirtsch. *15*, 150 (1934).

[11] W. H. GIEDT, *Investigation of Variation of Point Unit Heat Transfer Coefficient around a Cylinder Normal to an Air Stream*, Trans. ASME *71*, 375 (1949).

[12] W. H. GIEDT, *Effect of Turbulence Level of Incident Air Stream on Local Heat Transfer and Skin Friction on a Cylinder*, J. Aero. Sci. *18*, 725 (1951).

[13] R. SEBAN, *The Influence of Free Stream Turbulence on the Local Heat Transfer from Cylinders*, Trans. ASME Pt. C. (J. Heat Transfer) *82*, 101 (1960).

[14] H. H. SOGIN, V. S. SUBRAMANIAN, and R. J. SOGIN, *Heat Transfer from Surfaces of Non-Uniform Temperature Distribution*. Final report, Part. I: *Local Rates of Mass Transfer from Cylinders in Cross-Flow*, AFOSR Tech. Rep. 60–78 (May, 1960).

Zusammenfassung

Es wird das Problem des Einflusses der Turbulenz auf den Wärmeübergang an einem quer angeströmten Zylinder untersucht. Die Untersuchung beschränkt sich auf den Teil des Umfangs, über den sich die laminare Grenzschicht erstreckt. Einige ältere Messungen an der Vorderseite eines Zylinders werden miteinander verglichen, und es zeigt sich, dass ein wichtiger Parameter, nämlich die Intensität der Vorturbulenz bei den Untersuchungen nicht berücksichtigt worden ist. Die bekannten Messungen von Schmidt und Wenner werden kritisch untersucht und der genannte Effekt wird an ihnen aufgezeigt.

Weiter werden eigene Messungen der lokalen Nusseltschen Zahl beschrieben. Die Messungen waren durchgeführt worden an der Vorderseite eines einzelnen Zylinders im Querstrom, und zwar in drei sich nicht überdeckenden Gebieten der Intensität der Vorturbulenz. Die Versuchsanordnung wird beschrieben und mögliche Einflüsse der Veränderung der Druckverteilung am Zylinder werden diskutiert. Obwohl dieser letztere Effekt nicht völlig eliminiert worden war, zeigen die Versuche doch klar, dass steigende Turbulenz ein starkes Anwachsen der lokalen Nusselt-Zahl bedingt. Dieses Anwachsen ist bei kleiner Turbulenz besonders stark. Ein Vergleich mit der theoretischen Lösung Froesslings, die für Turbulenz 0 gilt, zeigt, dass die Turbulenz den Wärmeübergang in der Staulinie bis zu 80% erhöhen kann, bei einer Turbulenzvariation von 0–3%.

Diese Ergebnisse, die qualitativ interpretiert werden, stützen die Hypothese einer früheren Veröffentlichung, die annimmt, dass der Effekt durch Änderungen der laminaren Grenzschicht, die hervorgerufen werden durch Schwankungen von zunehmender Amplitude, wie sie bei zunehmenden Vorturbulenzen auftreten, bedingt ist.

(Received: September 22, 1960.)

Biharmonic Solutions to the Steady-State Thermoelastic Problems in Three Dimensions

By JERZY NOWINSKI, Madison, Wis., USA[1])

(An abstract of this paper has been presented on the International Conference on Partial Differential Equations and Continuum Mechanics in Madison, June 1960).

1. Introduction

Because of a rising interest in thermal problems, much recent literature has dealt with the complex question of thermoelastic fields in three dimensions. Thus, confining ourselves to the case of a steady state of temperature in an

[1]) Army Mathematics Research Center, University of Wisconsin.

isotropic body, we may cite the representative work by MINDLIN and CHENG [1][2]), STERNBERG and MCDOWELL [2], SNEDDON and LOCKET [3], and MCDOWELL and STERNBERG [4]. The first three papers treat the semi-infinite body[3]), while the last concerns a thick spherical shell in an axisymmetric temperature field[4]).

The diversity of methods used in these papers, even for related problems[5]), suggests that it would be expedient to look for still another method having a somewhat broader applicability. One such method already has been introduced in ordinary (isothermal) three-dimensional elasticity and is due apparently to KELVIN [8][6]), and ALMANSI [10]. It has been used extensively by TREFFTZ [11]. The method corresponds, to some extent, to the method of KOLOSOV-MUSKHELISHVILI, based on the Goursat representation of plane biharmonic functions, which has proved to be so effective in deducing explicit solutions to many important problems in two dimensions.

In what follows we deal with the application of the Kelvin-Almansi method to thermoelastic problems in three dimensions concerning infinite, semi-infinite and spherical regions. To make the paper self-contained we first briefly explain the basic equations, for future reference.

2. Basic Equations

Consider an isotropic homogeneous elastic medium occupying a region of space D with the boundary B. Let the body be in static equilibrium subject to a steady-state temperature field $T(P)$, P being a point in $D + B$ and T being measured above a uniform temperature in which the body remains unstrained. With no loss in generality, we may assume that surface tractions and body forces are absent, since by virtue of the linearity of the problem, postulated in the following, the influence of an external load can be determined by solving an ordinary elastic problem[7]).

Within the classical theory of elasticity, the pure thermoelastic problem (in the aforementioned sense) is governed by the linear strain-displacement

---

[2]) Numbers in brackets refer to References, page 148.

[3]) In the paper [3] the case of an infinite thick plate is also solved. Apparently, this case was previously solved by LURIE [6], page 193, using thermoelastic potential, and SHARMA [7] using Fourier integral representation.

[4]) The limiting cases being a solid sphere and an infinite medium with a spherical cavity.

[5]) In [1], an arbitrary distribution of temperature is treated by an extended scheme of GOODIER [5]; in [2] a steady-state heat flow is approached by the method of GREEN; and in [3] double Fourier transforms are used. In the paper [4] the method of thermoelastic displacement potential is employed.

[6]) See in this connection the book by SOKOLNIKOFF [9], p. 335 and 351.

[7]) It is implied that the temperature increase $T(P)$ does not effect the value of the elastic moduli and the coefficient of thermal expansion. In the last case the third term in the Duhamel-Neumann equations of state (2) takes the form $\frac{(1+\nu)}{(1-2\nu)} \int_0^T \alpha(\vartheta)\, d\vartheta$.

and stress-strain relations together with the homogeneous equations of equilibrium. With reference to a rectangular cartesian coordinate system x_i ($i = 1, 2, 3$) and in index notation, these conditions provide the following field equations:

$$2\,e_{ij} = u_{i,j} + u_{j,i}\,, \tag{1}$$

$$\tau_{ij} = 2\,\mu\left[e_{ij} + \left(\frac{\nu}{1-2\,\nu}\,e_{kk} - \frac{1+\nu}{1-2\,\nu}\,\alpha\,T\right)\delta_{ij}\right], \tag{2}$$

$$\tau_{ij,j} = 0\,, \tag{3}$$

where the usual conventions of summation (by repeating indices) and differentiation (by means of a comma) have been used. u_i, e_{ij} and τ_{ij} denote, as usual, the components of displacement, strain and stress, respectively; δ_{ij} is the Kronecker delta, μ the shear modulus, ν POISSON's ratio and α the coefficient of thermal expansion.

To the general field equations (1), (2), (3), which are valid throughout the region D occupied by the body, we must add the boundary conditions which, for the pure thermoelastic problem (i. e., for the boundary B free of tractions) take the form

$$\tau_{ij}\,\nu_j = 0 \quad \text{on } B\,, \tag{4}$$

ν_j being the components of a unit vector normal to the surface B.

Substitution of (1) and (2) into (3) provides the Duhamel-Neumann field equations in terms of displacement.

After changing from indicial notation to vector notation, which is more expedient at this stage, we obtain

$$\Delta\vec{u} + \varkappa\,\text{grad div}\,\vec{u} - \beta\,\text{grad}\,T = 0\,, \tag{5}$$

where $\vec{u}$ denotes the displacement vector, E YOUNG's modulus, Δ the Laplace space operator and $\varkappa = 1/(1-2\,\nu)$, $\beta = E\,\alpha\,\varkappa/\mu = 2\,(1+\nu)\,\alpha/(1-2\,\nu)$.

Let us now turn to the temperature field. Assume that the heat is generated at no more than a finite number of points situated in $D + B$. Then for a steady flow of heat, the governing temperature field equation is the Laplace equation

$$\Delta T = 0\,, \tag{6}$$

provided that the body is thermally isotropic and homogeneous. Thus $T(P)$ is a harmonic function, i. e. regular throughout the region $D + B$, except at the points of generation of heat where it may become singular[8]).

Denote the dilatation by

$$\theta \equiv \text{div}\,\vec{u} \tag{7}$$

[8]) By the boundary value or the value of a function at a singular point we understand in the sequel the value of the function obtained by a suitable limit process.

and take the divergence of both members of (5). Because of the temperature equation (6), this gives

$$\Delta\theta = 0\,, \tag{8}$$

a relation which is well known for the isothermal problem. Now, taking the Laplacian of both members of (5), we derive, in view of (8)

$$\Delta\Delta\vec{u} = 0\,. \tag{9}$$

Thus every component of the displacement field, in the steady-state thermoelastic problem under investigation, represents a biharmonic function, as in the isothermal case. This permits us to utilize in the solution of the thermoelastic problem a method which was worked out for the isothermal case.

In preparation for an application of the method[9]) let us observe that if $\phi(P)$ and $\psi(P)$ are two arbitrary functions harmonic inside the region D and if r is the modulus of a position vector $\vec{r} \equiv x_1, x_2, x_3$, then

$$\Psi(P) = \phi(P) + r^2\,\psi(P) \tag{10}$$

is a solution of the biharmonic equation in the region. This assertion may be proved by direct substitution of (10) into (9). Moreover, the converse is true[10]). Every biharmonic function $\Psi(P)$ in D can be expressed in the form (10), where $\phi(P)$ and $\psi(P)$ are harmonic in D. Thus we have a general representation of biharmonic functions in terms of pairs of harmonic functions. Since Equation (9) was derived from Equation (5) by differentiation we can assert that every solution of (5) is a biharmonic function, but the converse may not be true, i. e., not every biharmonic function is a solution of (5). In order to obtain a representation formula for the solution of the differential equation (5) we must fulfill the additional requirement (8), viz. that the divergence of the biharmonic vector function $\vec{u}$ must be harmonic function.

Represent the displacement vector in the form

$$\vec{u}(P) = \vec{\phi}(P) + r^2\,\mathrm{grad}\,\psi(P)\,, \tag{11}$$

where $\vec{\phi}(P)$ is a harmonic vector (a vector whose components are harmonic functions) and $\psi(P)$ is a harmonic scalar function. Since the components of the gradient of a harmonic function are themselves harmonic, the representation (11) provides, by virtue of what was said in connection with (10), s solution of the field equations (9). It may be shown by simple calculation that (11) also becomes a solution of (5) if the following relation between the harmonic functions $\psi(P)$ and $\vec{\phi}(P)$ exists:

$$\psi = \frac{r^{-\frac{1}{2+\varkappa}}}{4+2\varkappa} \int_0^r r^{\frac{1}{2+\varkappa}-1} D(P)\,dr\,. \tag{12}$$

[9]) See Almansi [10], Trefftz [11], Bergman and Schiffer [12].

[10]) See [12], page 230.

Here the integration is to be performed along a fixed position vector and

$$D(P) = 2\left[\psi + (2+\varkappa)\, r \frac{\partial \psi}{\partial r}\right] = -\varkappa \operatorname{div} \vec{\phi} + \beta T + C\,. \tag{13}$$

The constant of integration C which depends on the direction of integration has to be determined in such a way that $D(P)$ really is a harmonic function[11]). Then, by a known lemma[12]), ψ will also be harmonic, which implies the harmonicity of the divergence of $\vec{u}$ in (11), as was demanded. It is now possible to construct an infinite set of particular solutions of (5) by starting with an arbitrary harmonic vector function $\vec{\phi}$ (i. e. with three arbitrary harmonic scalar functions ϕ_i, $i = 1, 2, 3$) and deriving the fourth harmonic function ψ by means of the relation (12).

We now observe that since the stresses arise from the displacements by simple differentiation and the operator of partial differentiation commutes with the biharmonic operator, the stresses induced by the steady heat flow are biharmonic functions, a result known in ordinary elasticity.

3. Some Theorems on Harmonic Functions

As a further preliminary we shall quote, for future reference, two theorems concerning harmonic functions. The regions that we shall consider here are the half-space, the plate and completely regular regions. The latter are defined as closed finite or infinite regions that are bounded by closed smooth surface[13]). In the case of infinite regions, we shall assume that the harmonic functions considered are regular at the point at infinity. This means that the functions tend to zero at infinity no slower than $1/\varrho$ and their partial derivatives no slower that $1/\varrho^2$, where ϱ designates the distance from any fixed point.

Bearing this in mind we formulate the following theorems.

Theorem 1. A function which is harmonic in a completely regular region and vanishes at all points of the boundary must vanish identically in the region.

Theorem 2. A function which is harmonic in a half-space and vanishes at all points of the bounding plane must vanish identically in the half-space. The proof of the first theorem may be found in any book on potential theory[14]). A proof of the second theorem is given in the Appendix.

---

[11]) Of course the middle expression in (13) is harmonic, since ψ is harmonic by hypothesis and from this results the harmonicity of $r\,(\partial\psi/\partial r)$ as may be trivially proved. Clearly, the right-hand side of (13) is harmonic if C is harmonic, since the divergence of a harmonic function is harmonic and T is harmonic by (6).

[12]) [12], page 230.

[13]) A smooth surface is a surface with continuously turning tangent plane. An example of an infinite completely regular region provides the entire space exterior to a spherical surface. Our requirement of complete regularity of the region may be considerably weakened. See in this connection the regularity conditions introduced, e. g., in [13], page 113 and 217.

[14]) See e. g. [13], p. 213.

We now proceed to apply our general considerations to the steady-state thermoelastic problem for some fundamental regions.

4. The Half-Space

Denote now the cartesian coordinates by x, y, z. Let the half-space occupy the region $z > 0$ with the boundary $z = 0$.

We shall show that for a steady flow of heat, s simple particular solution of the type (11) permits us to obtain a general solution for the case considered.

To this end drop the nonessential constant in (13) and assume in addition that

$$\operatorname{div} \vec{\phi} = \frac{\beta}{\varkappa} T . \tag{14}$$

Then from (13) we find that $D(P) \equiv 0$ and from (12) that $\psi(P) \equiv 0$. This shows that we seek the solution to the problem in the form

$$u, v, w = \phi_1, \phi_2, \phi_3 , \tag{15}$$

where u, v, w denote the components of the displacement vector $\vec{u}$ and ϕ_i $(i = 1, 2, 3)$ are harmonic components of $\vec{\phi}$. Since from (7) in the case considered

$$\theta = \operatorname{div} \vec{\phi} , \tag{16}$$

we confirm the fulfillment of the condition (8) that the dilatation be harmonic and find

$$\theta = \frac{\beta}{\varkappa} T . \tag{17}$$

We shall show that the solution (15) constitutes the complete solution to our problem. To this end we change x_i $(i = 1, 2, 3)$ to x, y, z in (2) and using (17) write explicitly the components of stress acting on an element parallel to the plane $z = 0$:

$$\left.\begin{aligned} \tau_{zx} &= \mu (u_{,z} + w_{,x}) , \\ \tau_{zy} &= \mu (v_{,z} + w_{,y}) , \\ \tau_{zz} &= \mu \left(2 w_{,z} - \frac{\beta}{\varkappa} T\right). \end{aligned}\right\} \tag{18}$$

Since the partial derivatives of harmonic functions are themselves harmonic, and u, v, w and T are harmonic, this result shows that the stresses (18) are also harmonic.

In order that the displacement (15) respresents the complete solution to our problem it has, first of all, to meet the boundary conditions on the plane

$z = 0$. These are in terms of stresses:

$$\tau_{zx} = \tau_{zy} = \tau_{zz} = 0 \quad \text{on} \quad z = 0\,. \tag{19}$$

Furthermore, we shall require the fulfillment of the following conditions: a) the displacements and the stresses are regular except perhaps at the points of singularity, and except b) the components τ_{zx}, τ_{zy}, τ_{zz} which are bounded everywhere in the region $D + B$; c) the resultant of the stresses acting on any surface enclosing a point of singularity, if any, and lying in D must vanish; d) the stresses must vanish in infinity[15]).

Denote the stress vector acting on an element of area parallel to the plane $z = \text{const.}$ and having the components τ_{zx}, τ_{zy}, τ_{zz} by $\vec{t}_z$. It is bounded and vanishes on $z = 0$, by (19). Hence we may utilize Theorem 2 to conclude that it must vanish identically throughout the whole half-space. In other words, the stress field induced in the half-space by any steady-state temperature field is plane and parallel to the bounding plane.

This theorem which follows as a natural consequence of the theory of harmonic functions extends the remarkable result of STERNBERG and MCDOWELL [2] inferred in the special case of an arbitrarily prescribed surface temperature (bounded 'region of exposure'). It is important to note in connection with the Equations (18) that although their right hand sides represent bounded functions, the boundedness does not concern the individual terms in (18) taken separately. Thus the derivatives of the components of displacement as well as the temperature may not be bounded.

In the case of rotational symmetry around the z-axis we obtain instead of (18) by transformation to the cylindrical coordinates r, z

$$\left.\begin{aligned} \tau_{zr} &= \mu\,(u_{r,z} + w_{,r})\,, \\ \tau_{zz} &= \mu\left(2\,w_{,z} - \frac{\beta}{\varkappa}\,T\right), \end{aligned}\right\} \tag{18.1}$$

where u_r is the radial component of the displacement. In this case we put u_r, $w = \phi_1, \phi_3$, the tangential component of the displacement vanishing identically. Again instead of (19) we obtain

$$\tau_{zr} = \tau_{zz} = 0 \quad \text{on} \quad z = 0\,. \tag{20}$$

Since the right-hand members of Equation (18) or (19) vanish identically throughout the region $D + B$, they establish important general relations between the harmonic functions ϕ_i $(i = 1, 2, 3)$. A trivial integration, neglecting

[15]) The property d) is evident if one considers any hermispherical surface drawn in the body around a point on the boundary. For no resultant vector and moment of stresses acting on this surface, the stresses must go to zero with growing radius of the hemisphere. Apparently, we do not require that the displacements vanish at infinity and we shall see later that they may not vanish.

nonessential harmonic functions of integration, yields the following result in the non-symmetric case:

$$\left.\begin{aligned} u = \phi_1 &= -\int \phi_{3,x}\, dz\,, \\ v = \phi_2 &= -\int \phi_{3,y}\, dz\,, \\ w = \phi_3 &= \frac{\beta}{2\varkappa}\int T\, dz\,; \end{aligned}\right\} \tag{21}$$

and in the case of rotational symmetry

$$\left.\begin{aligned} u_r = \phi_1 &= -\int \phi_{3,r}\, dz\,, \\ w = \phi_3 &= \frac{\beta}{2\varkappa}\int T\, dz\,. \end{aligned}\right\} \tag{22}$$

Denote

$$\Phi_{,z} = \int T\, dz\,, \tag{23}$$

where Φ, of course, is harmonic. A comparison of (21) and (22) with the corresponding representation in [2][16]) shows that

$$\Phi = \frac{1}{2\pi}\chi\,, \tag{24}$$

where χ is the Boussinesq three-dimensional logarithmic potential applied in [2].

The strikingly simple result obtained in the preceding discussion permits us to solve a whole class of thermoelastic problems by a mere substitution of the expression for the temperature in (21) or (22), provided the temperature field for the prescribed steady-state heat flow is known.

A detailed study of particular problems being beyond the scope of this paper, we now turn to a brief outline of some characteristic solutions connected with the half-space.

1. At first consider a point source of heat located at the bounding plane $z = 0$. The solution of this problem was given by MELAN and PARKUS [14], p. 74, using thermoelastic displacement potential and LOVE's displacement function (the latter in order to remove the stress on the plane $z = 0$ created by the former function). The final result of [14] can be at once predicted from our previous argument, and the solution reduces to the following trivial reasoning.

For a thermally insulated bounding plane

$$T = \frac{Q}{4\,w\,K\,R}\,, \qquad R = (r^2 + z^2)^{1/2} \tag{25}$$

where Q is the constant rate of heat introduced per unit time and K the heat

[16]) Equations (31) and (32).

conductivity. By introduction of (25) into (22) we obtain the associated field of displacement

$$\left.\begin{aligned} u_r &= \frac{Q\,\alpha\,(1+\nu)}{4\,w\,K}\,\frac{r}{R+z}\,, \\ w &= \frac{Q\,\alpha\,(1+\nu)}{4\,\pi\,K}\log(R+z)\,. \end{aligned}\right\} \tag{26}$$

A simple inspection shows a singular behavior of displacements at the (singular) point of generation of heat, while at the point at infinity only w increases infinitely. The stress field generated by (26) renders the components τ_{zr} and τ_{zz} identically equal to zero, while the remaining nonvanishing components of stress become

$$\left.\begin{aligned} \tau_{rr} &= -\frac{Q\,E\,\alpha}{4\,\pi\,K}\,\frac{1}{R+z}\,, \\ \tau_{\phi\phi} &= -\frac{Q\,E\,\alpha}{4\,\pi\,K}\,\frac{z}{R\,(R+z)}\,. \end{aligned}\right\} \tag{27}$$

These components tend to zero at infinity in accordance with the property d) required previously.

2. The case of a given surface temperature in the region of exposure on $z = 0$ has been explored, as already mentioned, in [2] and [3], for two types of regions and distributions. Referring the reader to these papers for a detailed discussion, we borrow the formulae for the temperature field in the particular case in which a uniform temperature distribution exists over a circular region of exposure.

In Sternberg-McDowell representation, we thus obtain

$$T(r,z) = \frac{T_0}{\pi}\left\{K'\left[E(k,\theta) - F(k,\theta) - \frac{z}{r_2}\right] + E'\,F(k,\theta)\right\}, \tag{28}$$

$E(k,\theta)$ and $F(k,\theta)$ being the incomplete elliptic integrals of the first and second kind in the LEGENDRE's normalform referred to the modulus k and the argument θ, while K' and E' are the corresponding complete elliptic integrals referred to the complementary modulus k'. There designate

$$\left.\begin{aligned} k = \frac{r_1}{r_2}\,, \qquad k' &= \frac{2}{r_2}\,(a\,r)^{1/2}\,, \qquad r_1 = [(a-r)^2 + z^2]^{1/2}\,, \\ r_2 &= [(a+r)^2 + z^2]^{1/2}\,, \end{aligned}\right\} \tag{29}$$

and

$$\sin\theta = \frac{r_1}{r_2}\,, \qquad \cos\theta = \frac{r-a}{r_1} \qquad (0 \leqq \theta \leqq \pi)\,, \tag{30}$$

a being the radius of the (circular) region of exposure.

The representation by SNEDDON-LOCKETT leads to the following alternate formula in terms of the Bessel functions of the first kind:

$$T(r, z) = T_0 \int_0^\infty J_1(\varrho)\, J_0\left(\frac{r}{a}\varrho\right) e^{-\frac{z}{a}\varrho}\, d\varrho\,, \tag{31}$$

in which, in accordance with the notation of EASON, NOBLE and SNEDDON [15], the improper integral can be also written down as $I(1, 0; 0)$ with

$$I(\mu, \nu; \lambda) = \int_0^\infty J_\mu(a\,t)\, J_\nu(b\,t)\, e^{-c\,t}\, t^\lambda\, dt\,. \tag{32}$$

Since the elliptic integrals in (28) and the last integral have been extensively tabulated their numerical evaluation presents no difficulty. Of course, the two representations quoted above are equivalent to each other. This is shown in [15].

By utilizing either representation, e. g. (31), we obtain the associated field of displacement by a simple substitution into (22). In this way it may be trivially established that, in the case considered,

$$u_r = \alpha\,(1+\nu)\, a\, T_0\, I\,(1, 1; -1)\,, \quad w = -\alpha\,(1+\nu)\, a\, T_0\, I\,(1, 0; -1)\,, \tag{33}$$

in agreement with the result in [3], page 5.

Since the determination of the displacement and stress fields in the half-space demands a mere knowledge of the associated temperature fields, many thermoelastic problems for the half-space may be at once solved provided the respective steady-state temperature problems are already solved. Let us quote here some more characteristic examples of known temperature fields which may be of interest: a) circular region of exposure at uniform temperature with no flow of heat over the rest of the bounding plane [16]; b) uniform flow of heat over a circular region with no flow of heat over the rest of the bounding plane [16]; c) uniform flow of heat over a circular region and zero temperature of the rest of the bounding plane [16]; d) a point source soaring over the bounding plane at a fixed distance [17].

5. The Infinite Thick Plate

The foregoing analysis may be easily extended to the case of an elastic body bounded by two parallel planes, e. g. $z = 0$ and $z = h$, but otherwise unlimited, i. e. to an infinite thick plate. Apparently, we might start with a theorem corresponding to the Theorem 2[17]). It is simpler, however, to choose a more heuristic approach.

[17]) According to the oral communication of Professor C. WILCOX, the proof of such a theorem for the infinite plate, sketched by him, involves subtle mathematical argument.

Observe that since the stress vector $\vec{t}_z$ on the planes parallel to the bounding plane of the half-space vanishes throughout the body, no interactions between the horizontal layers of the half-space exist. Thus we may separate a layer, say $0 \leqq z \leqq h$, of the half-space from the remaining body without influencing the stresses in the disconnected parts. The complete solution to the problem is obtained by substitution into the Equations (21) or (22) of a solution of the equation of steady heat flow appropriate for an infinite plate.

As already mentioned, the case of an infinite plate has been treated in some detail for a suitably chosen and axially symmetric surface temperature distribution e. g. in [2]. Hence we confine ourselves to a particular illustrative example of a point source of heat of strength Q located at the upper face of the plate while the lower face of the plate is kept at zero temperature. In this case

$$T = \frac{Q}{2\pi K} \int_0^\infty \frac{J_0(\alpha r) \sinh \alpha (h - z)}{\cosh \alpha h} d\alpha , \tag{34}$$

with K as thermal conductivity.

By substituting (34) into Equations (22) we get in a trivial way

$$\left.\begin{aligned} u_r &= \frac{(1+\nu)\alpha Q}{2\pi K} \int_0^\infty \frac{J_1(\alpha r) \sinh \alpha (h - z)}{\alpha \cosh \alpha h} d\alpha , \\ w &= -\frac{(1+\nu)\alpha Q}{2\pi K} \int_0^\infty \frac{J_0(\alpha r) \cosh \alpha (h - z)}{\alpha \cosh \alpha h} d\alpha , \end{aligned}\right\} \tag{35}$$

in agreement with the result of LURIE [6], p. 196, obtained by a rather involved argument, using in the case of a layer equations similar to our general equations (21).

6. The Sphere

Let us now consider regions bounded by spherical surfaces. We shall confine ourselves to the solid sphere since the corresponding solutions for a thick spherical shell and a spherical cavity in an infinite medium may be obtained by a similar reasoning.

Take the center of the sphere at the origin of coordinates and denote the radius of the sphere by a. Let the sphere be immersed in an arbitrary steady-state temperature field[18]).

[18]) A formal solution in integral representation for the sphere subjected to an arbitrary temperature field was obtained by BORCHARDT [18] in 1873. For the axisymmetric temperature field, see [4] and Footnote 2.

We assume the following expressions for the components of the displacement

$$\left.\begin{aligned} u &= \phi_1 + (r^2 - a^2)\,\psi_{,x}\,, \\ v &= \phi_2 + (r^2 - a^2)\,\psi_{,y}\,, \\ w &= \phi_2 + (r^2 - a^2)\,\psi_{,z}\,, \end{aligned}\right\} \tag{36}$$

and we shall show that for a suitable choice of the functions ϕ_i $(i = 1, 2, 3)$ and ψ they may represent a complete solution to the problem.

We observe first that (36) becomes a solution of (5) if by virtue of (12)

$$\psi = \frac{1}{2\,(3 - 4\,\nu)}\, r^{-\lambda} \int_0^r [2\,(1 + \varkappa)\,\alpha\, T - \theta_0]\, r^{\lambda - 1}\, dr\,, \tag{37}$$

with the notation

$$\theta_0 = \phi_{1,x} + \phi_{2,y} + \phi_{3,z}\,, \qquad \lambda = \frac{1 - 2\,\nu}{3 - 4\,\nu}\,. \tag{37.1}$$

Hence the components of the associated field of stress become

$$\left.\begin{aligned} \tau_{xx} &= 2\,\mu\,(\phi_{1,x} + (r^2 - a^2)\,\psi_{,xx} + 2\,x\,\psi_{,x} + \Phi)\,, \\ \tau_{yy} &= 2\,\mu\,(\phi_{2,y} + (r^2 - a^2)\,\psi_{,yy} + 2\,y\,\psi_{,y} + \Phi)\,, \\ \tau_{zz} &= 2\,\mu\,(\phi_{3,z} + (r^2 - a^2)\,\psi_{,zz} + 2\,z\,\psi_{,z} + \Phi)\,, \\ \tau_{xy} &= \mu\,[\phi_{1,y} + \phi_{2,x} + 2\,(r^2 - a^2)\,\psi_{,xy} + 2\,(y\,\psi_{,x} + x\,\psi_{,y})]\,, \\ \tau_{zx} &= \mu\,[\phi_{1,z} + \phi_{3,x} + 2\,(r^2 - a^2)\,\psi_{,xz} + 2\,(x\,\psi_{,z} + z\,\psi_{,x})]\,, \\ \tau_{zy} &= \mu\,[\phi_{2,z} + \phi_{3,y} + 2\,(r^2 - a^2)\,\psi_{,yz} + 2\,(y\,\psi_{,z} + z\,\psi_{,y})]\,, \end{aligned}\right\} \tag{38}$$

where

$$\Phi = \frac{\nu}{1 - 2\,\nu}\,(\theta_0 + 2\,r\,\psi_{,r}) - \frac{\beta}{2}\,T\,. \tag{39}$$

In order that the stresses conform to the boundary conditions (4), in the absence of the surface tractions, the following equations must be satisfied by the functions ϕ_i $(i = 1, 2, 3)$ and ψ on the surface $r = a$:

$$\left.\begin{aligned} &2\,x\,\phi_{1,x} + y\,\phi_{2,x} + z\,\phi_{3,x} + y\,\phi_{1,y} + z\,\phi_{1,z} \\ &\quad + 2\,x\,r\,\psi_{,r} + 2\,r^2\,\psi_{,x} + \vartheta\,x = 0\,, \\ &x\,\phi_{1,y} + 2\,y\,\phi_{2,y} + z\,\phi_{3,y} + x\,\phi_{2,x} + z\,\phi_{2,z} \\ &\quad + 2\,y\,r\,\psi_{,r} + 2\,r^2\,\psi_{,y} + \vartheta\,y = 0\,, \\ &x\,\psi_{1,z} + y\,\phi_{2,z} + 2\,z\,\phi_{3,z} + x\,\phi_{3,x} + y\,\phi_{3,y} \\ &\quad + 2\,z\,r\,\psi_{,r} + 2\,r^2\,\psi_{,z} + \vartheta\,z = 0\,, \end{aligned}\right\} \tag{40}$$

with the notation

$$\vartheta = \frac{2}{1-2\nu}\left[\theta\,\nu - (1+\nu)\,\alpha\,T\right]. \tag{41}$$

It may be shown by direct substitution that by virtue of Equations (5) the left-hand members of the above equations are harmonic. Thus since they vanish on the boundary $r = a$ of a bounded region they must vanish identically throughout the entire region occupied by the body, according to the Theorem 1. From this fact we derive the important conclusion that the only nonvanishing components of the stress vector $\vec{t}_r\,(\Xi, H, Z)$ which act on elements of spherical surfaces centered at the center of the body are

$$\left.\begin{aligned} \Xi &= 2\,\mu\,\frac{r^2-a^2}{r}\,(\psi_{,xx}\,x + \psi_{,xy}\,y + \psi_{,xz}\,z)\,, \\ H &= 2\,\mu\,\frac{r^2-a^2}{r}\,(\psi_{,yy}\,y + \psi_{,xy}\,x + \psi_{,yz}\,z)\,, \\ Z &= 2\,\mu\,\frac{r^2-a^2}{r}\,(\psi_{,zz}\,z + \psi_{,xz}\,x + \psi_{,yz}\,y)\,. \end{aligned}\right\} \tag{42}$$

We turn now to the system of equations (40) which we have found valid for the whole interval $0 \leqq r \leqq a$. Simple computation reduces the system to one equation for the function ψ

$$r^2\,\psi_{,rr} + 2\,(1+\nu)\,r\,\psi_{,r} + (1+\nu)\,\psi + \frac{\alpha\,T}{2} = 0\,. \tag{43}$$

We assume now that the harmonic function ψ defined in the bounded simply connected region can be represented in a series of solid harmonics[19])

$$\psi = \sum_{n=0}^{\infty} a_n \left(\frac{r}{a}\right)^n Y_n(\theta, \phi)\,, \tag{44}$$

where a_n are unknown coefficients and θ and ϕ angles of latitude and longitude, respectively. We assume, furthermore, that the temperature, being an arbitrary harmonic function of coordinates, can be represented by a similar series

$$T = \sum_{n=0}^{\infty} \left(\frac{r}{a}\right)^n Y_n(\theta, \phi)\,. \tag{45}$$

Substituting of (44) and (45) into (43) and comparing of coefficients yields

$$a_n = -\frac{(1+\nu)}{2\,[n^2 + n\,(1+2\,\nu) + (1+\nu)]}\,\alpha\,, \tag{46}$$

the series representation (44) being now complete.

[19]) Evidently the solution of Equation (43) can be easily found in a closed form, but the method adopted in the sequel and modelled on the procedure of TREFFTZ seems to be more convenient for practical purposes.

Our next aim is to obtain the components τ_{rr}, $\tau_{r\theta}$ and $\tau_{r\phi}$ of the stress vector $\vec{t}_r$ resolved along the radius and the tangents to the meridian and the parallel at a point. By simple projection of (42) on the directions considered we find

$$\left.\begin{aligned}
\tau_{rr} &= \mu\,(r^2 - a^2)\,[2\,(\psi_{,xx}\cos^2\phi + \psi_{,yy}\sin^2\phi)\sin^2\theta + 2\,\psi_{,zz}\cos^2\theta \\
&\qquad + \psi_{,xy}\sin 2\phi\sin^2\theta + (\psi_{,xz}\cos\phi + \psi_{,yz}\sin\phi)\sin 2\theta]\,, \\
\tau_{r\theta} &= \mu\,(r^2 - a^2)\,[(\psi_{,xx}\cos^2\phi + \psi_{,yy}\sin^2\phi - \psi_{,zz} \\
&\qquad + \psi_{,xy}\sin 2\phi)\sin 2\theta + 2\,(\psi_{,xz}\cos\phi + \psi_{,yz}\sin\phi)\cos 2\theta]\,, \\
\tau_{r\phi} &= \mu\,(r^2 - a^2)\,[(-\psi_{,xx}\sin 2\phi + \psi_{,yy}\sin 2\phi \\
&\qquad + 2\,\psi_{,xy}\cos 2\phi)\sin\theta - 2\,(\psi_{,xz}\sin\phi - \psi_{,yz}\cos\phi)\cos\theta]\,.
\end{aligned}\right\} \tag{47}$$

We observe that the computation of the components of stress acting on the elements of area perpendicular to the radii does not require the knowledge of the functions ϕ_i $(i = 1, 2, 3)$. This important conclusion greatly simplifies the following calculations.

In order to find the effective equations for the stresses let us decompose (47) into the particular solutions corresponding to the separate terms of the series (44) and denoted by the superscript n. In this way we find by lengthy but trivial computation

$$\left.\begin{aligned}
\tau_{rr}^n &= \Gamma\, n\left(1 - \frac{a^2}{r^2}\right)\left(\frac{r}{a}\right)^n Y_n\,(\theta, \phi)\,, \\
\tau_{r\theta}^n &= \Gamma\left(1 - \frac{a^2}{r^2}\right)\left(\frac{r}{a}\right)^n Y_{n,\theta}\,(\theta, \phi)\,, \\
\tau_{r\phi}^n &= \Gamma\left(1 - \frac{a^2}{r^2}\right)\left(\frac{r}{a}\right)^n \frac{1}{\sin\theta}\, Y_{n,\phi}\,(\theta, \phi)\,,
\end{aligned}\right\} \tag{48}$$

where

$$\Gamma = -\frac{\mu\,(1 + \nu)\,(n - 1)\,\alpha}{n^2\,(1 + 2\,\nu)\,n + (1 + \nu)}\,. \tag{48.1}$$

In the event that the arbitrary temperature distribution becomes symmetric with regard to the axis through the poles, the surface harmonics reduce to zonal harmonics, or Legendre-polynomials $P_n(\rho)$ with $\rho = \cos\theta$. This reestablishes the known result for the axisymmetric problem derived in [4].

The preceding discussion hinges on the series representation of the function ψ (44). Since, by hypothesis, ψ is harmonic inside the region of the sphere its expansion in a series of solid harmonics is uniformly convergent in this region [13], p. 251 a. subs. Such a series, however, may also be regarded as a power series in three variables (x, y, z) according to the definition of the spherical

harmonics. Hence by virtue of the known theorem regarding power series[20]), any given partial deriivatives of ψ will be represented inside the sphere by a uniformly convergent series obtained by a termwise differentiation of the series (44). The series for the stresses τ_{rr}, $\tau_{r\theta}$, $\tau_{r\phi}$ (48) being obtained in this way these series must be uniformly convergent inside the region considered. Since the aforementioned stresses vanish on the boundary $r = a$, we need not investigate the convergence there.

Computation of the remaining components of the stress field $\tau_{\theta\theta}$, $\tau_{\phi\phi}$ and $\tau_{\theta\phi}$ as well as of the associated field of displacement requires the determination of the harmonic functions ϕ_i $(i = 1, 2, 3)$ from (40). With no essential difficulty involved, this can be done following the procedure outlined by TREFFTZ [11], p. 104, for the isothermal case.

It is obvious that using series representations (44) and (45) in negative or in negative as well as in positive powers of r we can obtain in a like manner the solution to the thermoelastic problems relative to arbitrary steady-state temperature distributions in a infinite medium exterior to a sphere (a spherical cavity in the infinite space) or in a thick spherical shell.

In the foregoing discussion the components of the stress field have been represented in terms of surface harmonics which, bearing in mind the expansion (45), can be assumed as being known if the associated temperature field $T(r, \theta, \phi)$ is known. Suppose for definiteness that the temperature distribution on the surface B of the sphere is prescribed, $T(a, \theta, \phi) = S(\theta, \phi)$; $S(\theta, \phi)$ being a sufficiently regular function of θ and ϕ, say, its square is integrable over B. Then the series

$$S(\theta, \phi) = \sum_{n=0}^{\infty} Y_n(\theta, \phi) \tag{49}$$

converges in the mean to $S(\theta, \phi)$ and the spherical harmonics $Y_n(\theta, \phi)$ can be represented by the given function $S(\theta, \phi)$ as well as by the extensively tabulated Legendre polynomials $P_n(\mu)$ and the associated Legendre functions $P_n^{(m)}(\mu)$, where $\mu = \cos\theta$. In fact, we have the following known representation:

$$Y_n(\theta, \phi) = c_0^{(n)} P_n(\mu) + \sum_{m=1}^{n} (c_m^{(n)} \cos m\phi + d_m^{(n)} \sin m\phi) P_n^{(m)}(\mu) , \tag{50}$$

where for $n \geq 1$

$$\left.\begin{aligned} c_m^{(n)} &= \delta_{m(n)} \int_{(B)} S(\theta, \phi)\, P_n^{(m)}(\mu) \cos m\phi \, d\sigma , \\ d_m^{(n)} &= \delta_{m(n)} \int_{(B)} S(\theta, \phi)\, P_n^{(m)}(\mu) \sin m\phi \, d\sigma , \end{aligned}\right\} \tag{51}$$

[20]) See e. g. [13], page 137.

and

$$\delta_{m(n)} = \frac{(2n+1)(n-m)!}{2\pi(n+m)!\,\varepsilon_m}. \tag{52}$$

Here $\varepsilon_m = 1$ if $m > 0$, $\varepsilon_m = 2$ if $m = 0$ and $P_n^{(0)}(\mu) = P_n(\mu)$. For $n = 0$ we get simply $Y_0(\theta, \phi) = c_0^{(0)}$, where $c_0^{(0)}$ has to be computed from the first equation (51).

APPENDIX

Proof of Theorem 2. Consider a harmonic function $u(P)$ satisfying the requirements of the Theorem 2.

Let the half-space occupy the infinite region $z > 0$. To prove the theorem[21]), define $u(P)$ for negative z as an odd function of z:

$$u(x, y, -z) = -u(x, y, z). \tag{a}$$

First let us show that this new (extended) function $u(x, y, z)$, $-\infty < z < \infty$, is harmonic throughout the entire space. To this end, construct a sphere S with an arbitrary radius ϱ, and the boundary Σ, the center of the sphere resting on the plane $z = 0$.

Define a new function $v(P)$ which is harmonic in S and which takes on Σ the same values as $u(P)$ on Σ:

$$v(P) = u(P) \quad \text{for} \quad P \text{ on } \Sigma. \tag{b}$$

It may be easily shown that $v(P) = 0$ on the plane $z = 0$. In fact, an auxiliary function $w(x, y, z) = 1/2\,[v(x, y, z) + v(x, y, -z)]$ is harmonic in S as a sum of two harmonic functions in S, and vanishes on Σ because of (a) and (b). Hence, by virtue of the Theorem 1, certainly

$$w(P) = 0 \text{ for } P \text{ on } z = 0. \tag{c}$$

But

$$v(P) = w(P) \text{ for } P \text{ on } z = 0 \tag{d}$$

by construction, hence the function $v(P)$ vanishes on the plane $z = 0$. This plane divides the sphere S in two hemispheres. On the bounding surface of each of these hemispheres the values of $v(P)$ coincide with the values of $u(P)$. In fact, on the hemispherical surface this results from (b) and on the plane $z = 0$ both functions are zero, $v(P)$ by (d) and $u(P)$ by hypothesis. Hence, by virtue of the Theorem 1, the difference $u - v$ vanishes inside any of the two hemispheres and $u \equiv v$ throughout the sphere S. Hence the extended function

[21]) The main line of the proof is modelled on SOBOLOV's proof of the uniqueness of solution of the Dirichlet problem for the half-space [19]. In the argument we use the Liouville theorem which states that a harmonic function bounded in the entire space is constant.

$u(P)$ is harmonic in S. Since the location of the origin and the radius of S are arbitrary, this conclusion concerns also the entire space.

Recall now that by hypothesis $u(P)$ is bounded in the entire space. Hence by virtue of the Liouville Theorem, it is constant in the entire space. But it vanishes on $z = 0$, thus it may be only zero everywhere. This completes the proof of the Theorem 2.

Acknowledgment

This work has been sponsored by the United States Army under contract No. DA-11-022-ORD-2059.

REFERENCES

[1] R. D. MINDLIN and D. H. CHENG, *Thermoelastic Stress in the Semi-Infinite Solid*, J. appl. Phys. *21*, 931 (1950).
[2] E. STERNBERG and E. L. MCDOWELL, *On the Steady-State Thermoelastic Problem for the Half-Space*, Quart. appl. Math. *14*, 381 (1957).
[3] I. N. SNEDDON and F. J. LOCKETT, *On the Steady-State Thermoelastic Problem for the Half-Space and the Thick Plate*, Rep. No. AF 18(600)–1341 (Duke University, 1959).
[4] E. L. MCDOWELL and E. STERNBERG, *Axisymmetric Thermal Stresses in a Spherical Shell of Arbitrary Thickness*, J. appl. Mech. *24*, 376 (1957).
[5] J. N. GOODIER, *On the Integration of the Thermoelastic Equations*, Phil. Mag. *23*, 1017 (1937).
[6] A. I. LURIE, *Three-Dimensional Problems of the Theory of Elasticity* (in Russian) (GITTL, Moscow, 1955).
[7] B. SHARMA, *Thermal Stresses in Infinite Elastic Disks*, J. appl. Mech. *78*, 527 (1956).
[8] W. THOMSON, *Mathematical and Physical Papers*, *3*, 351 (1890).
[9] I. SOKOLNIKOFF, *Mathematical Theory of Elasticity* (McGraw-Hill Book Co., 1956).
[10] E. ALMANSI, *Sull'integrazione dell'equazione differentiale* $\Delta^{2n} = 0$, Ann. Mat. Pura Appl. [3], *2*, 1 (1898–99).
[11] E. TREFFTZ, *Mechanik der elastischen Körper*, Handb. Phys. *6* (1928).
[12] S. BERGMAN and M. SCHIFFER, *Kernel Functions and Elliptic Differential Equations in Mathematical Physics* (Academic Press, New York, 1953).
[13] O. D. KELLOGG, *Foundations of Potential Theory* (Dover Publ., New York, 1953).
[14] E. MELAN and H. PARKUS, *Wärmespannungen* (Springer-Verlag, Wien 1953).
[15] G. EASON, B. NOBLE, and I. N. SNEDDON, *On Certain Integrals of Lipschitz-Hankel Type Involving Products of Bessel Functions*, Phil. Trans. [A], *247*, 529 (1955).
[16] H. S. CARSLAW and J. C. JAEGER, *Conduction of Heat in Solids* (Oxford University Press, 1959).
[17] P. H. THOMAS, *Some Conduction Problems in the Heating of Small Areas on Large Solids*, Quart. J. Mech. appl. Math., *10*, 482 (1957).
[18] C. W. BORCHARDT, *Untersuchungen über die Elastizität fester isotroper Körper unter Berücksichtigung der Wärme*, Mber. Akad. Wiss. Berlin, *9* (1873).
[19] S. L. SOBOLEV, *Equations of Mathematical Physics* (in Russian), (GITTL, Moscow, 1954).

Zusammenfassung

Die Kelvin-Almansi-Darstellung einer Bipotentialfunktion vermittelst zweier harmonischer Funktionen wird zur Lösung elastischer Wärmespannungsprobleme für stationäre Temperaturfelder angewendet.

Es werden die Wärmespannungen infolge willkürlicher stationärer Temperaturfelder in einigen fundamentalen Bereichen, nämlich im Halbraum, in der dicken Platte und in der Vollkugel untersucht.

(Received: Juli 25, 1960.)

On the Dynamics of Turbulent Vortical Flow

By Alan Reynolds, London, Great Britain[1])

The problem of the mathematical representation of the vortex flows occurring in nature has so far proved intractable. Two lines of attack have been used: the study of simple solutions of equations potentially capable of adequately representing the phenomena, and the study of flows with the necessary geometric complexity but satisfying simpler equations. The recent treatments of vortex flows by Deissler and Perlmutter, Lay, Long, Pengelley, Rott, and Vulis and Ustimenko ([1][2]) to [6]) illustrate various approaches to the same problem. Every contribution represents a compromise between conflicting demands of reality; as the fluid properties are specified more realistically, the geometric verisimilitude must be correspondingly reduced.

In most of the physical situations of interest the flows are turbulent. Nevertheless, most investigators have found it expedient to base their studies of vortices in real fluids on the Navier-Stokes equations, extending their conclusions to turbulent flows by introducing a constant eddy viscosity to represent the activity of turbulence.

Here the problem of the turbulent vortex will be attacked directly, using an order-of-magnitude analysis to pick out the important terms of Reynolds' equations. This approach does not lead to explicit solutions unless further, more arbitrary assumptions are made. But it does simplify the problem and thus provides considerable insight into the mechanisms operating to set up the basic flow patterns. Also, the reduced equations would seem to provide a suitable basis for further attempts at the detailed prediction of vortex flows.

From the outset we neglect the viscous terms in the momentum equations; however, account will be taken of density variations, in order that the study be applicable to the interesting problem of the Ranque-Hilsch vortex tube.

[1]) Imperial College of Science and Technology, Dpt. of Aeronautics.

[2]) Numbers in brackets refer to References, p. 158.

Thus the analysis can be valid only for flows in which there is a fairly high level of turbulent activity, high enough for the turbulent mixing stresses to far exceed the viscous terms. This neglect of viscosity means that the results apply only in the turbulent body of the flow, away from solid boundaries where turbulence is suppressed.

This investigation is particularly directed towards flows with large swirl. It is to such cases that the technique of approximation adopted is especially applicable. Thus the approximate results may be misleading if applied directly to 'swirling pipe flow' or other problems in which the swirl is small compared to the axial component of velocity.

Finally, it should be noted that body forces are neglected. Consequently, only those flows in which the typical centripetal accelerations greatly exceed that of gravity are within the scope of this treatment. This stricture is likely to apply only to flows of liquids since these are commonly much slower than gas flows.

1. The Governing Equations

From continuity and EULER's momentum equations we obtain, on taking mean values with respect to time and requiring the mean motion to be steady and axisymmetric:

$$\left.\begin{aligned}
&\frac{1}{r}\frac{\partial}{\partial r}(r\,\overline{\varrho\,u}) + \frac{\partial}{\partial z}(\overline{\varrho\,w}) = 0\,,\\
&\frac{1}{r}\frac{\partial}{\partial r}\left(r\,\overline{\varrho\,u^2}\right) + \frac{\partial}{\partial z}(\overline{\varrho\,u\,w}) - \frac{\overline{\varrho\,v^2}}{r} = -\frac{\partial P}{\partial r}\,,\\
&\frac{1}{r}\frac{\partial}{\partial r}(r\,\overline{\varrho\,u\,v}) + \frac{\partial}{\partial z}(\overline{\varrho\,v\,w}) + \frac{\overline{\varrho\,u\,v}}{r} = 0\,,\\
&\frac{1}{r}\frac{\partial}{\partial r}(r\,\overline{\varrho\,u\,w}) + \frac{\partial}{\partial z}\left(\overline{\varrho\,w^2}\right) = -\frac{\partial P}{\partial z}\,,
\end{aligned}\right\} \qquad (1)$$

where $\varrho = R + \varrho'$, $u = U + u'$, etc. We have then

$$\overline{\varrho\,u\,v} = R\,\overline{u\,v} + \overline{\varrho'\,(U\,v' + V\,u' + u'\,v')}\,,$$

etc.

The introduction of time-mean values has brought order into the system, but at a great price. For it is immediately apparent that this system of equations does not specify a determinate mathematical problem: we have now more dependent variables than governing equations. General principles on which further mathematical relationships might be based have not yet been devised. This is the fundamental problem facing us.

As we cannot investigate turbulent vortex flows by obtaining and studying explicit solutions of the governing equations, we are forced to extract what

information we can directly from the equations. To this end we shall simplify them by dropping the smaller terms, justifying these steps with an order-of-magnitude analysis. Three cases will be studied: nearly plane motions, nearly helical motions as would occur within long tubes, and finally a more general class including these as special cases.

2. Nearly Plane Swirling Flows

Exact integrals can be found for some of the governing equations if axial variations are restricted. Indeed, these first integrals can be obtained even with the viscous terms retained if the coefficient of viscosity is assumed constant The results are applicable to flows that are the same in every section perpendicular to the axis.

Consequently, in allowing small axial velocities and small axial gradients we are working away from a firm base. We can expect that neglect of less important terms will lead to considerable simplifications and that the accuracy of the approximate results will be reasonably high.

The scheme for the order-of-magnitude analysis is as follows. We take

$$U, V \sim O(1), \quad W \sim O(\varepsilon), \quad \frac{\partial}{\partial r} \sim O(1), \quad \frac{\partial}{\partial z} \sim O(\delta)$$

to represent the basic features of the flow, and

$$\overline{u'^2}, \quad \overline{v'^2}, \quad \overline{w'^2} \sim O(\beta), \quad \varrho' \sim O(\eta)$$

to represent the turbulence.

Units are chosen such that $r, U, V, \Delta P \sim O(1)$. Then $R \sim O(1)$ also, for consistency of these assumptions with the equation governing tangential momentum; this result will be seen more clearly a posteriori. The quantities $\beta, \delta, \varepsilon, \eta$ are, of course, assumed to be small compared with unity so that terms of higher orders in them can be neglected.

Introducing these orders into equations (1) we find:

$$\left.\begin{aligned} r\,R\,U &= C + O(\delta\,\varepsilon, \beta^{1/2}\,\eta)\,, \\ \frac{\partial P}{\partial r} + \frac{1}{r}\frac{\partial}{\partial r}(r\,R\,U^2) &= \frac{R\,V^2}{r} + O(\beta)\,, \\ r^2\,R\,\overline{u\,v} &= G + O(\delta\,\varepsilon, \beta\,\delta, \beta^{1/2}\,\eta)\,, \\ \underset{O(\delta)}{\frac{\partial P}{\partial z}} + \frac{1}{r}\frac{\partial}{\partial r}(r\,R\,\underset{O(\varepsilon,\beta)}{\overline{u\,w}}) &= O(\beta\,\delta, \beta^{1/2}\,\eta)\,, \end{aligned}\right\} \quad (2)$$

where only the lower order terms are indicated and those not marked $\sim O(1)$.

Note that residual errors due to non-zero compressibility remain in these relations even as $\delta, \varepsilon \to 0$ to give purely planar flow. The axial momentum

relation appears to be the least accurate of the simplified equations; it has come into being as the result of introducing perturbations to the planar flow.

Integration of the continuity and tangential relations has still been possible. A result of some interest can be derived from the integrated forms. We have

$$r^2 R \overline{u' v'} = -G_0 \quad \text{for} \quad U V = 0 .$$

If the radial variation of REYNOLDS' stress does not change decisively with U, we can write, for small radial flows:

$$R U V = -\frac{G}{r^2} + \frac{G_0}{r^2} \quad \text{or} \quad V = \left(\frac{G_0 - G}{C}\right) \frac{1}{r} .$$

Thus it appears that $V \sim 1/r$ for small or vanishing U's. This law is found to be obeyed in the fully turbulent region between two rotating cylinders, adjustments to particular boundary conditions taking place in boundary layers. But its justification for this case of zero radial flow is not simple unless the more general radial flow is considered first.

3. Flow in a Vortex Tube

Here the system of approximation is

$$V \sim O(1) , \quad U \sim O(\varepsilon) , \quad \frac{\partial}{\partial r} \sim O(1) , \quad \frac{\partial}{\partial z} \sim O(\delta) ,$$

$$\overline{u'^2}, \ \overline{v'^2}, \ \overline{w'^2} \sim O(\beta) , \quad \varrho' \sim O(\eta) .$$

Units are again chosen so that $r, V, \Delta P \sim O(1)$; as before, $R \sim O(1)$, for consistency.

The geometric specializations imposed seem natural in a problem of high-swirl flow in a tube, although they will not necessarily be valid near the ends of the tube if there are constrictions there. Introducing them into the continuity equation (1), we find that

$$W \sim O\left(\frac{\varepsilon}{\delta}\right),$$

at most, so that

$$\underset{O(\varepsilon)}{\frac{1}{r} \frac{\partial}{\partial r}(r R U)} + \underset{O(\varepsilon)}{\frac{\partial}{\partial z}(R W)} = O(\beta^{1/2} \eta) .$$

Also,

$$\left.\begin{aligned} &\frac{\partial P}{\partial r} = R \frac{V^2}{r} + O(\beta) , \\ &\underset{O(\varepsilon)}{\frac{\partial}{\partial z}(R V W)} + \frac{1}{r^2} \underset{O(\varepsilon, \beta)}{\frac{\partial}{\partial r}(r^2 R \overline{u v})} = O(\beta \delta, \ \beta^{1/2} \eta) , \\ &\underset{O(\delta)}{\frac{\partial P}{\partial z}} + \underset{O(\varepsilon^3/\delta)}{\frac{\partial}{\partial z}(R W^2)} + \frac{1}{r} \underset{O(\beta, \varepsilon^3/\delta)}{\frac{\partial}{\partial r}(r R \overline{u w})} = O\left(\beta \delta, \ \frac{\varepsilon}{\delta} \beta^{1/2} \eta\right) . \end{aligned}\right\} \quad (3)$$

The accuracy of these simplified results does not seem to be as high as that of equations (2). However, detailed investigations of the flow within a vortex tube have been made by the present writer; these experimental data allow estimates of the errors to be made for this particular case.

The vortex tube was about 7·5 cm (3 inches) in diameter and about 120 cm (48 inches) long. Air entered through slots cut tangentially through the wall near one end and escaped to the atmosphere through throttling devices at the ends of the tube. Internal flow measurements were made with a variety of blockages at the ends of the tube – solid end plates, orifice plates, perforated plates, or no blockage at all. Eight configurations were studied for overall pressure ratios of 2·0 and 2·3.

In the turbulent body of the flow we find, typically, $W/V \sim 1/4$, suggesting that $\varepsilon \sim \delta/4$. Considering the pressure distributions we find, typically,

$$\frac{\Delta P}{\Delta z} \Big/ \frac{\Delta P}{\Delta r} \sim \frac{1}{50},$$

relating changes down the length and across the radius of the tube, suggesting that $\delta \sim 1/50$, $\varepsilon \sim 1/200$. The experimental results indicate that for balance of the tangential and axial momentum equation we must have β not very different from δ and ε. Say $\beta \sim 2\,\varepsilon \sim \delta/2 \sim 1/100$. This implies that the intensity of turbulence in the tube $\sim 10\%$. As this is of the order expected, it offers a slight check on these estimates.

Finally we must estimate η, the order of the turbulent density fluctuations. The following considerations allow us to do this.

If the fluid is homogeneous (that is, such that it would be homogeneous on being brought to rest) the density fluctuations will be dependent on the turbulent velocity intensity. It seems plausible that these density differences are maintained by the centripetal pressure gradients within the eddies forming the turbulent velocity field. The pressure difference from core to periphery of a 'typical' eddy is related to the velocity field by

$$p' \sim R\,\overline{u'^2} \sim O(\beta).$$

We know that $\varrho'/p' \cong K$, the compressibility of the fluid. Hence, $\eta \sim K\,\beta$.

We have now only to estimate K, the compressibility, in the units appropriate to this study. We have taken ΔP, the pressure difference across the vortex, $\sim O(1)$. But in the high velocity air flow of the experimental situation we have also ΔR, the density difference across the vortex, $\sim R \sim O(1)$. Then

$$K \cong \frac{\Delta R}{\Delta P} \sim O(1)$$

in the appropriate units. Finally, $\eta \sim 1/100$.

We can now give estimates of the error terms in this situation as percentages of those retained:

$$\left.\begin{aligned}
\frac{1}{r}\frac{\partial}{\partial r}(r\,R\,U) + \frac{\partial}{\partial z}(R\,W) &= O(20\%)\,, && \text{1 term}\\
\frac{\partial P}{\partial r} &= R\,\frac{V^2}{r} + O(1\%)\,, && \text{2 terms}\\
\frac{\partial}{\partial z}(R\,V\,W) + \frac{1}{r^2}\frac{\partial}{\partial r}(r^2\,R\,\overline{u\,v}) &= O(15\%)\,, && \text{1 term}\\
\frac{\partial P}{\partial z} + \frac{\partial}{\partial z}(R\,W^2) + \frac{1}{r}\frac{\partial}{\partial r}(r\,R\,\overline{u\,w}) &= O(2\%)\,, && \text{1 term}
\end{aligned}\right\} \quad (3a)$$

or

$$\frac{\partial P}{\partial z} + \frac{1}{r}\frac{\partial}{\partial z}\left(r\,R\,\overline{u'\,w'}\right) = O(10\%)\,, \qquad \text{2 terms.}$$

The number of the larger rejected terms is indicated to the right.

Very likely the errors estimated for the continuity and tangential momentum equations are much too high. The more accurate forms of these equations are

$$\frac{1}{r}\frac{\partial}{\partial r}(r\,R\,U) + \frac{\partial}{\partial z}(R\,W) + \frac{1}{r}\frac{\partial}{\partial r}\left(r\,\overline{\varrho'\,u'}\right) = O(\delta\,\beta^{1/2}\,\eta)\,,$$

$$\frac{1}{r^2}\frac{\partial}{\partial r}(r^2\,R\,\overline{u\,v}) + \frac{\partial}{\partial z}(R\,V\,W) + \frac{1}{r^2}\frac{\partial}{\partial r}\left(r^2\,V\,\overline{\varrho'\,u'}\right) = O(\delta\,\varepsilon,\ \beta\,\delta)\,.$$

The estimates of the mixing terms were made on the basis of 100% correlation; for example, $\overline{\varrho'\,u'} \sim O(\beta^{1/2}\,\eta)$. In reality, the correlations will be much lower, and the error terms dependent on them correspondingly reduced. It seems likely that $\overline{\varrho'\,u'} > 0$ in vortex flows, since lighter lumps of the turbulent fluid will tend inwards under the action of Archimedean buoyancy forces. This finite correlation will definitely introduce errors into the simplified equations, although much smaller errors than those estimated above.

Finally, we conclude that the terms neglected in the simplified equations are probably only a few per cent of those retained. The simplified forms should represent the mass and momentum balances with accuracy sufficient for most purposes.

Although it is not possible to obtain integrals for this case, some of the gross features of the flows in the central part of the vortex tube can be grasped using the approximate relations (3, 3a).

The tangential momentum relation is no longer a simple balancing of the Reynolds' stress term against convection of mean vorticity; the effects of axial convection are not negligible here:

$$R\,U\left(\frac{\partial V}{\partial r} + \frac{V}{r}\right) + R\,W\,\frac{\partial V}{\partial z} = -\frac{1}{r^2}\frac{\partial}{\partial r}\left(r^2\,R\,\overline{u'\,v'}\right).$$

(Note that the simple continuity relations are sufficiently accurate in both systems of approximation to allow the mean-motion acceleration terms to be written in their more usual forms without altering the orders of the errors.)

The simple radial equilibrium relation,

$$\frac{\partial P}{\partial r} = R\frac{V^2}{r}$$

retains its applicability in this type of flow.

We have found in equations (3a) that the axial momentum equation can be simplified even farther, by dropping the mean-motion accelerations, without introducing disastrous errors. Although the final result is the least accurate of the set, it us sufficient to show that axial pressure changes are chiefly accountable to REYNOLDS' stresses. This result is in accord with the conclusion reached upon examination of the experimental results on which the estimates of the errors are based.

4. The Vortex Shape Hypothesis

A key feature of the two systems of approximation just considered is the relationship between the gradients within the vortex, the requirement that changes of any mean-value function be much more gradual in the axial direction than in the radial direction. It seems appropriate to term this a vortex shape hypothesis. The considerable simplifications of the equations of motion are chiefly accountable to the introduction of this concept.

The hypothesis has needed little justification in the two cases that have been examined. In the former, small perturbations were imposed on planar flows; in the latter, the elongated chamber in which the motion took place offered good reason for the assumption. But, as we shall now see, this approximation is useful for other vortex problems to which its applicability is not so immediately apparent.

On examining the swirling flow of water through a contracting conical chamber, BINNIE and TEARE [7] found a cylindrical air core. This parallel-sided streamsurface indicates that the hypothesis is valid away from the tapering sides of the chamber. The study of swirling flow through a convergent-divergent nozzle (BINNIE, HOOKINGS, and KAMEL [8]) revealed again a cylindrical air core in the contracting subcritical flow above the throat. The supercritical flow below the throat did not form a cylindrical core along the axis but fanned along the diverging walls. However, a supercritical flow will not necessarily violate the assumption that radial changes are very much more rapid than axial. If the flow is retained within a cylinder, the hypothesis may still be valid.

A somewhat similar situation is found in the vortices shed from lifting surfaces. Commonly they tighten in on the vortex core and the elongation hypothesis represents the pattern well. But a vortex burst phenomenon is sometimes encountered in trailing vortices [9], the tight core breaking up and the swirling fluid moving away from the axis. Another case of interest is a swirling jet emerging from an orifice or pipe into the atmosphere. Commonly the vortex spreads out, often leaving the core free for reversed flow.

Finally: there are cases for which the vortex shape hypothesis is not useful, but is does adequately represent the situation in the heart of the vortex for a variety of problems, not only flows confined within nozzles and tubes, but also some cases of unrestrained flow in the atmosphere.

The reasons for its wide applicability and the limitations to its applicability are not hard to see. In the first place, the radial and swirl velocity components must be zero on the vortex axis. Therefore, their gradients must be related as suggested by the elongation hypothesis. If, further, we have rapidly swirling fluid close to the axis (that is, a high angular velocity) the radial pressure gradient will be high in the core. This in turn leads to steep radial density gradients, whether by air core formation in a liquid or by the normal effect of compressibility in a gas.

Thus we see that the kinematical requirement of axisymmetry, together with the dynamical requirement of radial equilibrium for rapidly rotating flow, must specify a flow in which radial gradients are large compared to axial gradients. It is to be emphasized that this relationship will hold for the gradients of all the flow variables only if there is a high angular velocity in the fluid.

It is interesting to note that many of the highly developed branches of fluid mechanics depend on the assumption that changes in one direction are small compared to those in another. As examples we can mention boundary layer theory, the classical theory of surface waves, and the theory of the thin wing. The power of this hypothesis is not surprising. For fluid mechanical theory thrives on simplification of its initially difficult equations. And in a problem governed by equations with two independent variables a great simplification can almost always be made if the gradients in one direction are small. It seems safe to predict that this hypothesis has not yet reached the limit of its usefulness.

5. General Flow with High Swirl

We have seen that the vortex shape hypothesis used previously for the two special cases has a wider validity in high-swirl flows. We note also that the two sets of simplified equations (2, 3) contain, for the most part, the same terms. That is, only a few terms become important or lose their importance as we shift from one sort of flow to the other, while most of the terms of REYNOLDS' equations (1) are negligible for both categories.

It seems plausible that by combining the two sets, retaining the dominant terms of each class, we will obtain equations valid for a less restricted group of vortical flows, a group containing not only the two specified classes, but also the whole range of flows intermediate to them.

The combined set is

$$\left.\begin{aligned} \frac{1}{r}\frac{\partial}{\partial r}(r\,R\,U) + \frac{\partial}{\partial z}(R\,W) &= 0\,, \\ \frac{\partial P}{\partial r} &= R\,\frac{V^2}{r} - \frac{1}{r}\frac{\partial}{\partial r}(r\,R\,U^2)\,, \\ \frac{\partial}{\partial z}(R\,V\,W) + \frac{1}{r^2}\frac{\partial}{\partial r}(r^2\,R\,\overline{u\,v}) &= 0\,, \\ \frac{\partial P}{\partial z} + \frac{1}{r}\frac{\partial}{\partial r}(r\,R\,\overline{u\,w}) &= 0\,. \end{aligned}\right\} \tag{4}$$

We know that these equations are valid for large swirl so long as one of the other velocity components is small. But are they also valid when all the velocity components are of the same order? This is easily checked. Taking

$$U, V, W \sim O(1)\,, \quad \frac{\partial}{\partial r} \sim O(1)\,, \quad \frac{\partial}{\partial z} \sim O(\delta)\,, \quad \overline{u'^2},\ \overline{v'^2},\ \overline{w'^2} \sim O(\beta)\,,$$

we obtain the approximate forms

$$\left.\begin{aligned} r\,R\,U &= C + O(\delta)\,, \\ \frac{\partial P}{\partial r} &= R\,\frac{v^2}{r} - \frac{1}{r}\frac{\partial}{\partial r}(r\,R\,U^2) + O(\delta, \beta)\,, \\ r^2\,R\,U\,V &= G + O(\delta, \beta)\,, \\ r\,R\,U\,W &= F + O(\delta, \beta)\,. \end{aligned}\right\} \tag{5}$$

These results are contained in the general set (4). For this degenerate case all the REYNOLDS' stresses are found to be negligible and explicit solutions are possible.

The problem of the turbulent vortex is still intractable in the simplified form (4): we have two more dependent variables than governing equations. However, the order-of-magnitude analysis has been useful in displaying the essentials of the mechanics of flows with high swirl.

The effects of compressibility are now represented solely by the time-mean density; the continuity and radial equilibrium relations are not directly influenced by turbulence; only two of Reynolds' apparent stresses are found to be important in determining the motion – those acting on cylindrical surfaces.

Notation

r	radial co-ordinate;
z	axial co-ordinate;
u, U, u'	radial velocity component, its time-mean value, and the turbulent perturbation to it;
v, V, v'	tangential or swirl velocity component, etc.;
w, W, w'	axial velocity component, etc.;
p, P, p'	fluid pressure, etc.;
ϱ, R, ϱ'	fluid density, etc.;
$\beta, \delta, \varepsilon, \eta$	numbers small with respect to unity;
C, F, G, G_0	constants of integration.

REFERENCES

[1] R. G. DEISSLER and M. PERLMUTTER, *An Analysis of the Energy Separation in Laminar and Turbulent Compressible Vortex Flows*, Proc. 1958. Heat Transfer and Fluid Mechanics Institute, Stanford University, Palo Alto, California.

[2] J. E. LAY, *An Experimental and Analytical Study of Vortex-Flow Temperature Separation by Superposition of Spiral and Axial Flows*, Trans. ASME, *81* [C], 3, 202, 213 (1959).

[3] R. R. LONG, *Sources and Sinks at the Axis of a Rotating Liquid*, Johns Hopkins University, Civil Engineering Dept., Techn. Rep. *9* (1957).

[4] C. D. PENGELLEY, *Flow in a Viscous Vortex*, J. Appl. Phys., *28*, 1, 86 (1957).

[5] N. ROTT, *On the Viscous Core of a Line Vortex*, Z. angew. Math. Phys. IXb, 5/6, 543 (1958); X, 1, 73 (1959).

[6] L. A. VULIS and B. P. USTIMENKO, *Über die Aerodynamik der Zyklonfeuerungskammern*, Energietechnik, *5*, 6, 265 (1955).

[7] A. M. BINNIE and J. D. TEARE, *Experiments on the Flow of Swirling Water through a Pressure Nozzle and an Open Trumpet*, Proc. Roy. Soc. Lond., *A 235*, 78 (1956).

[8] A. M. BINNIE, G. A. HOOKINGS, and M. Y. M. KAMEL, *The Flow of Swirling Water through a Convergent-Divergent Nozzle*, J. Fl. Mech., *3*, 261 (1957–8).

[9] B. J. ELLE, *On the Breakdown at High Incidences of the Leading Edge Vortices on Delta Wings*, J. Roy. Aero. Soc., *64*, 596, 491 (1960).

Zusammenfassung

Die Wirbelströmung in einer turbulenten kompressiblen Flüssigkeit wird behandelt. Die Bewegungsgleichungen werden durch die Vernachlässigung der kleineren Glieder vereinfacht. Die experimentellen Ergebnisse erlauben eine Fehlerrechnung für einen Fall. Ein wichtiger Schritt in der Vereinfachung ist die Voraussetzung, dass die Radialgradienten viel grösser sind als die Axialgradienten. Für die kräftigen Wirbel erwies sich diese Annahme sowohl durch die Erfahrung als auch aus den wesentlichen theoretischen Betrachtungen heraus als begründet. Die vereinfachten Gleichungen zeigen einige wichtige Aspekte der schnelldrehenden Strömungen und geben einen Anhaltspunkt für die ausführlicheren Studien.

[Received: September 16, 1960.]

An Investigation into the Mechanism of Ice Crystal Nucleation by Proton Spin Resonance Spectroscopy

By Geoffrey T. Barnes and Raymund Sänger, Zürich[1])

In experiments on weather modification silver iodide is dispersed in the atmosphere and under certain conditions causes marked changes in the pattern of precipitation. These phenomena are due to the activity of silver iodide as an ice forming agent, but the mechanism of this process is not yet fully understood. This paper reports on some preliminary experiments in a program aimed at elucidating the mechanism of ice nucleation by silver iodide and other nucleants.

Three mechanisms have been considered in order to account for the formation of ice crystals when nuclei are introduced into a cloud of supercooled water droplets (e. g. see Mason and van den Heuvel [1][2]) and Sänger [2]).

(a) In 'freezing' nucleation the nuclei are thought to act by collision with supercooled droplets in the cloud, causing them to freeze. Statistical considerations and several experimental observations (Katz [3] and Koenig [4]) indicate that this process is relatively unimportant in cloud seeding experiments.

(b) In the 'pure sublimation' process the nuclei adsorb water vapour from the atmosphere directly into an ice-like structure.

(c) In what might be called condensation-freezing nucleation water vapour is first adsorbed onto the nuclei to form a liquid layer which later freezes.

In all three mechanisms the embryo ice crystals thus formed can grow further by transport (through the vapour) of water molecules from nearby liquid droplets in the cloud.

All three mechanisms are idealized cases as they assume that the surfaces of the nuclei are initially free of adsorbed water, but, unless special efforts have been made to achieve this condition, the assumption is undoubtedly incorrect for most, if not all, nucleants. For example, Birstein [5] has shown that at temperatures as high as 20°C and at 50% relative humidity there are some four to eight molecular layers of water on AgI and PbI_2 powders. We must therefore assume that, normally, ice forming nucleation follows a mechanism in which an appreciable amount of the water required to initiate the growth of ice crystals is already present on the nuclei when they are injected into the cloud.

The activity of the introduced nuclei thus depends on the physical state of this adsorbed water when the particles have assumed the temperature of the cloud. If the adsorbed water is all in a liquid-like or disordered state there will be no activity; if some or all is in an ice-like or ordered state the nuclei may be active if other factors, such as the aqueous vapour pressure, are favourable. Since particular nuclei may be inactive at one temperature and active at some lower temperature, these ideas imply that there must be a phase transition involving at least some of the adsorbed water as the nuclei change from an inactive to an active condition (or *vice versa*). Therefore, in order to demonstrate the feasibility of this ice nucleation

[1]) Laboratory of Atmospheric Physics, Swiss Federal Institute of Technology.

[2]) Numbers in brackets refer to references, page 163.

process it is first necessary to show that such phase transitions do occur on ice forming nuclei. This is the purpose of the experiments described here. In some other systems transitions in adsorbed layers have been observed previously (e. g. FISHER and MCMILLAN [6]; MAYS and BRADY [7].

It should be noted that the adsorbed water need not (and usually will not) be uniformly distributed over the surface. Nor is it necessary for the transition of the whole adsorbed layer on a particle to occur at the one temperature: water films on different parts of the particle may well have quite different transition points, either because of variations in the thickness of the adsorbed film or because of differences in the surface structure of the nucleus. Furthermore, the proposed model does not rule out the possibility that the first adsorbed layer is more or less immobile even at temperatures where the overlying layers are fluid.

At first sight it would appear that the formation of an ice embryo on a particular nucleus should be a function of the temperature only. However in experiments with silver iodide in clouds formed from salt solutions of various concentrations KATZ [8] has observed that a particular activity value[3]) was always reached at the same degree of supersaturation with respect to ice and *not* at the same temperature. Two alternative explanations consistent with our hypothesis on ice forming nucleation can be advanced: firstly, that the degree of supersaturation has no effect on the formation of stable ice embryos, but does markedly affect their further growth into visible ice crystals; or secondly, that initially the ordered zones are unstable and will revert to a disordered condition unless the supply of water vapour is sufficient to cause rapid growth to a stable size.

The model suggested would also provide an explanation for the effect of particle size, as observed by HOSLER and SPALDING [9] and by SANO, FUJITANI, and MAENA [10].

To demonstrate the existence of phase transitions in the adsorbed water films on ice forming nuclei we have made use of the nuclear spin resonance of the protons in the adsorbed water molecules. If the molecules are able to move fairly freely the local magnetic fields due to neighbouring water molecules tend to average out and the nuclear magnetic resonance (NMR) spectrum exhibits a sharp proton resonance line. However if movement is appreciably hindered, as in an ice-like structure, this averaging out is no longer possible and the local fields will vary somewhat from proton to proton leading to a broadening of the resonance line.

The NMR spectrometer is basically that described by PRIMAS and GÜNTHARD [11] modified by ARNDT [12] for low resolution work with solids. The B_0 field is provided by a permanent magnet of approximately 6,000 gauss, corresponding to a proton resonance frequency of 25 megacycles. The usual modulation method for solid state NMR was used, giving the first derivative of the absorption curve. In the present experiments the modulation amplitude was 43·2 milligauss. With AgI the sweep rate was 2·41 m gauss/sec, and with CuO it was 4·88 m gauss/sec. In both cases the time constant of the final amplifier stage was set at 2 sec.

Samples of AgI, CuO, Cu_2O, and CuS from the same batches as those used by KATZ [8, 13] were prepared by allowing them to stand in air saturated with water vapour at 0°C for several days. The surface areas of these samples have been determined by ZETTLEMOYER [14]; the values found by water vapour adsorption are given in Table 1.

Examination of the samples at room temperature showed a well defined proton resonance signal with CuO, a weaker signal with AgI, and no observable signals

[3]) The activity is defined as the ratio of the number of ice crystals observed in a supercooled cloud to the total number of nucleating particles introduced into the cloud.

with Cu_2O or CuS. Accordingly only AgI and CuO could be used in studying the effects of temperature on the proton resonance signal. Owing to the low concentrations of protons in these samples (ca. 10^{19} protons within the detector coil compared with 10^{22} for liquid water) it was necessary to operate the spectrometer near its maximum sensitivity. Consequently the signal to noise ratio was rather low and precise delineation of the spectra was not possible. Figure 1 shows some

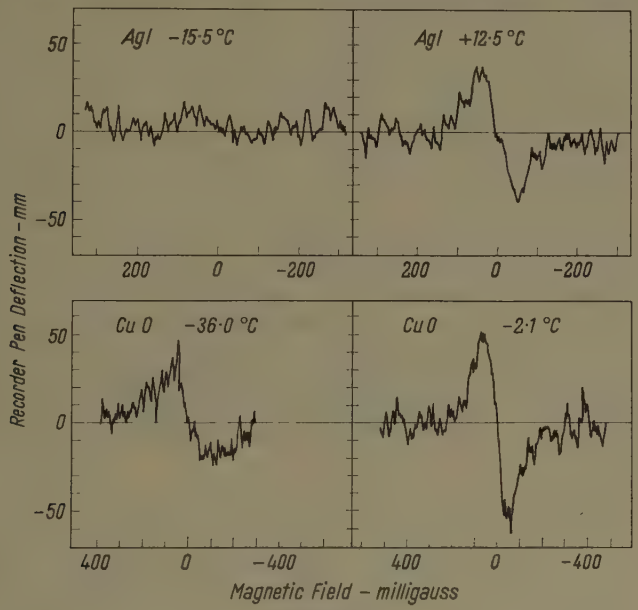

Figure 1

Typical proton spin resonance spectra (including noise) of the adsorbed water films on AgI and CuO powders at various temperatures.

typical records. Obviously with records similar to that of AgI at − 15·5°C (Figure 1) the existence of a spectral line can only be ascertained after scanning the region several times.

When the sample temperature was lowered there was at first no effect on the resonance signal, then at a certain temperature the wave height began to decrease. However the line width remained approximately constant throughout the entire temperature range with both samples, indicating that with decreasing temperature the observed signal from liquid-like adsorbed water was being replaced by a much broader, shallower signal from the ice-like state which we were unable to detect.

The effects of temperature on the amplitudes of the resonance signals (in arbitrary units) are shown in Figure 2. The wave height data for the two different samples cannot be directly compared as different B_1 (exciting) fields were used and no precise calibration was available. However this is of little importance at present as the most interesting observation for our purpose is in the comparison along the temperature scale.

For both samples the curves exhibit breaks which may be interpreted as the onset of ordering or 'freezing' (with falling temperature) or the completion of

disordering or 'melting' (with rising temperature) in the adsorbed water films. It is interesting to note also that the change in wave height, and hence the order-disorder transition, was not abrupt but was spread over a wide temperature range of more than twenty degrees. This spread could be due to differences in the transition temperatures for different particles in the sample or to heterogeneity in the films on individual particles. Probably both factors contribute.

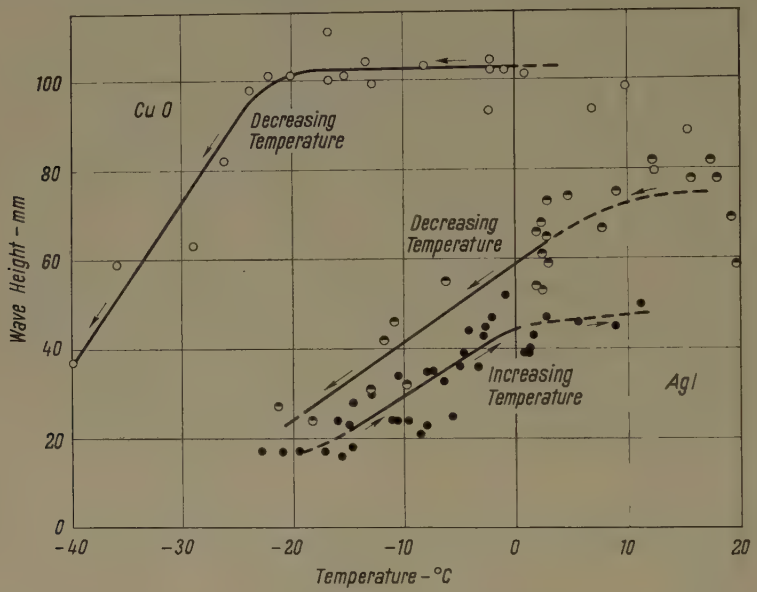

Figure 2

The effect of sample temperature on the wave height of the proton spin resonance signal from water adsorbed on AgI und CuO powders.

Thus it is clear from Figure 2 that the adsorbed film on AgI has a much higher transition temperature than that on CuO, and in accordance with the model for ice crystal nucleation outlined above there should be a corresponding difference in the temperatures at which these powders act as nuclei. This relationship is shown in Table 1, using the nucleation data of Katz [8, 13].

In comparing the results in Table 1 a number of complicating factors must be considered. Firstly, the high noise level in the NMR spectra introduces considerable error in the measurement of wave height; this is especially noticeable in the curve for AgI with decreasing temperature. Secondly, whereas it is possible to detect one active nucleus in 10^6 in the cloud chamber experiments, it is impossible to observe a decrease in wave height with this sensitivity. Thirdly, other conditions, such as the aqueous vapour pressure, may influence one or both types of experiment.

Bearing these difficulties in mind, the agreement between the nucleation and NMR data does appear to be good enough to support the mechanism of ice forming nucleation which we have discussed above. Further work with substances of higher specific area should yield more accurate spin resonance data and enable a more quantitative appraisal of the suggested nucleation mechanism to be made.

Table 1

Specific surface areas [14], ice crystal nucleation data [8, 13], and the onset of ordering or 'freezing' (transition temperature) in the adsorbed water films on nuclei as determined by proton spin resonance measurements.

Substance	Surface Area (by H_2O ads.) (m^2/g)	Nucleating Activity (fraction of active nuclei)	Nucleation Temperature (°C)	Transition Temperature (°C)
AgI	0·14	10^{-4} 10^{-3}	− 4 − 6	+ 5 (± 5) (cooling) − 1 (± 3) (warming)
CuO	4·7	10^{-4} 10^{-3}	− 18 − 26·5	− 22 (± 3) (cooling)

It is a pleasure to thank Prof. H. H. Günthard and Mr. R. Arndt, Laboratory for Physical Chemistry, ETH, for their cooperation and assistance in the spin resonance studies, and Prof. A. C. Zettlemoyer, Lehigh University, Bethlehem, Pa., for the surface area data. This work is partly supported by Federal Funds and partly by a grant to the ETH from Dr. D. Bührle, Werkzeugmaschinenfabrik, Oerlikon, Zürich. The investigation is part of the research program of the Swiss Federal Commission for the Study of Hail Formation and Prevention.

REFERENCES

[1] B. J. Mason, and A. P. van den Heuvel, Proc. Phys. Soc. *74*, 744 (1959).
[2] R. Sänger, Bull. Obs. Puy de Dôme *1957*, 75.
[3] U. Katz, Private Communication.
[4] L. R. Koenig, J. Met. *17*, 426 (1960).
[5] S. J. Birstein, J. Met. *12*, 324 (1955).
[6] B. B. Fisher, and W. G. McMillan, J. Chem. Phys. *28*. 549 (1958).
[7] J. M. Mays, and G. W. Brady, J. Chem. Phys. *25*, 583 (1956).
[8] U. Katz, Z. angew. Math. Phys. *12*, 76 (1961).
[9] C. L. Hosler, and G. R. Spalding, in: H. Weickmann and W. Smith, *Artificial Stimulation of Rain* (Pergamon Press, London 1957), p. 369.
[10] I. Sano, Y. Fujitani, and Y. Maena, J. met. Soc. Japan, Ser. II *34*, 104 (1956).
[11] H. Primas, and H. H. Günthard, Helv. Phys. Acta *30*, 315 (1957); Rev. Sci. Instr. *28*, 510 (1957).
[12] R. Arndt, Thesis, ETH, Zürich (1961).
[13] U. Katz, Z. angew. Math. Phys. *11*, 237 (1960).
[14] A. C. Zettlemoyer, Private Communication.

Zusammenfassung

Unter Heranziehung der Kernresonanzspektroskopie wird versucht, den Vorgang der Keimbildung an Eiskeimbildungskernen wie AgI und CuO abzuklären. Die Ergebnisse der ersten Versuche zeigen, dass die adsorbierte Wasserschicht unterhalb einer bestimmten Temperatur, die nahe der Schwellentemperatur für die Eis-

keimbildungsaktivität liegt, teilweise in einem flüssigkeitsartigen und teilweise in festkörperartigem Zustand auftritt. Bei abnehmender Temperatur wächst der feste Anteil der Schicht auf Kosten des flüssigen Bestandes. Der volle Verfestigungsvorgang wickelt sich dabei in einem Temperaturbereich von ca. 20°C ab. Die Beobachtungen legen es nahe, anzunehmen, dass zwischen dem Auftreten der eisartigen Struktur in der adsorbierten Schicht und der Eisbildungswirksamkeit der Kernstoffe eine Beziehung besteht.

(Received: January 3, 1961.)

Two-Dimensional Steady Temperature Fields in a Stratiform Half-Space

By Václav Vodička, Plzeň, Czechoslovakia

1. Statement of the problem. The half-space

$$x \geqq x_0, \quad -\infty < y < +\infty, \quad -\infty < z < +\infty$$

is made of n homogeneous isotropic parts

$$x_{k-1} \leqq x \leqq x_k, \quad -\infty < y < +\infty, \quad -\infty < z < +\infty, \quad 1 \leqq k \leqq n-1,$$

$$x \geqq x_{n-1}, \quad -\infty < y < +\infty, \quad -\infty < z < +\infty,$$

with thermal conductivities λ_k, respectively. The question is to determine the steady temperature distribution in the solid, provided that the front face $x = x_0$ is kept at the temperature $f(y)$ and that there is continuity both of the temperature and of the flux at the surfaces of separation between several parts of the body.

Mathematically speaking we have to find the solution $u_k = u_k(x, y)$ of the equations

$$\frac{\partial^2 u_k}{\partial x^2} + \frac{\partial^2 u_k}{\partial y^2} = 0, \quad x_{k-1} < x < x_k, \quad -\infty < y < +\infty, \quad 1 \leqq k \leqq n-1, \tag{1.1}$$

$$\frac{\partial^2 u_n}{\partial x^2} + \frac{\partial^2 u_n}{\partial y^2} = 0, \quad x > x_{n-1}, \quad -\infty < y < +\infty \tag{1.2}$$

with the following conditions:

$$\left.\begin{aligned} u_1(x_0, y) &= f(y), \quad -\infty < y < +\infty, \\ u_k(x_k, y) &= u_{k+1}(x_k, y), \quad -\infty < y < +\infty, \end{aligned}\right\} \tag{2.1}$$

$$\Lambda_k \frac{\partial u_k}{\partial x} = \frac{\partial u_{k+1}}{\partial x}, \quad x = x_k, \quad -\infty < y < +\infty, \quad \Lambda_k = \frac{\lambda_k}{\lambda_{k+1}}, \quad 1 \leqq k \leqq n-1 \tag{2.2}$$

$$\lim_{x \to +\infty} u_n(x, y) = 0, \quad -\infty < y < +\infty. \tag{2.3}$$

2. The Fourier transforms of $u_k(x, y)$. Making the usual assumptions on the disappearance of u_k and $\frac{\partial u_k}{\partial y}$ for $|y| \to \infty$ the familiar transformation

$$\left.\begin{aligned} \bar{h}(\eta) = F[h(y)] &= \frac{1}{\sqrt{2\pi}} \int_{-\infty}^{+\infty} h(y)\, e^{i\eta y}\, dy\,, \\ h(y) = F^{-1}[\bar{h}(\eta)] &= \frac{1}{\sqrt{2\pi}} \int_{-\infty}^{+\infty} \bar{h}(\eta)\, e^{-i\eta y}\, d\eta \end{aligned}\right\} \tag{3}$$

changes our problem (1. 1)–(2. 3) into the equations

$$\frac{d^2\bar{u}_k}{dx^2} - \eta^2\, \bar{u}_k = 0, \quad x_{k-1} < x < x_k, \quad k = 1, 2, \ldots, n-1\,, \tag{4.1}$$

$$\frac{d^2\bar{u}_n}{dx^2} - \eta^2\, \bar{u}_n = 0\,, \quad x > x_{n-1}\,, \tag{4.2}$$

$$\bar{u}_1(x_0, \eta) = \bar{f}(\eta)\,, \tag{5.1}$$

$$\bar{u}_{k+1}(x_k, \eta) = \bar{u}_k(x_k, \eta)\,, \quad \frac{d\bar{u}_{k+1}}{dx} = \Lambda_k \frac{d\bar{u}_k}{dx}\,, \quad x = x_k, \quad k = 1, 2, \ldots, n-1, \tag{5.2}$$

$$\lim_{x \to +\infty} \bar{u}_n(x, \eta) = 0 \tag{5.3}$$

for determining the Fourier transforms $\bar{u}_k(x, \eta)$ of the required functions $u_k(x, y)$.

Integrating (4.1) and (4.2) gives generally

$$\bar{u}_k(x, \eta) = A_k \cosh(x - x_{k-1})\, \eta + B_k \sinh(x - x_{k-1})\, \eta, \quad 1 \leqq k \leqq n\,, \tag{6}$$

where the coefficients A_k, B_k are to be found from (5.1)–(5.3) i. e. from the equations

$$A_1 = \bar{f}(\eta), \quad A_n + B_n = 0\,, \tag{7.1}$$

$$A_{k+1} = A_k \cosh l_k\, \eta + B_k \sinh l_k\, \eta\,,$$

$$B_{k+1} = \Lambda_k (A_k \sinh l_k\, \eta + B_k \cosh l_k\, \eta), \quad l_k = x_k - x_{k-1}, \quad 1 \leqq k \leqq n-1. \tag{7.2}$$

Introducing the matrices

$$K_k = \left\| \begin{matrix} A_k \\ B_k \end{matrix} \right\|, \quad 1 \leqq k \leqq n, \quad M_k(\eta) = \left\| \begin{matrix} \cosh l_k\, \eta, & \sinh l_k\, \eta \\ \Lambda_k \sinh l_k\, \eta, & \Lambda_k \cosh l_k\, \eta \end{matrix} \right\|, \quad 1 \leqq k \leqq n-1\,,$$

$$Q_k(\eta) = M_k(\eta)\, M_{k-1}(\eta) \cdots M_2(\eta)\, M_1(\eta), \quad 1 \leqq k \leqq n-1\,, \tag{8}$$

the well-known manipulation with (7.2) and with the first equation (7.1) gives us [2][1])

$$K_{k+1} = Q_k(\eta) \left\| \begin{matrix} \bar{f}(\eta) \\ B_1 \end{matrix} \right\|, \quad 1 \leqq k \leqq n-1\,. \tag{9}$$

[1]) Numbers in brackets refer to References, page 168.

Writing $Q_{n-1}(\eta) = \left\| q_{n-1}^{(r,s)}(\eta) \right\|$, $r, s = 1, 2$, expressing A_n and B_n from the last equation (9) and inserting into the second condition (7.1) yields the value of B_1. On the whole, one finds the following expressions for the coefficients A_k, B_k:

$$A_1 = \bar{f}(\eta), \quad B_1 = -\frac{Z(\eta)}{N(\eta)}\bar{f}(\eta),$$

$$\begin{Vmatrix} A_{k+1} \\ B_{k+1} \end{Vmatrix} = \frac{Q_k(\eta)}{N(\eta)} \begin{Vmatrix} N(\eta) \\ -Z(\eta) \end{Vmatrix} \bar{f}(\eta), \quad 1 \leqq k \leqq n-1,$$

$$Z(\eta) = q_{n-1}^{(11)}(\eta) + q_{n-1}^{(21)}(\eta), \quad N(\eta) = q_{n-1}^{(12)}(\eta) + q_{n-1}^{(22)}(\eta); \tag{10}$$

$\bar{f}(\eta)$ is the Fourier transform of $f(y)$.

The main difficulty lies in finding the matrices $Q_k(\eta)$. The first of them, $Q_1(\eta)$, $Q_2(\eta)$ and $Q_3(\eta)$, are given explicitely in [2].

3. General solution of the problem (1.1)–(2.3). Finding $A_k = A_k(\eta)$, $B_k = B_k(\eta)$ from (10) and substituting into (6) gives $\bar{u}_k(x, \eta)$ and from this one obtains, by aid of (3), the required solution

$$u_k(x, y) = \frac{1}{\sqrt{2\pi}} \int_{-\infty}^{+\infty} [A_k \cosh(x - x_{k-1})\eta + B_k \sinh(x - x_{k-1})\eta] e^{-i\eta y} d\eta, \quad 1 \leqq k \leqq n. \tag{11}$$

4. A homogeneous half-space. In this case we have $\Lambda_1 = \Lambda_2 = \cdots = \Lambda_{n-1} = 1$ and the matrices $Q_k(\eta)$ are expressible in closed form

$$Q_k(\eta) = \begin{Vmatrix} \cosh(x_k - x_0)\eta, & \sinh(x_k - x_0)\eta \\ \sinh(x_k - x_0)\eta, & \cosh(x_k - x_0)\eta \end{Vmatrix}, \quad 1 \leqq k \leqq n-1.$$

Using this, the formulae (10) give

$$Z(\eta) = N(\eta) = e^{(x_{n-1} - x_0)\eta},$$

$$A_1 = -B_1 = \bar{f}(\eta),$$

$$A_{k+1} = -B_{k+1} = e^{-(x_k - x_0)\eta}\bar{f}(\eta), \quad 1 \leqq k \leqq n-1$$

and the solution (11) appears in the form

$$u(x, y) = \frac{1}{\sqrt{2\pi}} \int_{-\infty}^{+\infty} \bar{f}(\eta) e^{-(x - x_0 + iy)\eta} d\eta \tag{12}$$

which is valid for the whole extent of the solid.

Using the well-known result

$$e^{-\alpha\eta} = \frac{2\alpha}{\pi} \int_0^{\infty} \frac{\cos \eta\varrho}{\alpha^2 + \varrho^2} d\varrho = \frac{\alpha}{\pi} \int_{-\infty}^{+\infty} \frac{e^{i\varrho\eta}}{\alpha^2 + \varrho^2} d\varrho$$

of LAPLACE shows – see (3) – that

$$e^{-\alpha\eta} = \alpha \sqrt{\frac{2}{\pi}} F\left[\frac{1}{\alpha^2 + y^2}\right] \tag{13}$$

and the convolution theorem for Fourier transforms changes the solution (12) into its customary form [3]

$$u(x, y) = \frac{x - x_0}{\pi} \int_{-\infty}^{+\infty} \frac{f(\varrho)}{(x - x_0)^2 + (y - \varrho)^2} \, d\varrho \,. \tag{14}$$

5. A half-space of two parts. Here we have $n = 2$ and the relations (10) give

$$Z(\eta) = e^{l_1 \eta} + (\Lambda_1 - 1) \sinh l_1 \eta, \qquad N(\eta) = e^{l_1 \eta} + (\Lambda_1 - 1) \cosh l_1 \eta \,,$$

$$N(\eta) \, [A_1 \cosh (x - x_0) \, \eta + B_1 \sinh (x - x_0) \, \eta]$$

$$= \bar{f}(\eta) \, [e^{(x_1 - x) \eta} + (\Lambda_1 - 1) \cosh (x_1 - x) \, \eta] \,,$$

$$N(\eta) \, [A_2 \cosh (x - x_1) \, \eta + B_2 \sinh (x - x_1) \, \eta] = \Lambda_1 \, e^{(x_1 - x) \eta} \, \bar{f}(\eta)$$

and the solution (11) appears in the form

$$u_1(x, y) = \frac{1}{\sqrt{2\pi}} \int_{-\infty}^{+\infty} \frac{\bar{f}(\eta)}{N(\eta)} \, [e^{(x_1 - x) \eta} + (\Lambda_1 - 1) \cosh (x_1 - x) \, \eta] \, e^{-i\eta y} \, d\eta \,,$$

$$u_2(x, y) = \frac{\Lambda_1}{\sqrt{2\pi}} \int_{-\infty}^{+\infty} \frac{\bar{f}(\eta)}{N(\eta)} \, e^{(x_1 - x) \eta - i\eta y} \, d\eta \,,$$

$$N(\eta) = e^{(x_1 - x_0) \eta} + (\Lambda_1 - 1) \cosh (x_1 - x_0) \eta \,. \tag{15}$$

If especially $\Lambda_1 = 1$, then our result (15) changes into (14). Generally, the integrations in (15) are to be accomplished by numerical methods, for the exact calculations are exceedingly difficult. Apart from the above special case $\Lambda_1 = 1$ and from the artificial cases characterized by $\Lambda_1 = 0$ or $\Lambda_1 = \infty$ the author of the present paper does not know any situation with arbitrary $f(y)$, where it would be possible to express the solution in any kind of closed form like that of ref. [2].

Nevertheless, there exist special functions $f(y)$ admitting fargoing simplifications of the above complicated result (15). To give an example let us take

$$f(y) = - \frac{l_1 \sqrt{2}}{\sqrt{\pi} \, (l_1^2 + y^2)} \,, \qquad - \infty < y < + \infty \,. \tag{16}$$

Writing this in the form,

$$f(y) = \frac{l_1}{\sqrt{2\pi}} \left(\frac{\Lambda_1 - 1}{l_1^2 + y^2} - \frac{\Lambda_1 + 1}{l_1^2 + y^2} \right)$$

and using (13) gives

$$\bar{f}(\eta) = \frac{l_1}{\sqrt{2\pi}} \left[\frac{(\Lambda_1 - 1) \sqrt{\pi}}{l_1 \sqrt{2}} \, e^{-l_1 \eta} + \frac{(\Lambda_1 + 1) \sqrt{\pi}}{l_1 \sqrt{2}} \, e^{l_1 \eta} \right]$$

$$= \frac{1}{2} \, [(\Lambda_1 - 1) \, e^{-l_1 \eta} + (\Lambda_1 + 1) \, e^{l_1 \eta}] = e^{l_1 \eta} + (\Lambda_1 - 1) \cosh l_1 \eta = N(\eta) \,.$$

Hence, applying again (13), the solution (15) becomes

$$u_1(x, y) = \sqrt{\frac{2}{\pi}} \cdot \frac{x - x_1}{(x - x_1)^2 + y^2}, \qquad u_2(x, y) = \Lambda_1 u_1(x, y) . \tag{17}$$

REFERENCES

[1] Vodička, V., *Some Problems on Heat Conduction in Stratiform Bodies*, J. phys. Soc. Jap. *14*, 216 (1959).
[2] Vodička, V., *Steady Temperature Field in a Composite Doubly Infinite Strip*, J. phys. Soc. Jap. *15* (1960).
[3] Carslaw, H. S., and Jaeger, J. C., *Conduction of Heat in Solids* (Oxford, 1947), p. 146.

Zusammenfassung

Für einen aus n Schichten verschiedener Wärmeleitfähigkeit bestehenden unendlichen Halbraum wird die Temperaturverteilung berechnet, die sich einstellt, wenn an der freien Oberfläche ein beliebiger Temperaturverlauf vorgeschrieben wird. Eine geschlossene Darstellung ist im allgemeinen nicht möglich, doch gibt es Fälle, wo die Lösung verhältnismässig einfach wird.

(Received: Juli 7, 1960.)

Varia – Miscellaneous – Divers

Numerische Methoden in der Meteorologie

Von Walter Kuhn[1]), Zürich

Zusammenfassender Bericht

1. Problemstellung, Vorläufer

Die Atmosphäre empfängt Strahlungsenergie von der Sonne und von der Erdoberfläche; sie sendet selber Strahlung aus. An der flüssigen und festen Erdoberfläche werden zwischen Erde und Atmosphäre Wärme und Wasser ausgetauscht. Die unterste Luftschicht unterliegt je nach ihrer Bewegung und je nach dem Zustand der Erdoberfläche veränderlichen Reibungskräften. Abgesehen von diesen äusseren Einwirkungen, die sich quantitativ erfassen lassen, kann die Atmosphäre als ein geschlossenes mechanisch-thermodynamisches System betrachtet werden. Auf jedes Luftteilchen wirkt die Gravitation und die von der Rotation der Erde herrührende Corioliskraft.

Die Gesetze, welche die Zustandsänderungen im Innern der Atmosphäre beherrschen, sind im wesentlichen bekannt: 1. Die hydrodynamische Bewegungs-

[1]) Schweizerische Meteorologische Zentralanstalt.

gleichung, aufspaltbar in drei Komponenten, 2. die Kontinuitätsgleichung, 3. die Zustandsgleichung idealer Gase, 4. der erste und zweite Hauptsatz der Thermodynamik, 5. die Gesetze der Phasenumwandlungen des Wassers, 6. die Gesetze des turbulenten Austausches von Impuls, Wärme und Wasserdampf, 7. die Strahlungsgesetze.

Im Sinne der deterministischen Physik bestimmt ein momentaner Zustand alle späteren Zustände. Es stellt sich deshalb die Frage: Wie lassen sich bei hinreichend genauer Kenntnis eines Anfangszustandes spätere Zustände *berechnen*?

Bjerknes [1][2]), der Schöpfer der dynamischen Meteorologie, hat dieses Problem bereits 1904 exakt formuliert und seine Schwierigkeiten klar erkannt. Sie liegen auf vier Gebieten:

a) Lückenhafte und ungenaue Beobachtungen über den dreidimensionalen Anfangszustand, b) theoretisch-physikalische Schwierigkeiten: Erfassung der meteorologisch bedeutsamen Vorgänge und Herausfilterung kleinräumiger Störungen durch gezielte Vereinfachung der Grundgleichungen, c) mathematische: Integration eines komplizierten Systems partieller Differentialgleichungen mit unsicheren Randbedingungen, d) Arbeitsaufwand im Hinblick auf routinemässige Anwendung.

Bjerknes war sich klar darüber, dass eine strenge analytische Lösung des Problems in voller Allgemeinheit kaum je in Frage kommen dürfte. Er empfahl, sich zuerst auf die rein hydrodynamische Seite zu beschränken und die Verquikkung mit thermodynamischen Prozessen einer späteren Erweiterung vorzubehalten. Auch erkannte er, dass nur *numerische* oder *graphische* Integrationsmethoden zum Ziele führen würden. Bjerknes wurde in der Folge durch seine Polarfrontlehre so stark in Anspruch genommen, dass er sich selber dem Problem der rechnerischen Wettervorhersage nicht mehr widmen konnte.

Einen originellen und scharfsinnig angelegten Versuch unternahm in den Jahren 1911–1921 der Engländer F. L. Richardson [2]. Leider stimmte das Ergebnis seiner mühevollen Rechnungen schlecht mit der Wirklichkeit überein, ohne dass er und seine Zeitgenossen die Ursachen des Misserfolges völlig klar erkennen konnten.

Es war naheliegend, dass man neben den hydrodynamischen Bewegungsgleichungen vorab die Kontinuitätsgleichung heranzog, weil sie Änderungen der Dichte mit *Vergenzen* (Divergenzen und Konvergenzen) des Strömungsfeldes in Verbindung bringt. Da man über die vertikale Komponente der Luftbewegung a priori nichts wusste, versuchte man den Vergenzeffekt längs einer vertikalen Luftsäule vom Boden bis zur oberen Grenze der Atmosphäre zu integrieren (sogenannte Tendenzgleichung), um die Druckänderung am Boden zu berechnen. Dabei machte man aber zwei entmutigende Feststellungen: 1. Die Genauigkeit der Windmessungen reichte nicht entfernt zur Berechnung der Vergenzen aus. 2. In einer vertikalen Luftsäule überlagern sich jederzeit gegensinnige Vergenzen, so dass der integrierte Effekt viel kleiner ist als die Beiträge einzelner Schichten.

Damit war das Problem der Vorausberechnung von Wetterkarten einstweilen in eine hoffnungslose Sackgasse geraten, aus der es erst 1948 durch die bahnbrechenden Untersuchungen von Charney und seinen Mitarbeitern befreit wurde.

Inzwischen hatte die Aerologie, dh. die direkte Erforschung der freien Atmosphäre, durch die Schaffung eines weltweiten Netzes täglicher Radiosondierungen einen ungeahnten Aufschwung genommen. Aber auch die Dynamik der Luftströmungen hatte einige Fortschritte aufzuweisen:

[2]) Ziffern in eckigen Klammern verweisen auf das Literaturverzeichnis; Ziffern in runden Klammern auf die Formeln am Ende dieses Berichtes.

Rossby [3] hatte 1939 eine bestimmte Wirbelgrösse, die sogenannte *absolute Vorticity*, in die Meteorologie eingeführt und mit Erfolg auf die Verlagerung langer Wellen in einer zonalen Grundströmung angewendet. Die absolute Vorticity ist definiert als Vertikalkomponente des absoluten Rotors, wobei wir unter dem absoluten Rotor den Drehvektor in bezug auf ein nicht mit der Erde rotierendes Inertialsystem verstehen. Demnach setzt sich die absolute Vorticity zusammen aus der relativen Vorticity, welche von der Drehung und Scheerung des horizontalen Windfeldes herrührt, und der Projektion des Erdrotations-Vektors auf die Vertikale; diese Komponente, Coriolis-Parameter genannt, hängt nur von der geographischen Breite ab. Für die absolute Vorticity gelten gewisse Erhaltungssätze, welche als Verallgemeinerungen des Helmholtzschen Wirbelsatzes für kompressible Medien anzusehen sind.

Sutcliffe [6] hatte 1947 mit Hilfe der Vorticity und der temperaturbedingten vertikalen Abstände isobarer Flächen eine Theorie der Entwicklung thermisch asymmetrischer Zyklonen geschaffen.

2. Das barotrope Modell als Grundlage

Als die elektronischen Rechenautomaten aufkamen, legte der Mathematiker John von Neumann 1946 einer Gruppe von Forschern am Institute for Advanced Study in Princeton die Frage vor, ob diese Geräte nicht neue Perspektiven für die Vorausberechnung atmosphärischer Strömungen eröffneten. Unter der Führung von Charney wandte sich diese Arbeitsgruppe dem Studium grossräumiger Strömungen zu. Charney [7] unterzog insbesondere die Grössenordnung aller in den dynamischen Gleichungen auftretenden Glieder einer eingehenden Untersuchung, wobei ihre Abhängigkeit vom Maßstab der betrachteten Phänomene klar zutage trat.

Es ergab sich, dass die bei Schall- und Gravitationswellen wesentlichen Vergenzen für grossräumige meteorologische Strömungen nicht charakteristisch sind. Diese schienen praktisch *vergenzfrei* abzulaufen, und es musste also möglich sein, durch Unterdrückung der Vergenzen in den dynamischen Gleichungen die kleinen Störungen, den «meteorologischen Lärm», herauszufiltern.

Anderseits erwies sich die absolute Vorticity als eine in erster Näherung invariante, für grossräumige Strömungen in hohem Grade charakteristische Grösse. Auch spielten Temperaturunterschiede längs der Stromlinien dynamisch eine viel kleinere Rolle, als früher angenommen worden war. In dem für meteorologische Zwecke interessanten Bereich des Spektrums atmosphärischer Bewegungen durfte man also auch in erster Näherung *Barotropie* voraussetzen; darunter versteht man das Zusammenfallen der Flächen konstanter Temperatur mit Flächen konstanten Druckes.

Wenn man kleinräumige Störungen durch entsprechende Glättung des Stromfeldes eliminierte, schien sich die Luft in ihrem dynamischen Verhalten einer *inkompressiblen* Flüssigkeit zu nähern. Dieses vergenzfreie und quasi-barotrope Verhalten erwies sich vorzüglich als eine Eigenschaft der *mittleren Troposphäre*, während in den unteren und oberen Stockwerken der Troposphäre grössere Abweichungen gefunden wurden. Deshalb konzentrierte man die Berechnungsversuche naturgemäss zuerst auf die im Wetterdienst ohnehin geläufige 500-Millibar-Fläche, die im Durchschnitt etwa in 5,5 km Höhe über dem Meeresniveau liegt.

Hier ist eine Bemerkung über das in der theoretischen Meteorologie übliche *Koordinatensystem* am Platze. Als vertikale Koordinate verwendet man an Stelle der Höhe oder des Geopotentials mit Vorteil den Luftdruck p, während die Ebenen $x = \text{const}$ und $y = \text{const}$ wie in der Mechanik orthogonale Vertikalebenen

sind. Die Höhe z oder besser das Geopotential Φ erscheint dann als abhängige Variable und wird meist dazu benützt, die Topographie einer isobaren Fläche p = const zu charakterisieren. Die Neigung isobarer Flächen ist übrigens von der Grössenordnung 1:10000 und beträgt nur in extremen Fällen 1:1000. Das (x, y, p)-System ermöglicht die Elimination der Luftdichte aus sämtlichen dynamischen Gleichungen [8].

Bei Untersuchungen, die sich auf die Erdatmosphäre als Ganzes beziehen, muss man die horizontalen Koordinaten (x, y) durch sphärische ersetzen; erstrekken sich die zugrundeliegenden Wetterkarten auf eine Hemisphäre oder auf grosse Teile einer solchen, verwendet man in der Regel eine stereographische Projektion und transformiert die dynamischen Gleichungen entsprechend.

CHARNEY und Mitarbeiter zeigten nun auch, wie man die Vorticity prognostisch verwerten kann [9, 10]. Durch kreuzweises Differenzieren der beiden Bewegungsgleichungen (1) nach y bzw. x und Subtraktion, also durch Rotorbildung, erhält man unter Berücksichtigung der Kontinuitätsgleichung (2) die allgemeine Vorticitygleichung (3). Es sei darauf hingewiesen, dass hierin nur die Reibungs- bzw. Austauschkräfte und die von der vertikalen Windkomponente herrührende Komponente der Corioliskraft vernachlässigt wurden; die letztgenannte Vernachlässigung ist bei grossräumigen Strömungen belanglos, da die Vertikalgeschwindigkeit im grossräumigen Durchschnitt rund 1000 mal kleiner ist als die horizontale.

Im vergenzfreien, barotropen Fall verschwindet die rechte Seite von (3) und das Vorticitygesetz reduziert sich auf einen einfachen Erhaltungssatz (4). Er besagt, dass die absolute Vorticity einer Luftmasse im Laufe der Bewegung erhalten bleibt, d.h. sich mit dem Wind verlagert. Dabei ist zu beachten, dass infolge der Breitenabhängigkeit des Coriolisparameters die relative Vorticity im allgemeinen nicht konstant bleibt: wandert eine Luftmasse gegen den Äquator, so nimmt ihre Drehbewegung relativ zur Erde in zyklonalem Sinne zu, und umgekehrt.

Nun ergibt sich aber eine weitere Vereinfachung aus der unter gewissen Voraussetzungen zulässigen *geostrophischen* Näherung. Als geostrophischen Wind bezeichnet man einen Wind, der sich bei stationärer Strömung, d.h. bei Abwesenheit von Reibung und Beschleunigungen, aus dem Gleichgewicht von horizontaler Druckkraft und Corioliskraft ergibt. Aus den aerologischen Karten weiss man seit langem, dass der Wind in der freien Atmosphäre, und zwar namentlich in der Mitte der Troposphäre, im grossen und ganzen dem geostrophischen Näherungsgesetz sehr gut gehorcht. Merkliche Abweichungen treten nur bei scharfer Krümmung, Diffluenz oder Konfluenz der Stromlinien auf.

Der geostrophische Wind weht parallel zu den Isohypsen (Höhenkurven) der isobaren Flächen mit einer Stärke, die nur von der Neigung der isobaren Flächen und von der geographischen Breite abhängt.

Bei Verwendung der geostrophischen Näherung können wir die oft nur ungenau gemessenen Winde durch einen horizontalen Vektor ersetzen, der sich in einfacher Weise aus der viel genauer bestimmbaren Topographie isobarer Flächen berechnen lässt. So ergibt sich aus (4) eine recht einfache Prognosengleichung für die zeitliche Änderung des Geopotentials (6); sie hat die Form einer Poissonschen Differentialgleichung, wobei die rechte Seite ausschliesslich von topographischen Eigenschaften (Krümmung und Neigung) der betrachteten isobaren Fläche und von der geographischen Breite abhängt. Die Auflösung dieser Gleichung nach $\partial\Phi/\partial t$ hat eine gewisse Verwandtschaft mit der Berechnung des elektrostatischen Feldes aus einer gegebenen Raumladung, ist aber hier nur für ein zweidimensionales Problem durchzuführen.

Ist $\partial\Phi/\partial t$ einmal für jeden Punkt der Fläche berechnet, so genügt Multiplikation mit einem bestimmten Zeitintervall Δt und Addition zum Ausgangswert für die Berechnung des Geopotentials am Ende des Zeitintervalles (7). Der Zeitschritt Δt ist allerdings begrenzt durch die Forderung, dass die rechte Seite der Prognosengleichung (6) während dieser Zeitspanne innerhalb der Fehlergrenzen konstant bleibe. Bei den in Betracht kommenden Feldänderungen beträgt die höchstzulässige *Prognosendauer* für einen Schritt 2 Stunden. Eine Prognose auf 24 Stunden bedingt deshalb 12 malige Wiederholung des Verfahrens, wobei die bei jedem Schritt erhaltene Φ-Verteilung als Ausgangsverteilung für den nächsten Schritt zu verwenden ist.

Für die Durchführung solcher Aufgaben stehen sowohl numerische wie graphische Verfahren zur Verfügung.

Die hauptsächlich von Fjörtoft [12] und Estoque [16] entwickelten *graphischen* Verfahren sind den numerischen im Prinzip ähnlich; durch einen besonderen Kunstgriff konnte der Zeitschritt für eine graphische Prognose ohne starke Beeinträchtigung der Genauigkeit sogar auf 24 Stunden erhöht werden; auch ist der finanzielle Aufwand für graphische Prognosen bedeutend geringer als derjenige für numerische Prognosen mit Hilfe elektronischer Rechenanlagen. Da die graphischen Verfahren aber das Zeichnen einer grossen Zahl von Hilfskarten erfordern, haben sie sich für Routinezwecke neben den numerischen nicht durchsetzen können. Im folgenden befassen wir uns ausschliesslich mit den numerischen Methoden.

3. Numerische Berechnung

Um irgend ein physikalisches Feld numerischer Behandlung zugänglich zu machen, muss man seine Zahlenwerte in regelmässig angeordneten diskreten Punkten des Raumes kennen; das heisst, man muss den kontinuierlichen Raum durch ein sogenanntes *Gitter* unterteilen. Die Wahl der Gitterkonstanten oder *Maschenweite* richtet sich nach der räumlichen Ausdehnung der zu untersuchenden Feldschwankungen. Für die Bearbeitung grossräumiger atmosphärischer «Störungen» (Wirbel und Wellen) hat sich eine horizontale Maschenweite von etwa 400 km als zweckmässig erwiesen [25].

Nun sind aber die aerologischen Beobachtungsdaten zunächst nicht in den Punkten eines regulären Gitters, sondern an unregelmässig verteilten Stationen gegeben. (Eine Anzahl stationärer Wetterschiffe sorgt für Sondenaufstiege von den Ozeanen aus; über den Landgebieten ist die Stationsdichte wesentlich grösser). Jeder Prognose hat deshalb eine *Analyse* des Beobachtungsmateriales voranzugehen, durch welche man die wahrscheinlichen Werte der meteorologischen Variablen in den Gitterpunkten für einen bestimmten Ausgangstermin festlegt. In der konventionellen Meteorologie erfolgt diese Analyse, indem man in die Karte durch Interpolation zwischen den vorliegenden Stationswerten von Hand möglichst glatte Isolinien zeichnet. Beim Zeichnen der Isohypsen einer isobaren Fläche nimmt man auf das geostrophische Näherungsgesetz Rücksicht, indem man versucht, die Tangentenrichtung und den Abstand der Kurven möglichst gut in Übereinstimmung mit den gemessenen Winden zu bringen. Offensichtlich falsche Meldungen sind dabei nach Möglichkeit zu korrigieren oder zu ignorieren. Nach Beendigung einer solchen Analyse sind für numerische Zwecke die Werte in den Gitterpunkten abzulesen, das heisst durch Schätzung zu interpolieren.

Bei diesem Arbeitsprozess ist eine gewisse persönliche Willkür namentlich in Gebieten, wo die Beobachtungsstationen weit auseinanderliegen, nicht zu umgehen. Um solche persönliche Fehler auszuschalten, haben Cressman und andere

objektive Analysenmethoden [24] erfunden, welche mit Hilfe elektronischer Rechenautomaten nach dem Prinzip der kleinsten Quadrate und mit geostrophischer Berücksichtigung des Windes auf rein maschinellem Wege zu den Ausgangswerten führen. Diese Ausgangswerte werden dann der Prognosenmaschine «verfüttert». Im einfachsten Fall der barotropen Prognose einer 500-Millibar-Karte besteht das Ausgangsmaterial aus der zweidimensionalen Φ-Verteilung, dh. aus den Werten des Geopotentials der 500-Millibarfläche an einem bestimmten Termin.

Die im Speicherwerk des Computers ein für allemal festgelegte Rechenvorschrift stützt sich auf die im Anhang mitgeteilten Formeln. Dabei sind Differentialquotienten durch entsprechende Differenzenquotienten anzunähern. Die Maschine hat also im wesentlichen die ersten und zweiten Differenzen des Geopotentials Φ nach den Koordinatenrichtungen x und y und daraus die relative Vorticity ζ zu bilden; durch Addition des zeitlich konstanten Coriolisparameters f wird die absolute Vorticity η erhalten. Von ihr sind wiederum die ersten Differenzen zu bilden, damit der Jacobi-Ausdruck $J(\eta, \Phi)$ berechnet werden kann. Für die Auflösung der Poisson-Gleichung (6) nach $\partial\Phi/\partial t$ dient ein *Relaxationsverfahren* [4, 11, 13]; der Rest besteht aus elementaren Operationen gemäss (7).

Bisher haben wir die *Randwertprobleme* übergangen. Bei jeder Differenzbildung würde das nutzbare Gitter an allen Rändern um eine Maschenbreite verkleinert, wodurch das Prognosengebiet sehr rasch zusammenschrumpfen würde. Man ist also gezwungen, an den Rändern bei jeder Zwischenoperation willkürliche Φ-Werte vorzugeben. Dies ist namentlich am Westrand eines Kartengebietes eine sehr bedenkliche Massnahme, da durch die vorherrschenden Westwinde der Einfluss der Randwerte rasch ins Innere des Kartengebietes fortgepflanzt wird. Um diese Fehler zu vermeiden, gibt es nur eine radikale Lösung: Das *Kartengebiet* muss womöglich auf eine von Parallelkreisen begrenzte, um die ganze Erde herumlaufende Zone oder noch besser auf eine Kugelkalotte, ja Hemisphäre ausgedehnt werden. Da in den Tropen Φ erfahrungsgemäss nur wenig ändert, ist dort die Vorgabe konstanter Φ-Werte zulässig.

Heute wird in den USA bei numerischen Routineprognosen ein auf eine stereographische Projektion gelegtes, achteckig begrenztes Gitter verwendet, das fast die ganze Nordhalbkugel bis zum 10. nördlichen Breitengrad bedeckt. Dieses im Innern in lauter Quadrate unterteilte Gitter weist nahezu 2000 innere Netzpunkte auf.

Das Ergebnis einer numerischen Prognose besteht aus Zahlen, die von der Maschine in richtiger Anordnung auf eine stereographische Karte gedruckt werden, worauf ein Zeichner bloss noch Isolinien des neuen (vorausberechneten) Geopotentials ($\simeq$ Stromlinien) einzuzeichnen hat. Diese Prognosenkarte wird dann durch drahtlose Facsimile-(Bildfunk-)Übertragung in kürzester Zeit allen Interessenten zugestellt. Der ganze Arbeitsprozess von der Eingabe der Stationsbeobachtungen bis zur Ausgabe der Prognosenkarte dauert etwa eine Stunde und läuft praktisch ohne menschliches Dazutun ab.

4. Barokline und ageostrophische Modelle

Es ist klar, dass die barotropen Gleichungen nicht streng richtige Vorhersagen liefern können; denn sie verlangen ja Konstanz der Wirbelintensität, während anhand von Wetterkarten immer wieder festgestellt werden kann, wie sich Wirbel von einem Tag zum nächsten verstärken, abschwächen, auflösen oder neu bilden. Nach der Entwicklungstheorie von SUTCLIFFE [6] liegt die Ursache solcher Wirbeländerungen wenigstens zum Teil in *baroklinen* Effekten, d.h. in isobaren Temperaturunterschieden.

Um ihnen Rechnung zu tragen, muss man das erste Glied auf der rechten Seite der allgemeinen Vorticitygleichung (3) berücksichtigen. Ein Zusammenhang zwischen Temperaturänderungen und Vertikalgeschwindigkeit wird durch den ersten Hauptsatz der Wärmelehre hergestellt, wobei man sich anfänglich auf adiabatische Vorgänge beschränken darf.

Zur Erfassung isobarer Temperaturunterschiede genügt eine einzige isobare Fläche als Ausgangsmaterial nicht mehr; man braucht mindestens zwei solcher Flächen, wobei ihr vertikaler Abstand über die Mitteltemperatur der dazwischen liegenden Luftschicht Aufschluss gibt. Bei Verwendung von zwei isobaren Flächen kann man die Temperatur in der Horizontalen varieren lassen, muss aber einen einheitlichen vertikalen Temperaturgradienten voraussetzen. Will man auch diesen von Ort zu Ort varieren lassen, muss eine dritte isobare Fläche herangezogen werden; eine vierte erlaubt Änderungen des vertikalen Temperaturgradienten auch in vertikaler Richtung, usw. So werden der theoretischen Modellatmosphäre sukzessive weitere Freiheitsgrade eingeräumt, wodurch aber das zu verarbeitende Material immer umfangreicher wird [13, 14].

Bei diesen *Mehrschichtmodellen* liefert die Maschine als Ergebnis die vorausberechnete Topographie sämtlicher isobaren Flächen, deren Anfangstopographie ihr mitgeteilt wurde. Die Anforderungen an die Speicherkapazität der Computers sind dadurch gegenüber der barotropen Rechnungsweise vervielfacht worden.

Interessanterweise liefern die baroklinen Modelle für die Topographie der 500-Millibar-Fläche im allgemeinen kaum bessere Prognosen als das barotrope Modell – ein indirekter Beweis für das quasi-barotrope Verhalten der mittleren Troposphärenschichten. Für höher oder tiefer gelegene Schichten ist dagegen die barokline Berechnung unumgänglich.

Wie primitiv das barotrope Modell ist, geht schon aus der Tatsache hervor, dass bei barotroper Temperaturschichtung der Wind von der Höhe unabhängig wäre. In Wirklichkeit sieht aber das Stromfeld in verschiedenen Höhen oft ganz anders aus.

Alle bisher besprochenen Modelle leiden aber an einer gemeinsamen Schwäche, nämlich an der *geostrophischen* Näherung. Diese ist zwar sehr bequem, aber physikalisch durchaus nicht gerechtfertigt. Ein streng geostrophischer, also parallel zu den Niveaulinien der isobaren Flächen wehender Wind bewirkt nämlich keine Dichteverlagerung und könnte infolgedessen überhaupt zu keinen Änderungen der Druckverteilung Anlass geben. Dass man mit den geostrophischen Modellen Änderungen des Druck- und Windfeldes vorhersagen kann, liegt nur an gewissen Inkonsequenzen in der Anwendung der geostrophischen Näherung.

Es bedeutet einen prinzipiellen Fortschritt, dass es 1955 Charney [15], Bolin [20] und anderen [19] gelang, die geostrophische Fessel durch die sogenannte *Balance-Equation* (8) zu sprengen.

Bei der Ableitung dieser Gleichung geht man von der Tatsache aus, dass grossräumige Strömungen in guter Näherung vergenzfrei sind, sich also durch eine Stromfunktion Ψ darstellen lassen. Durch Einsetzen der Stromfunktion in die ursprünglichen hydrodynamischen Bewegungsgleichungen (1) und Divergenzbildung erhält man nach leichter Umgruppierung die Balance-Equation (8). Sie stellt eine Differentialgleichung zur Bestimmung der zunächst unbekannten Stromfunktion Ψ dar, falls die Topographie Φ einer isobaren Fläche gegeben ist, und kann mittels eines *Relaxationsverfahrens* [4] numerisch gelöst werden. Die aus der Stromfunktion sich ergebenden Winde besitzen im allgemeinen eine kleine *ageostrophische* Komponente; die Stromlinien $\Psi = \text{const}$ verlaufen nicht mehr genau entlang den Isohypsen.

Zur Berücksichtigung ageostrophischer Effekte ist das Rechnungsprogramm der numerischen Wetterprognose in der Weise abzuändern, dass zunächst von Φ ausgehend die Stromfunktion Ψ berechnet wird; alle weiteren Operationen werden dann mit dieser Stromfunktion ausgeführt; erst beim Schlussresultat geht man wieder zur Topographie über. Dieses Verfahren hat sich namentlich in den Fällen bewährt, wo mit grossen Beschleunigungen zu rechnen ist, zum Beispiel bei tropischen Wirbelstürmen [21].

Weitere Verbesserungen sind zu erwarten von der Berücksichtigung der Gelände-, Reibungs- und Strahlungseinflüsse sowie der Kondensationsprozesse.

5. Bisherige Erfolge und Zukunftsaussichten

Unsere Darstellung nimmt im wesentlichen Bezug auf die Arbeiten der *Joint Numerical Weather Prediction Unit* (JNWP) in Suitland (Maryland, USA). Dieses von der US-Air-Force, der amerikanischen Marine und dem staatlichen Wetterbureau gemeinsam finanzierte und betriebene Institut macht seit 1955 tägliche Routineprognosen; es verwendet einen «Digital Computer» vom Typ IBM-704, der demnächst durch eine Anlage vom Typ IBM-7090 ersetzt wird, also durch eine der grössten bisher gebauten Rechenmaschinen.

Die Produkte der JNWP werden laufend durch Facsimile-Funkübertragung ausgestrahlt. Das gegenwärtige Tagesprogramm umfasst: Eine 72-stündige Vorausberechnung der 500-Millibar-Karte (Niveau 5½ km), eine 24-stündige und zwei in Abständen von 12 Stunden ausgegebene 36-stündige Prognosen der 700-Millibar-Karte (Niveau 3 km), je zwei 12-, 24- und 36-stündige Prognosen der 300-Millibar-Karte (Niveau 9 km), eine 24-stündige Prognosenkarte der grossräumigen Vertikalbewegung.

Die 300-Millibar-Prognosen sind von unmittelbarer Wichtigkeit für den Düsen-Luftverkehr. Vertikalbewegungskarten sollen eine Abschätzung der Bewölkung und Niederschläge ermöglichen.

Auf Grund von Prognosen der Vertikalbewegung und der im Ausgangszeitpunkt bekannten dreidimensionalen Feuchtigkeitsverteilung ist es übrigens bereits gelungen, *quantitative Niederschlagsprognosen* zu machen, wobei sogar die durch das Gelände bedingten Aufwinde näherungsweise in Rechnung gestellt werden konnten. Diese Niederschlagsprognosen gaben die grossräumige Verteilung des Niederschlages im allgemeinen recht zutreffend wieder, wogegen Instabilitätserscheinungen regionalen und lokalen Charakters (Schauer und Gewitterregen) natürlich nicht erfasst werden konnten.

Es gibt auch schon brauchbare Verfahren zur Voraussage des *Meereszustandes*. Hierbei wird der Wellengang auf Grund von numerischen Vorhersagen des Windes in der untersten Luftschicht berechnet.

Diese Beispiele zeigen, dass neuerdings numerische Methoden auch auf andere Grössen als den Wind oder das Geopotential isobarer Flächen angewendet werden. Im Übrigen sei jedoch hervorgehoben, dass numerische Prognosen vorläufig nur ein *grossräumiges* Bild über die Verteilung des Windes oder allenfalls eines anderen meteorologischen Elementes geben. Die *Interpretation* dieses Bildes im Hinblick auf *regionale Wettervorhersagen* bleibt nach wie vor Aufgabe erfahrener Meteorologen, die ihre Regeln teils aus physikalischen Gesetzen, teils aus dem Studium vergangener Wetterabläufe herleiten. Wer aber im Wetterdienst arbeitet, weiss, wieviel für die regionale Wettervorhersage schon mit einer zuverlässigen Prognose des grossräumigen Strömungsfeldes gewonnen ist.

Wie steht es heute mit der *Güte numerischer Prognosen*? Um diese objektiv zu prüfen, hat man Korrelationskoeffizienten zwischen vorausberechneten und ein-

getroffenen Änderungen bestimmter Elemente an den Punkten eines Gitters berechnet. Dabei ergaben sich bisher folgende Resultate:

Im 500-Millibar-Niveau sind die numerischen Eintages-Prognosen den empirischen ebenbürtig; bei längerer Prognosenfrist (2 oder 3 Tage) sind die numerischen Prognosen den empirischen deutlich überlegen. In anderen Stockwerken der Atmosphäre, insbesondere am Erdboden, ist die Zuverlässigkeit der empirischen Methoden von den numerischen bisher erst knapp erreicht worden. Doch besteht kaum ein Zweifel, dass mit der weiteren Verfeinerung der Modelle die numerischen Methoden mehr und mehr den Vorrang erhalten werden.

Ihre künftige Entwicklung richtet sich aber noch auf ein anderes Anwendungsgebiet: Die *Mittel- und Langfristprognosen.*

Unter «Mittelfrist» verstehen wir in der Meteorologie einen Zeitraum, der mit der Dissipationszeit einer normalen Depression vergleichbar ist (etwa 5–7 Tage). Für solche Zeitspannen ist eine exakte dynamische Vorhersage auf Grund des Anfangszustandes heute nicht möglich. Dagegen scheint es auf Grund von Beziehungen zwischen räumlichen und zeitlichen Mitteln, die u.a. von österreichischen Meteorologen [18] untersucht wurden, zu gelingen, generelle Aussagen über die wesentlichen Züge des atmosphärischen Strömungsbildes am Ende eines mittelfristigen Zeitraumes zu machen [22].

Unter Langfristprognosen verstehen wir Voraussagen auf Monate, Jahreszeiten oder Jahre hinaus. Bei solchen Zeiträumen spielen Einzelheiten des Anfangszustandes, soweit man sie heute erfassen kann, keine Rolle mehr. Es handelt sich vielmehr darum, die Abweichungen der sogenannten *«allgemeinen Zirkulation»* der Erdatmosphäre vom mittleren Verlauf vorauszuberechnen.

Nach heutiger dynamischer Auffassung ist die allgemeine Zirkulation das, was von einem momentanen Strömungszustand der Erdatmosphäre übrig bleibt, wenn man durch eine starke Glättung alle Störungen von der Grössenordnung kleiner bis mittlerer Depressionen weggeschliffen hat. Sie zeigt zyklonale und antizyklonale Wirbel oder auch Wellen grossen Ausmasses, welche sich einer zonalen Grundströmung überlagern und für den meridionalen Wärmeaustausch zwischen den verschiedenen Breitenzonen verantwortlich sind. Bei Mittelbildung über längere Zeiträume (Jahre) bleibt abgesehen von Land-Meer-Effekten nur die zonale Grundströmung erhalten, die das dynamische Geschehen nur zu einem kleinen Teil widerspiegelt. Die Theorie der allgemeinen Zirkulation steckt noch in ihren Anfängen.

Die numerischen Methoden sind berufen, Licht in diese Theorie zu bringen; denn sie geben uns ein Mittel in die Hand, mit theoretischen Modellen zu *experimentieren* [17], was in natura nicht möglich ist. Wir können der Rechnungsmaschine z.B. gewisse Grundtypen einer allgemeinen Zirkulation eingeben und untersuchen, wie sich die Zirkulation im Laufe der Zeit unter bekannten äusseren Einwirkungen verändert. Dabei müssen selbstverständlich Strahlung, Reibung, Kondensationsprozesse und topographische Einflüsse in Rechnung gestellt werden; vielleicht sind aber auch extraterrestrische Einflüsse wie die Schwankungen der Sonnenstrahlung zu berücksichtigen.

Verheissungsvolle Ansätze zur Lösung dieser Probleme sind bereits vorhanden. Die Ergebnisse sind zum Teil überraschend. So scheint die über halbe Erdquadranten sich erstreckende «Grossturbulenz» mit ihren thermisch asymmetrischen Wirbeln energetisch ganz anders zu wirken als die bekannte Kleinturbulenz.

Parallel zu diesen numerischen Versuchen werden in Laboratorien *physikalische Modellversuche* mit rotierenden, beheizten Flüssigkeiten gemacht, wobei sich zum Teil verblüffende Übereinstimmungen mit den aus Wetterkarten bekannten Strömungsbildern und auch mit den numerischen Experimenten ergaben [23].

Für die Durchführung von Routineprognosen genügen beim heutigen Stand der Übermittlungstechnik einige wenige Zentren, zum Beispiel eines pro Kontinent. Zur Entwicklung der theoretischen Grundlagen sind dagegen Forscher aller Länder aufgerufen.

Die in unserer Übersicht besprochenen Methoden verdanken wir in der Hauptsache nordamerikanischen Universitäten und Forschungsinstituten; wesentliche Beiträge stammen von schwedischen, norwegischen, englischen, deutschen und japanischen Forschern. Russland geht mit den Methoden von I. A. KIBEL [5] eigene Wege. In manchen Ländern wird auch versucht, die Resultate numerischer Berechnungen durch empirische Korrekturen zu verbessern. Das Entscheidende sind aber wohl die Entdeckungen von CHARNEY [7, 9] und seinen Mitarbeitern, durch welche eine physikalische Grundlage für objektive, mathematische Prognosen des atmosphärischen Strömungsfeldes auf Grund hydrodynamischer Gesetze geschaffen wurde.

Symbole

x, y rechtwinklige, horizontale Koordinaten;

p Luftdruck;

u, v Geschwindigkeitskomponenten nach x, y (Horizontalwind);

$\omega = \frac{dp}{dt}$ sog. generalisierte Vertikalgeschwindigkeit;

$\Phi = \Phi(p; x, y; t)$ Geopotential;

$\frac{d}{dt} = \frac{\partial}{\partial t} + u\frac{\partial}{\partial x} + v\frac{\partial}{\partial y} + \omega\frac{\partial}{\partial p}$ individuelle (das heisst massengebundene) Ableitung nach der Zeit;

$\nabla = \left(\frac{\partial}{\partial x}, \frac{\partial}{\partial y}\right)_p$ Nabla-Operator auf einer isobaren Fläche;

$\nabla^2 = \left(\frac{\partial^2}{\partial x^2} + \frac{\partial^2}{\partial y^2}\right)_p$ Laplace-Operator auf einer isobaren Fläche;

$J(a, b) = \frac{\partial a}{\partial x}\frac{\partial b}{\partial y} - \frac{\partial a}{\partial y}\frac{\partial b}{\partial x}$ Jacobi-Operator;

Ψ Stromfunktion, definiert durch $u = -\frac{\partial \Psi}{\partial y}$, $v = \frac{\partial \Psi}{\partial x}$;

$u_g = -\frac{1}{f}\frac{\partial \Phi}{\partial y}$, $v_g = \frac{1}{f}\frac{\partial \Phi}{\partial x}$ geostrophischer Wind;

$f = 2\,\Omega \cdot \sin\varphi$ Coriolis-Parameter;

Ω Rotationsgeschwindigkeit der Erde;

φ geographische Breite;

$\zeta = \frac{\partial v}{\partial x} - \frac{\partial u}{\partial y} = \nabla^2\Psi$ relative Vorticity;

$\eta = \zeta + f$ absolute Vorticity.

Wichtigste Formeln

(1) $$\left.\begin{aligned} \frac{\partial u}{\partial t} + u\frac{\partial u}{\partial x} + v\frac{\partial u}{\partial y} + \omega\frac{\partial u}{\partial p} &= -\frac{\partial \Phi}{\partial x} + f v \\ \frac{\partial v}{\partial t} + u\frac{\partial v}{\partial x} + v\frac{\partial v}{\partial y} + \omega\frac{\partial v}{\partial p} &= -\frac{\partial \Phi}{\partial y} - f u \end{aligned}\right\}$$ Horizontalkomponenten der Eulerschen Bewegungsgleichung im (x, y, p)-System.

(2) $$\frac{\partial u}{\partial x} + \frac{\partial v}{\partial y} + \frac{\partial \omega}{\partial p} = 0$$ Kontinuitätsgleichung im (x, y, p)-System.

(3) $$\frac{d\eta}{dt} = \eta\frac{\partial \omega}{\partial p} + \frac{\partial u}{\partial p}\frac{\partial \omega}{\partial y} - \frac{\partial v}{\partial p}\frac{\partial \omega}{\partial x}$$ Allgemeine Vorticitygleichung.

(4) $$\frac{d\eta}{dt} = 0 \text{ oder } \frac{\partial \eta}{\partial t} = -u\frac{\partial \eta}{\partial x} - v\frac{\partial \eta}{\partial y} - \omega\frac{\partial \eta}{\partial p}$$ Barotrope Vorticitygleichung.

(5) $$\nabla^2\frac{\partial \Psi}{\partial t} = J(\eta, \Psi) - \omega\frac{\partial \eta}{\partial p} \quad \text{mit} \quad \eta = \nabla^2\Psi + f$$ Barotrope Prognosengleichung.

(6) $$\nabla^2\frac{\partial \Phi}{\partial t} = J(\eta, \Phi) \quad \text{mit} \quad \eta = \frac{1}{f}\nabla^2\Phi + f$$ Genäherte geostrophisch-barotrope Prognosengleichung.

(7) $$\Psi(t + \Delta t) = \Psi(t) + \Delta t\frac{\partial \Psi}{\partial t} \quad \text{bzw.} \quad \Phi(t + \Delta t) = \Phi(t) + \Delta t\frac{\partial \Phi}{\partial t}.$$

(8) $$f\nabla^2\Psi + \nabla f\,\nabla\Psi + 2\left[\frac{\partial^2\Psi}{\partial x^2}\frac{\partial^2\Psi}{\partial y^2} - \left(\frac{\partial^2\Psi}{\partial x\,\partial y}\right)^2\right] = \nabla^2\Phi$$ Balance-Equation.

LITERATURVERZEICHNIS

[1] V. Bjerknes, *Das Problem der Wettervorhersage, betrachtet vom Standpunkte der Mechanik und Physik.* – Met. Z. *39*, 1–7 (1904).

[2] L. F. Richardson, *Weather Prediction by Numerical Process.* – (Cambridge University Press, 1922).

[3] C. G. Rossby, *Planetary Flow Patterns in the Atmosphere.* – Quart. J. roy. Met. Soc. *66*, Suppl., 68–87 (1940).

[4] R. V. Southwell, *Relaxation Methods in Theoretical Physics.* – (Oxford, Clarendon Press, 1946).

[5] B. J. Izvekov, *Professor I. A. Kibel's Theoretical Method of Weather Forecasting.* – Bull. amer. Met. Soc. *27*, 488–498 (1946).

[6] R. C. Sutcliffe, *A Contribution to the Problem of Development.* – Quart. J. roy. Met. Soc. *73*, 370–383 (1947).

[7] J. G. Charney, *On the Scale of Atmospheric Motions.* – Geofys. Publ. *17* (2), (1948).

[8] A. Eliassen, *The Quasi-Static Equations of Motion with Pressure as Independent Variable.* – Geofys. Publ. *17* (3), (1949).

[9] J. G. Charney, *On a Physical Basis for Numerical Prediction of Large-Scale Motions in the Atmosphere.* – J. Met. *6*, 371–385 (1949).

[10] J. G. Charney, R. Fjörtoft, J. von Neumann, *Numerical Integration of the Barotropic Vorticity Equation.* – Tellus *2*, 237–254 (1950).

[11] F. H. Bushby, *Relaxation Methods and their Application to Meteorological Problems.* – Met. Mag. *80*, 71–77 (1951).

[12] R. Fjörtoft, *Graphical Integration of the Barotropic Vorticity Equation.* – Norske Videnskaps-Akad., Inst. f. Vaer-og Klimaforskning, Rep. No. *6*, (1952).

[13] K. Hinkelmann, O. Essenwanger, G. Reymann und F. Wippermann, *Physikalisch-mathematische Grundlagen der numerischen Integration in einer baroklinen Atmosphäre.* – Ber. dtsch. Wetterdienstes US-Zone *6* (38), 416–427 (1952).

[14] J. G. Charney, N. A. Phillips, *Numerical Integration of the Quasi-Geostrophic Equations for Barotropic and Simple Baroclinic Flows.* – J. Met. *10*, 71–99 (1953).

[15] J. G. Charney, *The Use of the Primitive Equations of Motion in Numerical Prediction.* – Tellus *7*, 22–26 (1955).

[16] M. A. Estoque, *A Prediction Model for Cyclone Development Integrated by Fjörtoft's Method.* – J. Met. *13*, 203–206 (1956).

[17] N. A. Phillips, *The General Circulation of the Atmosphere: A Numerical Experiment.* – Quart. J. roy. Met. Soc. *82*, 123–164 (1956).

[18] H. Reuter, *Über die Voraussage zeitlich gemittelter Höhenkarten für Zwecke mittelfristiger Wetterprognosen.* – Arch. Met., Geo. [A] *9*, 433–438 (1956).

[19] P. D. Thompson, *A Theory of Large-Scale Disturbances in Non-Geostrophic Flow.* – J. Met. *13*, 251–261 (1956).

[20] B. Bolin, *An Improved Barotropic Model and Some Aspects of Using the Balance Equation for Three-Dimensional Flow.* – Tellus *8*, 61–75 (1956).

[21] Y. Masuda, H. Itoo, *The Use of a Stream Function for the Barotropic Forecast of the Typhoon Movement.* – J. Met. Soc. Japan, 75th Anniversary 296–303 (1957).

[22] J. Namias and collabor., *Application of Numerical Methods to Extended Forecasting Practices in the U. S. Weather Bureau.* – Mon. Weath. Rev. *86*, 467–476 (1958).

[23] H. Riehl, D. Fultz, *The General Circulation in a Steady Rotating Dishpan Experiment.* – Quart. J. roy. Met. Soc. *84*, 389–417 (1958).

[24] G. Cressman, *An Operational Objective Analysis System.* – Mon. Weath. Rev. *87*, 367–374 (1959).

[25] E. Knighting, *On the Grid Length to be Adopted in Numerical Weather Prediction.* – Quart. J. roy. Met. Soc. *86*, 265–270 (1960).

Résumé

Le but de cet article est d'exposer à des physiciens et des mathématiciens les problèmes et principes de la prévision dynamique du temps et leur solution par des méthodes numériques.

Summary

The purpose of the present article is to acquaint physicists and mathematicians with the problems and principles of dynamical weather prediction and their solution by numerical methods.

(Eingegangen: 21. Juli 1960.)

Tagungen über Elektronenmikroskopie

1. Die Jahrestagung der Deutschen Gesellschaft für Elektronenmikroskopie e. V. findet vom 24. bis 27. September 1961 in Kiel im Anatomischen Institut (Dir. Prof. W. BARGMANN) statt. Anfragen sind zu richten an: Dr. H. KEHLER, p. Adr. Farbwerke Hoechst AG., Frankfurt (Main)-Höchst.

2. Der alle vier Jahre stattfindende Internationale Kongress der International Federation of Electron Microscopy Societies wird auf Einladung der Amerikanischen Gesellschaft für Elektronenmikroskopie vom 29. August bis 5. September 1962 in Philadelphia stattfinden. Anfragen sind zu richten an: Fifth International Congress for Electronic Microscopy, 7701 Burholme Avenue, Philadelphia 11, Pennsylvania, USA.

H. KEHLER

Buchbesprechungen – Book Reviews – Notices bibliographiques

Games and Decision: Introduction and Critical Survey. Von R. D. LUCE und H. RAIFFA (John Wiley & Sons, Inc., New York 1957). 509 S., 59 Fig.; $8.75.

Nach den Worten der Verfasser ist dies ein Buch über Spieltheorie und keine Darstellung der Theorie selbst. Dies kommt vor allem darin zum Ausdruck, dass es fast keine Beweise enthält – auch keinen für die Existenz der Lösung des Zwei-Personen-Nullsummen-Spiels. Das Buch ist somit vor allem solchen Lesern zu empfehlen, für welche mathematische Beweise die Darstellung mehr verdunkeln als erhellen. – Nach einer allgemeinen Einleitung wird die Normalform von KUHN dargestellt, welche Spiele als Bäume (im Sinne der Graphentheorie) interpretiert. Dann wird das Zwei-Personen-Spiel und das allgemeine n-Personen-Spiel behandelt, wofür der Lösungsbegriff von v. NEUMANN-MORGENSTERN ausführlich erläutert und mit Experimenten verglichen wird, welche bei RAND gemacht worden sind. In weiteren Paragraphen wird das Problem einer individuellen Entscheidung bei unvollständiger Information und jenes von Gruppenentscheidungen besprochen. Einige Anhänge erweitern die Darstellung des Hauptteiles nach der mathematischen Seite. Es wird so das Minimaxtheorem exakt formuliert und sein Beweis auf den Beweis eines Fixpunktsatzes zurückgeführt, und es werden die verschiedenen geometrischen Interpretationen des Zwei-Personen-Nullsummen-Spiels besprochen sowie auf den Zusammenhang mit der linearen Programmierung eingegangen.

E. SPECKER

Handbuch der Physik - Encyclopedia of Physics. Herausgegeben von S. FLÜGGE, Band 53: *Astrophysik* IV: *Sternsysteme* (Springer-Verlag, Berlin 1959). Mitarbeiter: F. K. Edmondson, B. Lindblad, J. H. Oort, H. S. Hogg, R. H. Brown, B. Y. Mills, G. de Vaucouleurs, F. Zwicky, J. Neyman, E. L. Scott, G. C. McVittie, O. Heckmann und E. Schücking. 565 S., 189 Abb.; DM. 142.–.

Der vorliegende letzte der die Ergebnisse der astrophysikalischen Forschung enthaltenden vier Bände behandelt die Sternsysteme und die Kosmologie. Das galaktische System nimmt 240 Seiten in Anspruch, die extragalaktischen Systeme 200 und die Kosmologie 100 Seiten. Der Band gibt mehr eine lockere Aneinanderreihung ausgewählter aktueller Kapitel als eine kompakte und geschlossene Darstellung. Diese Kapitel behandeln die Kinematik und Dynamik des galaktischen Systems, die radioastronomische Erforschung der Milchstrasse, die Sternhaufen, die «Punktquellen», die radioastronomische Erforschung, Klassifikation und Be-

schreibung der extragalaktischen Systeme, die Haufenbildung und die räumliche Verteilung derselben, Entfernung- und Altersbestimmungen und schliesslich die kosmologischen Theorien.

Der Band enthält eine reiche Fülle neuer und neuester Beobachtungsergebnisse und vorzügliches Bildmaterial. Die Darstellung geht je nach Gegenstand und Autor von der reinen Beschreibung, welche vorherrscht, bis zur reinen Theorie. Vielfach geben die Beiträge mehr eine Übersicht der vom Verfasser und seinen Mitarbeitern gepflegten Forschungsrichtung als einen gesamthaften Überblick. Einzelne Gebiete haben in neuester Zeit bereits eine monographische Darstellung, zum Teil von denselben Autoren, erfahren, denen der Handbuchartikel kaum wesentlich Neues beizufügen hat. Andere aktuelle Gebiete, für welche dies nicht zutrifft, sind auch im vorliegenden Band übergangen worden. Insbesondere vermisst man einen Beitrag über interstellare Materie und magnetische Felder des galaktischen Systems. Die drei radioastronomischen Beiträge, welche zusammen nur 100 Seiten umfassen, hätte man gerne in grösserer Breite gesehen. So mag zwar der Leser nicht alles finden, was er sucht, aber was er findet, ist von bestem Standard und von der Höhe der Forschung geschrieben. Ein Vergleich mit dem vor einem Vierteljahrhundert erschienenen Handbuch der Astrophysik zeigt die erstaunliche Fülle neuer Kenntnisse, denen leider keine entsprechende Mehrung des Verstehens folgte. Die Lösung des kosmologischen Problems ist noch in weiter Ferne, die meisten radioastronomischen Beobachtungen sind unverstanden und die Entwicklung der Sternsysteme rätselhaft, wissen wir doch nicht einmal mit Sicherheit, in welcher Richtung sie sich drehen! M. Waldmeier

Figures of Equilibrium of Celestial Bodies. Von Zdeněk Kopal (The University of Wisconsin Press, Madison 1960). 153 S., 3 Fig.; $3.–.

Die Theorie der Gleichgewichtsfigur einer kompressiblen Flüssigkeit unter der Wirkung der Eigengravitation wurde von Clairaut, Legendre und Laplace im wesentlichen bis zur 1. Ordnung des Einflusses der Deformation entwickelt. Im vorliegenden Buch gibt Kopal zunächst eine Zusammenfassung der Clairautschen Theorie, die explizite Ausdrücke für das Potential liefert und die äussere Form als Äquipotentialfläche definiert. Im besonderen werden die Lösungen der Clairautschen Gleichung für spezielle Dichteverteilungen angegeben und ebenso die iterative Lösung im Falle beliebiger Dichteverteilungen, wie sie durch Ljapunov und Kopal entwickelt wurde, dargestellt. Das Hauptziel des Buches ist die erstmalige Darstellung der vollständigen hydrostatischen Theorie 2. Ordnung. Es werden zu diesem Zwecke zunächst die expliziten Ausdrücke für die Äquipotentialflächen und das äussere Gravitationspotential abgeleitet für den Fall von Gezeitenstörungen und Rotationseffekten bei beliebiger Dichteverteilung. Speziell werden dann das homogene Modell und das Rochesche Modell betrachtet. Ebenso werden die Trägheitsmomente berechnet. Im weitern werden die recht komplizierten Terme bestimmt, die aus der Wechselwirkung von Gezeiten und Rotation auftreten und hier nicht mehr vernachlässigt werden dürfen. Schliesslich untersucht Kopal noch die nichtradialen Schwingungen, insbesondere die Möglichkeit von Resonanzen zwischen freien und erzwungenen Schwingungen, wobei aber keine definitiven Aussagen gemacht werden können und offensichtlich die dynamische Theorie herangezogen werden muss. Die entwickelte Theorie 2. Ordnung ist von wesentlicher Bedeutung für die Theorie enger Doppelsterne und die genaue Erfassung der Bewegung künstlicher Erdsatelliten. Die Theorie sollte beispielsweise in der Lage sein, die freie Gestalt der Erdoberfläche (als Äquipotentialfläche) mit einer Genauigkeit von der Grössenordnung 20 cm wiederzugeben. E. Roth-Desmeules

Grenzschichtforschung - Boundary Layer Research. Symposium der Internationalen Union für Theoretische und Angewandte Mechanik (IUTAM), Freiburg i. Br., 26. bis 29. August 1957. Herausgegeben von H. Görtler (Springer-Verlag, Berlin 1958). 411 S., 206 Abb.; DM 67.50.

Ein Gremium von 90 Strömungs-Wissenschaftlern aus 17 Ländern versammelte sich zur ersten IUTAM-Arbeitstagung 1957 in Freiburg i. Br. Während 8 Sitzungen gaben 32 Vortragende und 21 Diskussionsredner ihre Beiträge zu den Fortschritten der Grenzschichtforschung bekannt.

Während der Tagung wurde das Interesse auf die physikalischen Probleme der Grenzschichtforschung konzentriert, obschon dieser Zweig der Strömungsmechanik für die Technik von massgebender Bedeutung ist. Die inhaltsreichen Manuskripte der Referenten und die Diskussionsbeiträge sind in diesem Buch zusammengestellt und in der gewohnten, mustergültigen Art beim Springer-Verlag gedruckt worden. Im Rahmen einer kurzen Buchbesprechung ist es nicht möglich, auf Details des von den zahlreichen Autoren behandelten Stoffes einzugehen; kurze Hinweise auf die Themen (und Angabe der Verfasser) mögen zur Einführung dieses bedeutenden Sammelwerkes genügen:

Beiträge zur turbulenten Reibungsgrenzschicht (Townsend, Björgum, Wieghardt), spezielle stationäre Grenzschichten (Ackeret, Ludwig, Seth, Stewartson, Glauert, Thwaites, Görtler), Stabilitätstheorien und Umschlagsbedingungen (Schubauer, Görtler und Witting, Zaat, Laufer, Pfenninger, Dryden, Wille, Scholz, Tatsumi, Lin, Howard, Eichelbrenner und Michel, Bergh, van Driest), Temperatur- und Reibungsgrenzschichten bei Überschallströmungen und in Gasen kleiner Dichte (Ostrach, Schuh, Popper und Reiner, Schaaf und Talbot, Łunc und Lubonski, Käppeler und Zaddach, Scherberg), Wechselwirkung zwischen Grenzschichten und Verdichtungsstössen (Gadd, Ferrari, Mirels, Massignon, Iberall), Grenzschichten bei instationären Vorgängen und bei periodischer Absaugung (Moore, Persen, Wuest, Pfenninger, Wortmann, Tani), Grenzschichttheorie bei entstehender Ablösung und für Zweikomponenten-Flüssigkeit (Nikolskij, Rachmatulin), dreidimensionale Grenzschichten, Ablösebedingungen, laminar-turbulenter Übergang im Freistrahl und anderes (Timman, Oswatitsch, Walz, Tani, Wehrmann und Wille, Nickel, Frössling, de Krasinski).

Physiker und Ingenieure, die sich mit den Phänomenen der Reibungsgrenzschichten zu befassen haben, finden in dem Buche nicht nur neueste Forschungsergebnisse, sondern auch die dazu gehörenden Literaturhinweise. Die Beiträge sind in deutscher oder englischer Sprache geschrieben. H. Sprenger

Physical Climatology, 2. Aufl. Von Helmut Landsberg, U. S. Weather Bureau, Washington (Gray Printing Co., Inc., DuBois, Pennsylvania, 1958). 446 S., 109 Fig.; $ 6.00.

Die erste Auflage dieser grundlegenden Einführung in die Klimatologie erschien 1941. Nachdem das Werk in kurzer Zeit vier Neudrucke erlebt hatte, wurde es in der jetzt vorliegenden zweiten Auflage einer ebenso notwendigen wie gründlichen Revision unterzogen. Das Buch, das keine Kenntnisse der höheren Mathematik voraussetzt, gliedert sich in vier Kapitel. Im ersten Kapitel, das sich mit der Sammlung und dem Gebrauch von klimatologischen Daten befasst, werden neben den Untersuchungsmethoden und der Einrichtung der Instrumente, vor allem auch die statistischen Methoden behandelt. Das zweite Kapitel geht auf die klimatologischen Elemente selber ein. Es ist erfreulich, dass die immer wichtiger werdende Wärmebilanz der Atmosphäre hier eine eigene Darstellung erfährt. Unter der Ver-

bindung der klimatologischen Elemente, die den Inhalt des dritten Kapitels ausmacht, versteht H. LANDSBERG ihre Vereinigung zu Bildern des Klimas der Welt, grosser Regionen der Erde oder auch ganz kleiner Bezirke, also des Klimas der bodennahen Luftschichten im Sinne von R. GEIGER. Das letzte Kapitel schliesslich handelt von der angewandten Klimatologie.

Das sehr anschaulich und instruktiv geschriebene Buch ist nicht nur eine ausgezeichnete Einführung in die Klimatologie für Studierende der Meteorologie; auch der Fachmann wird es mit Vorteil lesen. J. C. THAMS

Theorie und Anwendung der direkten Methode von *Ljapunov*. Von WOLFGANG HAHN. Ergebnisse der Mathematik und ihrer Grenzgebiete. Neue Folge, Heft 22 (Springer-Verlag, Berlin-Göttingen-Heidelberg 1959). 142 S., DM 28.–.

Die Frage nach der Stabilität spielt bei Bewegungen und vor allem bei Schwingungsproblemen, insbesondere in der Regelungstechnik, praktisch eine hervorragende Rolle. Zu ihrer Untersuchung erweist sich die zweite oder direkte Methode von LJAPUNOV (die die Kenntnis der Lösungen der Differentialgleichungen nicht voraussetzt) als sehr geeignet, und sie lässt sich auch zum Aufbau einer allgemeinen Stabilitätstheorie heranziehen. Die Theorie der direkten Methode ist in den letzten Jahren vor allem durch russische Mathematiker stark gefördert worden, und da heute ein gewisser Abschluss erreicht wurde, erscheint eine Übersicht dringend notwendig, besonders auch deshalb, weil manche Originalarbeiten nur schwer zugänglich sind. Diese Übersicht vermittelt in ausgezeichneter Weise die Darstellung von W. HAHN. Die beiden ersten Kapitel entwickeln die elementare Theorie (hinreichende Bedingungen), das dritte bringt Anwendungen auf technische Probleme, während die restlichen dem Ausbau der Theorie (Umkehrung der Hauptsätze, Empfindlichkeit gegen Störungen, kritische Fälle) und dem Aufbau einer allgemeinen Stabilitätstheorie gewidmet sind. Im Vordergrund stehen naturgemäss die Stabilitätskriterien für gewöhnliche Differentialgleichungen; nur das letzte Kapitel bringt die Erweiterung auf partielle Differentialgleichungen und Differenzengleichungen. Die Darstellung schliesst mit einem Literaturverzeichnis, das bis zum Jahre 1957 möglichste Vollständigkeit anstrebt. Das Buch füllt im deutschen Sprachgebiet eine empfindliche Lücke aus, und sein Erscheinen ist daher sehr zu begrüssen. E. ROTH-DESMEULES

Plasma Physics and the Problem of Controlled Thermonuclear Reactions, Vol. III. Herausgegeben von M. A. LEONTOVICH. Übersetzung von J. B. SYKES, Harwell. (Pergamon Press, London 1959). 422 S., 114 Fig. £ 8.–.

Der vorliegende Band ist Teil einer vierbändigen Reihe und enthält eine Serie von kürzlich zur Publikation freigegebenen Arbeiten des Institutes für Kernphysik der USSR. Die meisten Artikel stammen aus den Jahren 1955–1957 und vermitteln ein eindrucksvolles Bild von den Fortschritten Russlands auf dem Gebiet der Fusionsforschung bis zum Zeitpunkt der Genfer Konferenz 1958. Der dritte Band enthält 26, vorwiegend theoretische Arbeiten, an denen etwa 20 Autoren beteiligt sind. Die behandelten Probleme sind in erster Linie die Erzeugung hoher Temperaturen, die magnetische Führung geladener Teilchen, Rekombinationseffekte in ionisierten Gasen, Strahlungsverluste usw.

G. I. BUDKER diskutiert Methoden zur direkten Umwandlung thermonuklearer Energie in elektrische Arbeit. Einen besonders interessanten Beitrag liefert B. A. TRUBNIKOW, in dem er zeigt, dass die magnetische Bremsstrahlung einer Plasmaschicht die Minimalgrösse eines selbsterhaltenden Fusionsreaktors bestimmt und dass diese kritischen Dimensionen selbst im Falle eines D–T–Reaktors sehr beträcht-

lich sind. Einer der wenigen experimentellen Artikel ist der von N. V. FILIPPOV, in dem er eine Methode zur Messung von Drucken in gepulsten Gasentladungen mit Hilfe von Piezoelementen beschreibt. L. I. RUDAKOV und R. Z. SADGEEV schlagen eine Methode der Plasmaerhitzung durch Hochfrequenz vor, die von der Zyklotronresonanz Gebrauch macht. In einer Arbeit von V. I. KOGAN wird die Rekombinationsstrahlung aus einem Wasserstoffplasma berechnet und mit der Intensität der Bremsstrahlung verglichen. S. I. BRADINSKII und B. B. KADOMTSEV zeigen, dass es mit Hilfe einer «Guardring»-Methode möglich sein sollte, die Form einer Plasmaoberfläche zugunsten einer möglichst stabilen Konfiguration zu beeinflussen. A. A. VEDENOV und R. Z. SADGEEV weisen die Möglichkeit auf, dass für eine anisotrope Geschwindigkeitsverteilung Plasmainstabilitäten auftreten können, die bei der hydromagnetischen Behandlung in älteren Arbeiten eventuell übersehen wurden. Im Ganzen beurteilt, dürfte dieses Buch ein neuer Beweis dafür sein, dass die vielseitigen Bemühungen des Pergamon Institutes, dem westlichen Leser die Literatur der USSR zugänglich zu machen, ausserordentlich fruchtbar sind.

F. HEINRICH

Kommunikation und Kybernetik in Einzeldarstellungen. Band 1: *Grundlagen und Anwendungen der Informationstheorie.* Von Prof. Dr. W. MEYER-EPPLER. (Springer-Verlag, Berlin 1959). 446 S., 178 Abb., 1 Tafel; DM 98.–.

Das Buch ist als erster Band einer Reihe über Kommunikation und Kybernetik in Einzeldarstellungen erschienen, deren Herausgeber ebenfalls der Autor war. Es ist nur zu hoffen, dass durch den leider zu früh erfolgten Hinschied von W. MEYER-EPPLER (Juli 1960) die Herausgabe der Reihe keinen Unterbruch erfährt und die folgenden Bände eine ähnliche Höhe der Qualität aufweisen werden. Die Darstellung der Informationstheorie hätte in keine bessern Hände gelegt werden können. Es ist erstaunlich, wie originell und gut fasslich die bereits bestehende zahlreiche Literatur mithinein verarbeitet wurde. Der Quellennachweis wurde aufs sorgfältigste geführt; und doch erscheint das Buch wie aus einem Guss.

Inhaltlich ist es in die folgenden elf Kapitel gegliedert, wobei die Klammern die Seitenzahlen angeben: *Die Kommunikationskette* (5) – *Strukturtheorie der Signale* (34) – *Eigenschaften linearer Übertragungssysteme* (14) – *Symbolstatistik* (80) – *Gestörte Systeme* (20) – *Sicherung gegen Übertragungsfehler* (19) – *Die Sinnesorgane als Informationsempfänger* (78) – *Signal und Zeichen* (32) – *Akustische und optische Valenzklassen als Zeichenträger* (47) – *Formstrukturen und Konstruktionen* (25) – *Die gestörte sprachliche Kommunikation* (48) – *Anhang mit einer Tabelle der Funktion -pld p und getrenntem Namen- und Sachverzeichnis* (15).

Besonders ausführlich – und mit Recht – sind die Kapitel über Symbolstatistik und die Sinnesorgane als Informationsempfänger gehalten. Im erstern sind die Kernsätze der Informationstheorie am Beispiel der Sprache entwickelt, und im andern finden die Eigenschaften der Sinnesorgane bezüglich ihrer Zellenstruktur, ihrer Reizschwellen, ihrer Unterscheidbarkeitsgrenzen und der Darstellung der Reizempfindungen (Farbdreieck, Phoneme, Vokaldreieck) ihren Platz. Erst durch die eingehende Kenntnis beider lässt sich die Kommunikationskette informationstheoretisch untersuchen, was in den dem oben genannten Kapitel folgenden durchgeführt wird.

Das vorliegende Buch schliesst eine Lücke im Schrifttum, es befriedigt nicht nur den Theoretiker, sondern auch den Fernmeldeingenieur, und selbst der Linguist wird es mit grossem Gewinn zu seinen Arbeiten verwenden können. W. MEYER-EPPLER hat sich mit diesem Buch selbst das schönste Denkmal gesetzt.

H. WEBER

Symposium on the numerical treatment of ordinary differential equations, integral and integro-differential equations

Proceedings of the Rome Symposium (20–24 Septembre 1960)
Organized by the Provisional International Computation Centre

Symposium sur le traitement numérique des équations différentielles ordinaires, des équations intégrales et intégro-différentielles

Actes du Symposium de Rome (20–24 septembre 1960)
Organisé par le Centre International Provisoire de Calcul

(1960) 680 pp. Fr. 35.— (DM 35.—)

Authors/Auteurs: M. Altmann, Z. Alterman, H. A. Antosiewicz, N. Artemiadis, W. D. Ashton, Ch. Blanc, K. Bochener, R. A. Buckingham, H. F. Bueckner, E. Bukovics, G. Capriz, J. Carteron, F. Ceschino, C. W. Clenshaw, R. Courant, B. Dejon, J. Delsarte, J. B. Diaz, A. S. Douglas, J. Douglas Jr., S. Fenyö, M. Fiedler, L. Finkelstein, T. Frey, F. Genuys, J. H. Giese, D. C. Gilles, M. Goto, D. Graffi, K. Grossman, K. Hain, P. Henrici, F. Hertweck, E. Isaacson, H. B. Keller, F. Krückeberg, G. N. Lance, C. Lanczos, R. Lattes, M. Laudet, P. Lesky, J. L. Lions, L. Lukaszewicz, G. J. Makinson, R. Mc Carroll, E. Martensen, A. Meallier, S. Moriguti, J. Moser, R. Nicolovius, B. Noble, H. Oulès, C. L. Pekeris, R. Pennacchi, T. Popoviciu, P. Pouzet, C. Pucci, K. A. Redish, M. H. Rogers, G. Seegmüller, M. A. Sneider, N. Teodorescu, J. Todd, L. H. Underhill, H. Unger, R. Van Norton, O. Vejvoda, A. Walther, A. Young

Symposium on questions of numerical analysis

Proceedings of the Rome Symposium (30 June–1 July 1958)
Organized by the Provisional International Computation Centre

(1958) 80 pp Fr. 10.— (DM 10.—)

Symposium on the numerical treatment of partial differential equations with real characteristics

Proceedings of the Rome Symposium (28–29–30 January 1959)
Organized by the Provisional Computation Centre

(1959) 158 pp Fr. 14.— (DM 14.—)

Zu beziehen durch Ihre Buchhandlung – Obtainable from your bookseller
Commandes à votre libraire

BIRKHÄUSER VERLAG · BASEL UND STUTTGART